TABLE OF CONTENTS

LIST OF FIGURES

Chapter 1

1. INTRODUCTION

Real world application is the inherent driver for the majority of research in robotics. It is often the current limitations in technology or design constraints that lead the way to new advances, and often works around to the development of these robots. In developing these airborne entities, the primary concerns are size, weight, sensors, communication and computational power. By **Defense Advanced Research Projects Agency** (DARPA), Micro Air Vehicles are small (usually defined to be less than 15 cm in length and below 100 g in weight) autonomous aircrafts, which have a great potential in fact-finding missions in confined spaces or inside buildings, including both civilian search-and-rescue missions and military surveillance and reconnaissance missions. The vehicle must fly 30 to 60 m/sec, fast enough to overcome head winds and have an endurance of 20 to 60 min to provide adequate range and mission time. The small size of Micro Air Vehicles makes them ideal to search for survivors in damaged buildings or to locate terrorists or kidnappers within building complexes. [1]

The predicted spectrum of conflict for 21st Century war fighters has influenced and motivated the new development. The shift toward a more diverse array of military operations, often involving small teams of individual soldiers operating in non-traditional environments (e.g. urban centers), is already more than evident in the post-cold war experience. MAVs are envisioned as an asset at the platoon level or below. Locally owned and operated, they will greatly reduce the latency inherent in current reconnaissance assets. They will give the individual soldier on-demand information about his surroundings resulting in unprecedented situational awareness, greater effectiveness and fewer casualties. Technological feasibility follows from advances in several micro technologies, including the rapid evolution of Micro Electro Mechanical System (MEMS) technology. These systems

combine micro electronics components with comparable sized mechanical elements of varying complexity to achieve useful and often unique functionality (e.g. integrated systems of sensors, actuators and processors).

In many cases, these devices are produced with established micro fabrication techniques, providing a high degree of optimism for eventual low-cost production potential. Other maturing micro systems such as tiny CCD-array cameras, equally small infra-red sensors and chip-sized hazardous substance detectors, have been catalytic in providing the motivation for like-sized delivery platforms. Yet formidable technical challenges must be met to successfully integrate these payloads into functional MAV systems. Innovative technical solutions must be found for aerodynamics, control, propulsion, power, navigation and communication. The earliest suggestions of technical viability appeared in the early 1990's from studies such as Research & Development Corporation's investigation of micro systems, and MIT Lincoln Laboratory's early investigations of micro flyers. [1]

The latter more recent study helped energize a DARPA workshop on Micro Air Vehicle feasibility in the fall of 1995. The outcome of that effort has been a newly created DARPA program to develop this new dimension in flight. The DARPA program was initiated through the Small Business Innovation Research (SBIR) Program together with a more detailed study by Lincoln Laboratory. The term Micro Air Vehicle may be somewhat misleading if interpreted too literally. We tend to think of flying model aircraft as "Miniature", so the term "Micro" now alludes to a class of significantly smaller vehicles. But MAVs are not small versions of larger aircraft. They are affordable, fully functional and militarily capable, small flight vehicles. The definition employed in DARPA's program limits these craft to a size less than 15 cm (about 6 inches) in length, width or height. MAVs should be thought of as aerial robots, as six degree of freedom machines whose mobility can deploy a useful micro payload to a remote or otherwise hazardous location where it may

perform any of a variety of missions including reconnaissance and surveillance, targeting, tagging and bio-chemical sensing. Although the 15 cm limitation may appear somewhat arbitrary, it derives from both physics and technology considerations.

Following types of MAVs are considered:

1. Fixed wing

2. Rotary wing

3. Flapping wing

a) Ornithopters (bird-like flapping)

b) Entomopters (insect-like flapping)

Each type has different advantages and disadvantages, different scenarios may call for different types of MAV. Fixed-wing MAVs can currently achieve higher efficiency and longer flight times, so are well suited to tasks that require extended loitering times, but are generally unable to enter buildings, as they cannot hover or make the tight turns required. Rotary-wings allow hovering and movement in any direction, at the cost of shorter flight time. Flapping wings offer the most potential for miniaturization and maneuverability, but are currently far inferior to fixed and rotary wing MAVs.

The range of Reynolds number at which they fly is similar to that of an insect or bird. Thus some researchers think that understanding bird flight or insect flight will be useful in designing MAVs. A new trend in the MAV community is to take inspiration from flying insects or birds to achieve unprecedented flight capabilities. Biological systems are not only interesting for their smart way of relying on unsteady aerodynamics using flapping wings, they are more and more inspiring engineers for other aspects such as distributed sensing and acting, sensor fusion and information processing.

An Ornithopter is an aircraft that uses flapping wing motion to fly. This type of flight offers potential advantages over fixed-wing flight, such as maneuverability, at slow speeds (1-40m/s). Natural Ornithopter range in size from small flying insects to large birds and flap their wings from about 5 to 200Hz. The DARPA largely motivates Micro Aerial/Air Vehicle development in military application for reconnaissance missions in confined spaces or under dangerous circumstances. The discreetness of a flapping wing MAV adds appeal for these types of covert operations. Employment in civilian search and rescue missions under dangerous or questionable circumstances such as fire or earthquake also fuels MAV development. Inspiration to mimic insect flight, which combines oscillating and rotating wings, is detailed in and points to the adeptness that can be obtained through this type of flight. Another important insight from is the focus on simple control loops in place of the complex control loops prevalent in modern aircraft. This focus spawns from the combination of limited on-board processing power with the need for many sensors and high-frequency update rates.

1.1. HISTORY OF ORNITHOPTER

History of Ornithopter [2] begins in the year 1490 with the Leonardo de Vinci's human powered design, though it is not capable of flying but showed a great deal of thought that feathers are not required for successful flapping-wing flight. The first flights of mechanical flapping wing aircraft in 1874 were performed by Alphonse Penaud [2] and this work took place in France which established a template for subsequent prototype of Ornithopters built by hobbyists and manufactured as toys. The first human powered Ornithopter had performed power glides after being towed into the air in the year 1929 by good amount of research carried out in Germany by Alexander Lippisch [2]. Research work of Jeremy Harris and James DeLaurier [3] in the University of Toronto lead a technological foundation for developing a full-scale engine powered piloted aircraft. Aircraft has

self-accelerated (flapping alone) on level pavements to lift-off speed in 1999 as shown in figure 1.

Figure 1: Harris/DeLaurier Model of Engine-Powered Piloted Ornithopter [3]

1.2. FLAPPING WING MAV

In just over 100 years from the first piloted flight of a powered aircraft in 1903, the field of aeronautics has produced an astonishing set of advancements. A great number of these advancements have been driven by the desire for aircraft with unique capabilities, or high performance for military applications. The most advanced military organizations in the world today have been using unmanned aerial vehicles (UAVs) for decades to provide reconnaissance, and are rapidly approaching the use of UAVs for combat missions. The popularity and increasing dependence on UAVs can be attributed to their great operational success, which has provided surveillance data of equal or higher quality to previous methods, while reducing the need to put humans in high risk situations. Wealth of civilian organizations is beginning to embrace the UAV as a tool for applications such as law enforcement, search and rescue, border patrol, and agriculture [4].

The Mini/Micro Aerial Vehicles (MAV) are classified based on the size. The Mini aerial vehicle size is typically varies from 1 feet to 8 feet and that of micro aerial vehicle will be less than 1 feet. Current Research aims at developing a Mini/Micro sized Ornithopters for military surveillance missions and spy missions unseen by airfield observers. Technological progress in the areas include aerodynamics, microelectronics, sensors, Micro Electro Mechanical Systems (MEMS), micro machining and more is ushering in the possibility for the affordable development for this new class of Micro Aerial Vehicles. Recent advances in miniaturization may make these vehicles possible that can carry out certain missions heretofore were beyond our reach or could only be achieved with at risk and expenditure. These missions would be possible if MAVs fulfill certain characteristic attributes like low cost, low weight, mission versatility, range, endurance, stealth and precision. Micro Aerial Vehicles represent a pioneer advancement to achieve these advantages.

Georgia Tech is pursuing a flapping wing design "micro-flyer" [5]. This micro-air vehicle employs a reciprocating chemical muscle shown in figure 1.5 is driven by catalyzed chemical reaction which uses a monopropellant fuel to generate up and down or back and forth motion such as beating of wings or scurrying the feet. This reciprocating muscle also generates electricity which can be used to power sensors and other onboard systems. Research is heading for micro-flyer to gather fuel from environment to continue their operations.

Figure 2: Reciprocating Chemical Muscle [5]

Berkeley Micro Mechanical Flying Insect project [6] aims to build a tiny Ornithopter for fly on wall reconnaissance purpose. This project aims to design a 25mm (wing-tip to wing-tip) capable of sustained autonomous flight based on biomimetic principles to capture some of the exceptional flight performance achieved by true flies. This project took ambitious approach of starting small rather than scaling down a working prototype. This Entomopters uses piezoelectric actuators that can match the power output of insect muscle shown in the figure 3.

Figure 3: Micro Mechanical Flying Insect [6]

Mentor [7] shown in figure 4 is a project of SRI International and University of Toronto aims at developing first radio controlled hovering Ornithopter. Mentor came into being in response to a vision of "fly on wall spy" at US Defense Advanced Research Agency. James DeLaurier professor at University of Toronto choose the humming bird model for its ability to "hover" as well as its "smooth, elegant style of switching from hovering to horizontal flight" though the transition is very shaky with battery powered motors. This and host of other sophisticated features allow Mentor to remain airborne for as many as 10 minutes which is a record for small scale Ornithopters.

Figure 4: Mentor Hovering Ornithopter [6]

1.3. POSSIBLE ROLES FOR MICRO AIR VEHICLES

1.3.1. Military Applications

- Over the hill reconnaissance and surveillance
- Communication relays
- Observation through windows, building interiors
- Bio chemical sensing, map, size and shape of hazardous cloud
- Search and rescue operation of ejected pilot
- Targeting and battle damage assessment
- Bomb damage indication

1.3.2. Civil Applications

- Traffic monitoring
- Border surveillance
- Sea rescue operation
- Forestry
- Wild life survey

- Power line inspection
- Real estate aerial photography
- Crowd control
- Snap inspection of pollution
- Road accident documentation
- Urban traffic management
- Search for survivors
- Pipeline inspection
- High risk indoor inspection

1.4. TECHNICAL CHALLENGES OF MICRO AERIAL VEHICLES

Micro Air Vehicle (MAV) is defined as a small flying vehicle which is designed for performing useful work. Its construction should enable a single person to operate it together with a complete Ground Control Station (GCS). Moreover, Micro Air Vehicle (MAV) should be safe and even collision with a human does not have any harmful consequences. In most cases, Micro Air Vehicles (MAVs) are envisaged to provide direct reconnaissance in various environments. These environments impose various requirements on the vehicle and hence there are different concepts of MAVs design exhibiting different characteristics allowing them to match these requirements. However, all these concepts pose certain problems which have to be solved before MAVs can be utilized.

Basic problems faced by micro air vehicles are as following:

1.4.1. The Physical Integration

The physical integration challenge is the most difficult problem, the degree of which increases dramatically with decreasing vehicle size or increasing functional complexity. Most of the system functions will be provided by the microelectronics or MEMS based components.

1.4.2. Flight Control

Flight control is the area which has the largest number of unknowns for MAV design. Steady aerodynamics is difficult and unsteady aerodynamics is more difficult because of inertias being non-existent. Platform stabilization and guidance will require rapid, highly autonomous control system.

1.4.3. Low Reynolds Number

Fully 3D aerodynamics is required, 2D low Reynolds number data is less and 3D it is still less. MAVs will experience highly unsteady flow due to natural gustiness. Still lesser data for Flapping wings, Natural flyers, unsteady aerodynamics being the major problem. Low Reynolds number effects will have to be mastered using highly integrated flight control system with autonomous stabilization.

1.4.4. Acoustically Quiet MAV Systems

Small-scale propulsion systems will have to satisfy extraordinary requirements for high energy density and high power density. Acoustically quiet systems have to be developed to assure covertness.

1.4.5. Power and Propulsive System

Poor L/D ratios & low propulsive efficiency result due to low Reynolds number. Battery power or exotic technologies like fuel cells may be required.

1.4.6. Navigation

Mission constraints will not permit real time human interaction to provide vehicle stabilization and guidance, also necessary vehicle agility or gust response

may well surpass a human operator's ability. Significant advances in miniature navigation, guidance & control are necessary.

1.4.7. Communication

Due to small vehicle size, small antennae size, limits power availability and support the bandwidth requirement (2-4 megabits/sec) for image transmission, Control function demands lower bandwidth in the 100 Kbits range. Image compression helps reduce the bandwidth but increases onboard processing and hence power requirements. Omni directional signal will be weak hence directional ground antennae is required to track the vehicle using line of sight transmission. Line of sight is not suitable for urban operations, so other approaches like cellular communications architecture may be required.

1.4.8. Payloads

Micro sensor technologies, optical, IR, chemical, nuclear and other sensors are likely payloads. On-board camera is also considered as payload.

1.4.9. Wireless Power Transmission

One possible means of reducing weight is to beam microwave energy to the vehicle, which is then converted to a digital signal that drives the motor, an approach called Wireless Power Transmission (WPT). Since WPT eliminates the need for batteries on-board, the potential volume and weight savings are significant. Current Research and Development effort for the US Navy's defense involves using existing surface search radar to power the vehicle.

1.4.10. Miniaturization

Development of miniaturization yet capable electronic auto-pilot modules is an important area of MAV research. MAVs are the size and shape of small, radio control hobby aircrafts. However, with the miniaturization of avionics and sensors they are becoming valuable armored battlement assets. Researcher is combining war fighting requirement and the latest avionics technology to develop auto-pilots that enable effective MAV systems.

1.4.11. VTOL, Hover and Stare Capabilities

To employ MAV in a variety of armored war fighting environments like hilly terrain, desert, urban areas, confined spaces, interiors of complex structures, hidden troops concentration centers, armored assets storages et cetera, it must have vertical take-off and landing (VTOL), hovering, staring (real time 3-D remote monitoring) capabilities. Initial MAV Research and Development programs in late nineties were primarily focused on flight control, navigation and communication.

1.4.12. Gust Response

One common trend in aircrafts and in nature is that smaller flyers travel slower and tend to have higher ratio of wing area to vehicle weight. So MAVs have to copy with fully three-dimensional aerodynamics. Here, there are even less low Reynolds number data available than there are for two-dimensional airfoils. Apart from this MAVs experience highly unsteady flows due to the natural gustiness (turbulence) of the atmosphere. Interestingly, nature's flyers of the same scale use another source of unsteady aerodynamics, flapping wings, to create both lift and propulsive thrust. For some applications, MAVs may ultimately have to do the same.

1.4.13. Low Weight Challenge

In reference to the power equation, there is nothing more effective than low weight to reduce power required. Technically like MEMs, low power electricity and component multi-functionality can contribute towards achieving high energy density (i.e. light weight). Battery-based system will likely power the first generation MAVs but more exotic technologies like fuel cells and 'off-board systems' are being developed for follow on systems.

1.5. CURRENT RESEARCH

Scientists study insect flight for a variety of reasons, biological development and understanding of the animals, a purely scientific interest in unsteady aerodynamics, or the engineering interest to develop Micro Air Vehicles (MAVs) or similar devices. Based on the size of the MAV, different flight methods make more sense. Currently, most MAVs are larger than insects and fly at Reynolds numbers closer to bird flight. For this reason, they generally are rotorcraft or use fixed-wings and propellers. For a smaller MAV flying at a smaller Reynolds number, the flight mechanics of insects become attractive. Additionally, MAVs that are the size of insects can accomplish a number of tasks that larger vehicles cannot.

In 1993 the RAND Corporation determined that the development of insect-size flying and crawling systems were possible and could give the United States a significant military advantage. In 1996, DARPA funded research into MAVs through the Small Business Innovation Research program. At this time, it was concluded that a six-inch (152 mm) MAV was feasible and capable of performing extremely useful missions. A successful MAV could be used for search and rescue, military or law enforcement surveillance, chemical, biological agent detection and for more unsavory purposes such as assassinations and other targeted killings. The primary use, however, would be reconnaissance in confined spaces.

The potential benefits of MAVs are extremely promising. Possible uses include detection of poisons and drugs or search and rescue in burning buildings or after natural disasters. Some things that an MAV could do are obviously destructive. Small explosives or chemical and biological agents could be delivered to a precise location for assassination attempts or any number of missions that would be dangerous for a soldier. The existence of MAVs means that humans do not need to risk their lives in some situations. At the same time, these missions directly result in the deaths or casualties of enemies. Other military applications are reconnaissance and surveillance. With the changing nature of warfare, precise urban tactics require reliable intelligence to minimize civilian casualties and property damage. In this sense, more and better information also may save lives.

MAVs must be designed to be safe and simple to operate, preferably by an individual soldier. The launch system must accommodate possible severe initial conditions, such as being launched at speed or at an extreme angle. Electronic connectivity must be rapid and secure. And control interfaces must involve minimal concentration, freeing the operator to perform other duties. The MAV must have a simple logistic tail. It must either be expendable or it must be easy to repair under field conditions. It must easily integrate into the combatant's field pack, and must be well-protected from hazards, including shock, until it is operated. Finally, the MAV must be affordable. Affordability is, to some extent, dictated by the complexity and importance of the mission. But MAVs will not be fielded in large numbers if their cost is prohibitive. For many of the routine missions being considered, an expendable MAV must cost no more than an anti-tank round. Despite the significant challenges facing the MAV developer, all indications are that these systems can be developed with today's emerging electronic and related technologies. Recognize that this statement permits an evolution of capability over time that will begin with the simplest of systems and missions. While small scale poses enormous technical

challenges, it offers major advantages, not just in terms of enabling new missions but in terms of potentially short fabrication and testing time scales.

1.6. PROBLEM IDENTIFICATION

The term Micro Air Vehicles (MAVs) is used for a new type of remotely controlled, semi-autonomous or autonomous aircraft that is significantly smaller than conventional aircrafts. The key advantage of Flapping Wing Micro Air Vehicle (FMAV), called Ornithopter, is its superior maneuverability at very low speeds and low noise levels. Hovering capability can, however, add more versatility. To apply Micro Electro Mechanical Systems (MEMS) inertial sensors for the Guidance, Navigation and Control (GNC) of Micro Air Vehicle (MAV) is an extremely challenging area. INS/GPS based navigation for flapping micro air vehicle is proposed. The major components of the navigation system of micro air vehicles are the onboard sensors. This thesis presents an approach for the implementation of on board sensors for Micro Air Vehicles and the application of a Seven State Discrete Time Extended Kalman Filter.. This research work presents an approach of applying an Inertial Navigation System (INS) using MEMS inertial sensors and Global Positioning System (GPS) receiver with a Single Seven State Discrete Time Extended Kalman Filter. Inertial navigation system (INS) includes MEMS gyro, accelerometer, magnetometer and barometer. MEMS inertial sensors are of utmost importance in the GNC system. The system considered is non-linear and it is first linearized for application of the Kalman Filter. A Single Seven State Discrete Time Extended Kalman Filter is used for state estimation. Process covariance matrix and measurement covariance matrix are derived.

So designing an INS/GPS based navigation system for Ornithopter/Flapping Micro Air Vehicle with the help of Extended Kalman Filter is addressed in this research work and comparison of the following three Discrete Time Extended Kalman Filtering Schemes is done:

1. Single seven State Discrete Time Extended Kalman Filter
2. 2 stage Cascaded Discrete Time Extended Kalman Filter
3. 3 Stage Cascaded Discrete Time Extended Kalman Filter

1.7. ORGANIZATION OF THE REPORT

This chapter deals with an introduction to Ornithopter and historical development and current research in the development of Ornithopter MAVs. It also deals with introduction to bird's flight.

Chapter 2 describes the detail of successful prototypes of Micro Air Vehicles.

Chapter 3 deals with the system requirement including the technical requirements of the system. It includes the description of the on-board sensors of Micro Air Vehicle for navigation purpose. It explains the guidance and navigation loops as well.

Chapter 4 explains the mathematical working of the system which includes the basic assumption as well. It explains the implementation of extended Kalman Filter on the system as well.

Chapter 5 explains the results obtained from implementation of Extended Kalman Filter and deals with the discussion of results obtained and conclusion.

Chapter 2

2. LITERATURE SURVEY

Several GPS-INS integration techniques have been implemented. Some of them are described here briefly. Schmidt [8] describes in detail the computations for a gimbaled INS and the strap down INS. The 9 state Kalman Filter which is discussed by him uses a barometric altimeter to correct for the height. Bar-Itzhack et al [9] describes a control theoretical approach to INS/GPS integration using Kalman Filtering in his paper. The psi-angle error model explained has been used extensively in many models of the INS/GPS Kalman Filter and also has been used in this project. Grewal et al [10, 11] have discussed in their books the working of the INS, GPS and Kalman Filtering in detail and have given a complicated model of a possible Kalman Filter with 54 states.

Wolf et al [12] use Systron Donner's MotionPak inertial measurement unit (IMU) and a Trimble Advanced Navigation Sensor (TANS) Vector receiver system (as the GPS component), which is a multi-antenna, attitude determination and position location system. They have developed real-time navigation software to calculate position, velocity and attitude from the outputs of the MotionPak gyroscopes and accelerometers. Besides giving position and velocity updates, TANS also gives attitude measurement data. A Kalman Filter with 27 states has been implemented by them. A Packard Bell 486 computer was used to carry out the computations.

Grejner-Brzezinska et al [13] have tested the feasibility of attitude estimation improvement by using high accuracy deection of vertical (DOV) information in the integrated GPS/INS navigation system. The estimability of attitude components improves by adding partially compensated gravity information. A fully digital Airborne. Integrated Mapping System (AIMS) has been designed and the integrated INS/GPS forms an integral part of this AIMS. A dual frequency differential GPS

(DGPS) and the Litton LN100 IMU are tightly integrated. IMU data was updated at 256Hz. A centralized 21 state Kalman Filter was used to process the GPS L1/L2 signals as well as the errors from the INS. Accuracy of order of 10cm was achieved.

Srikumar and Deori [14] have used an airdata based dead reckoning system to calculate position of their MAV. Navigation accuracy has been improved by using updates from a GPS receiver as well as a ground-based tracking system. A Pentium 90MHz personal computer has been used to control navigation and many other features of the aircraft. Randle and Horton [15] describe in their works the integration of GPS/INS using a low cost IMU consisting of micro-machined sensors and on-board calibration. Simulations have been done for both flight and automotive navigation. With complete loss of GPS signals, position accuracy is shown to be less than 10m after 30s. Kalman Filter has 23 states and a DGPS was simulated to give measurement updates.

Navigation for reusable launch vehicles has been studied by Gaylor et al [16]. A number of navigation sensors have been studied and the GPS/INS integrated system was settled for. Error models of INS and GPS operating in the vicinity of the International Space Station have been developed. Effects of signal blockage and multipath errors of the GPS have been modeled. An extended Kalman Filter with 18 states was developed.

Brown and Sullivan [17] have described test results for a system that uses an improved kinematic alignment algorithm suite providing high quality navigation solution using direct carrier-phase and pseudo-range GPS measurements, tightly coupled with measurements from a low cost IMU system. A 32 state Kalman Filter has been implemented using InterNav software made by Navsys Corporation.

Moon et al [18] first process the GPS values before sending it to their 9 state Kalman Filter. Honeywell's HG1700 IMU has been used along with a Motorola UT Oncore GPS, which can track 8 GPS satellites simultaneously. Salychev et al [19] use

MotionPak IMU and integrate it with GPS (GPS - GLONASS) and DGPS information, to provide navigation capability to bridge GPS outages for tens of seconds.

Airborne and ground tests have been conducted and robustness of the system has been studied. IMU data was recorded at 46Hz. A 21 state Filter using tightly coupled integration scheme was implemented by Wang et al [20] and two digital signal processors were used to carry out the computations. A sensitivity performance has been analyzed in their research thesis. Kwon [21] has studied airborne gravimetry and compared it to ground measurement of gravity. The combination of GPS/INS is known to show very good performances for recovering the gravity signal. A new algorithm using acceleration updates instead of conventional position or velocity updates has been developed. It is computationally proven to be less expensive since navigation equations need not be integrated. Real flight data has been tested upon the system designed by Kwon and the simulations have been discussed in his works in detail. A comparative study of the Kalman Filter using traditional approach and the new approach has been done.

Ronnback [22] has tested his INS/GPS navigation Filter written in C++ on an air vehicle. A redundant 4 axes IMU called Tetrad has been used. A 9 state Kalman Filter was implemented with measurements of position and velocity from the GPS. Gautier [23] has designed GPS INS generalized evaluation tool (GIGET) which aids in the selection of sensor combinations for any general application or set of requirements. It includes a unique have antenna, forty channel GPS receiver providing attitude, position and timing. Honeywell's HG1700 tactical grade IMU is integrated with this GPS using a 21 state extended Kalman Filter and tested on their homemade Dragonfly Unmanned Air Vehicle.

In his work, Mayhew [24] proposes several methods for improving the position estimation capabilities of a system by incorporating other sensor and data technologies, including Kalman Filtered inertial navigational systems, rule-based

and fuzzy-based sensor fusion techniques, and a unique map-matching algorithm. Ground testing of the system has been done. Dead reckoning sensors are used to collect odometry data. A Pentium 133MHz computer was used to carry out all the computations and control handling of the aircraft. The 9 state Kalman Filter was run every time a measurement update from the INS took place.

Moore and Qi [25] have implemented a direct Kalman _Filtering technique to integrate their GPS and INS systems, where they use two stage GPS Filtering to preprocess the GPS data before the Kalman Filter can use it. Their eight state direct Kalman Filter uses the position and velocity as its state vector. Shang et al [26] use two GPS receivers to not only estimate the position but also the azimuth alignment. They use a PC/104 microcomputer to carry out their computations. They have carried out a tightly coupled implementation of the Kalman Filter.

Cao et al [27] have implemented a 15 state Kalman Filter successfully using MEMS based sensors for intelligent transport systems. They have used a strap down INS system. Panzieri et al [28] have implemented a 5 state extended Kalman Filter to maneuver a robot's movements. They use a GPS because the usage of the robot is outdoors.

Dorobantu and Zebhauser [29] have implemented an extended Kalman Filter of have states for a 2-D case as they are using it on a land vehicle. They use a DGPS to get measurement updates every 1s and have discussed results when there are regular GPS outages.

Chapter 3

3. SUCCESSFUL MAV PROTOTYPES

3.1. AEROVIRONMENT BLACK WIDOW

In 1999, AeroVironment won DARPA's Award for Outstanding Performance by a Small Business Innovation Research Contractor and the Shepherds Press Unmanned Vehicles Magazine Readership Design Award for the Black Widow MAV. The Black Widow is a conventional propeller driven MAV. It flies using a hotwired foam rectangular wing with tapered corners, as shown in Figure. The propeller is directly driven. The electrical propulsion system is powered by Lithium batteries. The MAV has a 6in wingspan and configuration-dependant weight of around 80g. [30]

Figure 5: AeroVironment Black Widow [31]

The Black Widow has demonstrated an endurance of 30-minutes, maximum range of 1.8km, and maximum altitude of 769 feet. The MAV flies at 30 mph. The

custom designed and built electronics, include a 3g color camera, 2g video transmitter, 5g fully proportional radio control receiver, 0.5g actuators, and an autopilot. The autopilot includes single-axis magnetometer, piezoelectric gyro, and pitot-static pressure sensors. With these components and a central processor, the autopilot is currently capable of maintaining airspeed, altitude, or heading. The autopilot also features active yaw damping. Similar to all MAVs, in flight, the Black Widow is extremely difficult to observe and must be flown via down-linked video imagery and sensor data when operated more than a short distance from the pilot.

3.2. AEROVIRONMENT WASP

In August of 2002 the Wasp recorded the longest flight of a MAV at 107 minutes. The Wasp, shown in Figure 15, was developed as part of DARPA's Synthetic Multifunction Materials Program by Telcordia Technologies and NRL and built by AeroVironment. The project's intent was to improve overall efficiency and performance by combining the function of structure with other critical aircraft functions. The Wasp combined the function of power-supply and wing-structure. The multifunctional structure/battery supplies electrical energy for the motor and avionics and doubles as a mechanical structure for transferring aerodynamic forces on the main wing. In essence, the 4.25 ounce Wasp plastic lithium-ion battery (6 ounce vehicle weight) was designed, shaped, and fabricated to be the main lifting wing. The 13 inch wingspan flying wing configuration is equipped with off-the-shelf avionics including a 3-channel receiver controlling throttle, rudder, and elevator. The Wasp did not carry a camera, autopilot, or flight augmentation system. [32]

3.3. AEROVIRONMENT HORNET

In conjunction with Lynntech Incorporated, Aerovironment completed the first documented flight of a MAV powered entirely by a hydrogen fuel cell as part of DARPA's Synthetic Multifunction Materials Program in March of 2003. The hydrogen generator and fuel cell was developed and tested by Lynntech. The fuel cell was fabricated using a stiff metal mesh that doubles as the wing's mechanical structure. No batteries were carried onboard; the motor and all avionics were powered by the fuel cell. The 6 ounce MAV was a flying-wing configuration with a 15 inch wingspan. A three-channel receiver controlled the rudder, elevator, and rate of hydrogen generation. The Hornet was developed to show the potential of fuel cells for powering high endurance MAVs. Although the fuel cell's endurance was designed to be 45 minutes, the Hornet accomplished three flights for a total endurance of 15 minutes, due to moisture problems in the fuel cell. The Hornet did not carry a camera, autopilot, or flight augmentation system. [32]

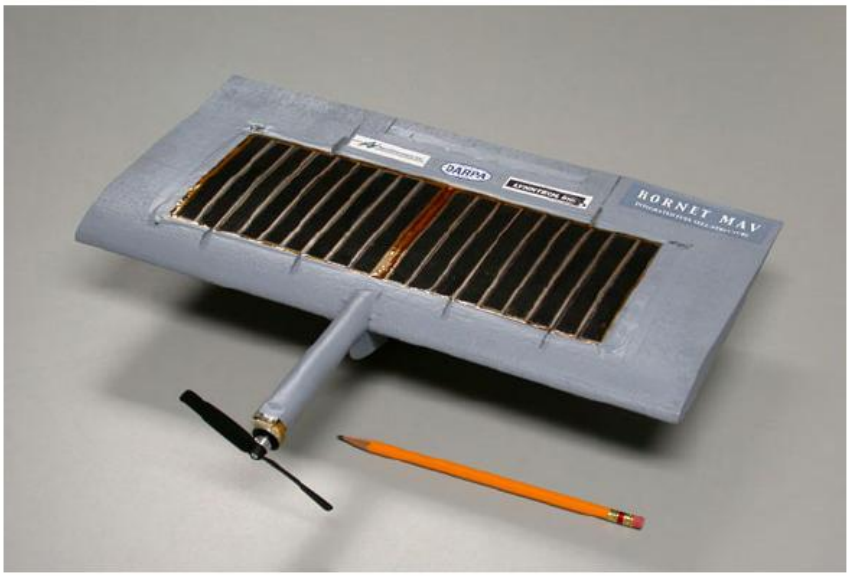

3.4. AEROVIRONMENT MICROBAT

The Microbat is a flapping MAV designed in conjunction by CalTech, UCLA, and AeroVironment for DARPA. The motor flaps the left and right wings in a near sinusoidal motion with a minimal phase difference. The Microbat was tested using flap amplitudes from 40 to 60 degrees (comparable to flap amplitudes used by small birds.) Although intended to be tailless, the complex flight control system necessary to differentially control both Microbat wings for three-axis control was abandoned for a simpler tailed design. Turning, speed, and climb rate were controlled by rudder, elevators, and throttle respectively. The Black Widow inspired 3-channel receiver comprised only 0.9g of the vehicle's 14g total mass. The Microbat used electrically stimulated muscle wires for deflecting its control surfaces. Originally, a 50mAh NiCd single cell battery weighing 3.5g powered the coreless DC brush (vibrating pager and mobile-phone) motor. In flight tests, the NiCd cell powered the Microbat for a 42 second flight in 2000. After numerous modifications, including the replacement of the NiCd cell for two small rechargeable lithium batteries, AeroVironment has achieved 25 minutes in flight. [33]

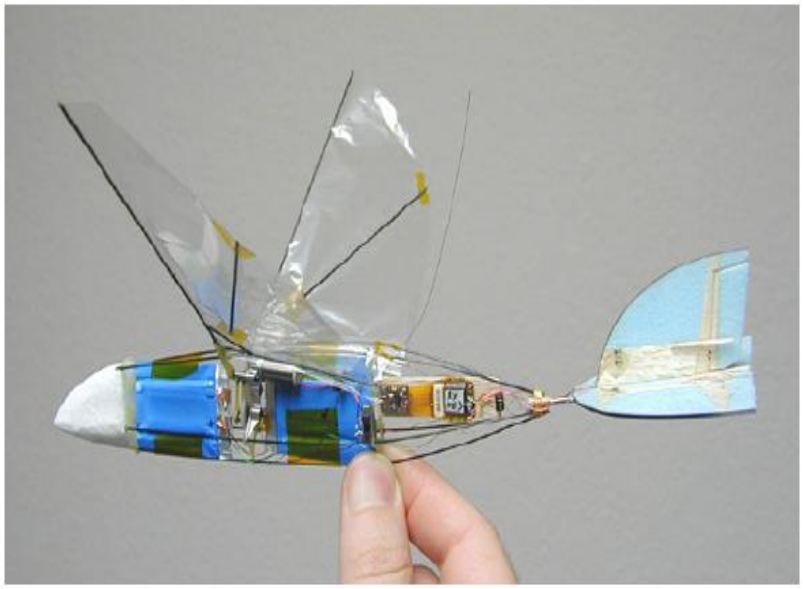

3.5. IAI MOSQUITO

The Mosquito flew its first flight in January of 2003. The 40 minute flight was flown by the original 250g, 12 inch wingspan design. Little performance or avionics data has been released by IAI. IAI has published the Mosquito's ability to stream live video from and onboard camera. IAI is currently developing the Mosquito 1.5 in hopes to achieve 60 minutes of flight endurance. The Mosquito 1.5's advances include two gimbals and electronic image stabilization software for enhanced video quality. IAI is also developing custom avionics for fully autonomous mission capability. [34]

Figure 9 (a): Mosquito 1.0 **(b): Mosquito 1.5 (right) [34]**

3.6. LOCKHEED MARTIN MICROSTAR

Lockheed's initial teardrop bodied cropped delta wing design had a single vertical stabilizer. The final platform swapped the vertical stabilizer for winglets and added a propeller in a tractor configuration vice the original pusher configuration. Test platforms were constructed with 6.0, 9.0, 15.0, and 24.0 inch wingspans. Maxtek Components fabricated the 5.0g navigation system including processor and data MCMs. The autopilot accepted directional commands from the ground station and was capable of maintaining heading or orbiting a target.

MicroSTAR flight testing demonstrated altitudes up to 200ft, 30mph max velocity, and an endurance of 20 minutes. The MicroSTAR project never entered mass-production; however, Lockheed continues to develop the autopilot system for use on its larger UAVs. [35,36]

Figure 10: Lockheed Martin MicroSTAR [37]

3.7. MLB FIXED WING ELECTRIC

This aircraft completed a one minute flight using a 0.18 watt-hour nickel-cadmium battery pack and two electric motors in a tractor configuration. The 9in wingspan model's configuration was achieved through trial and error. Twin engines kept disc loading low because the motors operated at high RPM for propeller efficiency. The airframe used a one-channel commercially available receiver for rudder deflection. Flight testing resulted in a maximum altitude of 40 feet and a cruise velocity of 27 fps. The limited performance capabilities of the aircraft made it unstable in moderate winds or turbulence. This design, along with the Flyswatter and Helirocket, were the first of many MAV designs tested by MLB starting in 1997. [38]

3.8. MLB FLYSWATTER

This 8.5 inch wingspan model was powered by a Cox 0.010 cubic inch internal combustion engine. The aircraft configuration included a cambered rectangular wing and winglets, as shown. [38]

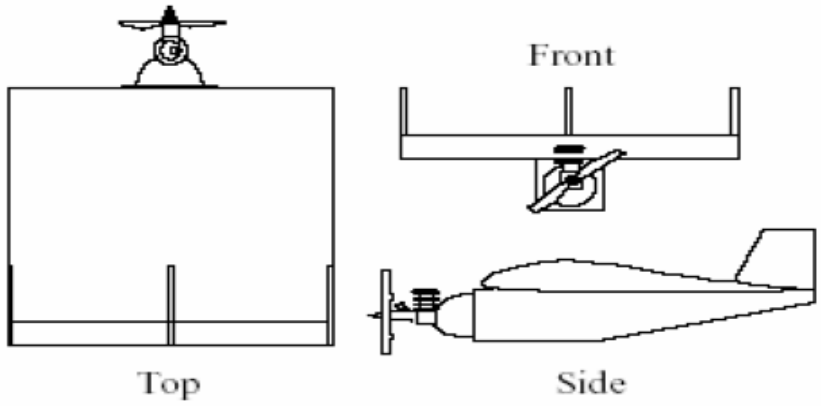

Figure 11: MLB Flyswatter

The Flyswatter was controlled by a two channel commercially available receiver. Flight testing at full throttle resulted in a two-minute endurance, 20 foot turning radius, altitudes greater than 50 feet, and 30fps velocity. The aircraft's configuration was based around a low aspect ratio lifting wing. The development of the tip vortex played a large role in sustaining lift at high angles of attack. The increased lift improved the aircraft's performance in turns and at low speeds. In addition, the Flyswatter flight tests showed that lower aspect ratios and higher wing loadings decreased gust sensitivity. Flyswatter was stable in winds up to 15mph whereas their previous fixed-wing model could not sustain flight in winds over 5mph. As with most MAVs, rudder control provided sufficient roll authority.

3.9. MLB HELIROCKET

Powered by the Cox 0.049 cubic inch internal combustion engine, the MLB Helirocket turned a 7 inch propeller and controlled flight using four control vanes, as shown in Figure 21. Using a 0.4 ounce fuel tank, the Helirocket sustained stable flight for 2.5 minutes. The VTOL aircraft has been flown with payloads up to 1.5 ounces. The Helirocket has demonstrated stability in translational flight in light winds.[38]

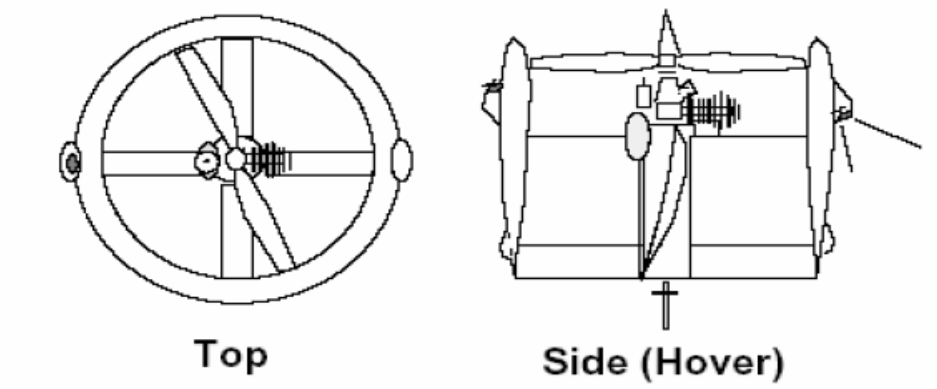

Figure 12: MLB Helirocket [39]

3.10. LB TROCHOID

MLB Company's most recent and successful MAV, the Trochoid, had a wingspan of less than 8 inches. The configuration was a near delta wing with fixed twin vertical stabilizers. Unlike most MAVs, the Trochoid used ailerons for roll control as opposed to relying on the strong yaw-roll coupling of rudders. Flight tests have demonstrated flight speeds from 10 to 60mph and a 15ft turn radius. Trochoid was able to sustain stable flight in winds up to 20mph.

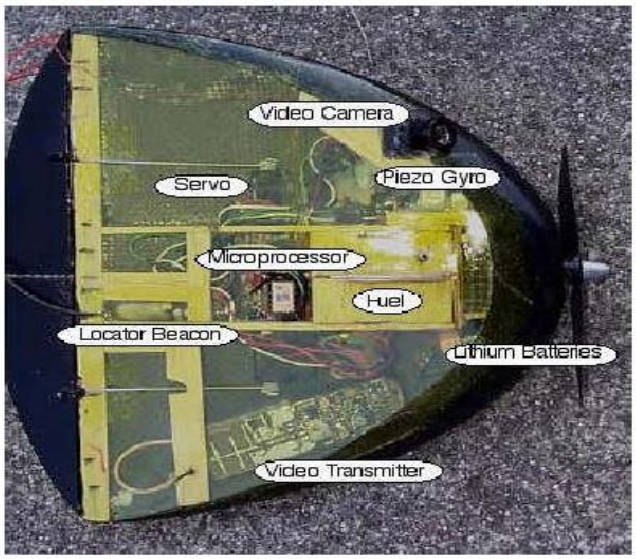

Figure 13: MLB Trochoid [40]

The Trochoid MAV, shown in Figure 22, was equipped with a camera and video transmitter. The gas powered MAV used a small lithium battery for payload and auxiliary power. An active stability augmentation system included a microprocessor and gyros and was capable of yaw damping. No other capabilities of the augmentation system have been specified. A locator beacon was also integrated among the MAVs internal components. [39]

3.11. PS FLAPPING-WING MAV

The NPS flapping-wing MAV has a large lifting wing forward and two counter-plunging flapping wings trailing behind the main wing. This design is superior to many configurations because the flapping wings are mechanically balanced. It is also believed that the symmetry of the twin wings may mimic ground effect. Testing of the flapping wing model in a smoke-tunnel shows that the phenomenon of flow entrainment keeps the flow close to the main wings. This effect makes the aircraft very resistant to the unstable and unpredictable effects of separated flow. 10.5g and 13.4g models have been successfully flown. A 2-channel receiver controls rudder deflection and throttle setting. Both altitude and velocity are controlled using throttle position. The MAV must be trimmed for level-flight velocity before launch. Roll-yaw coupling and rudder are used for turning. The MAV is best suited for low speeds slightly above walking speed, roughly between 4 and 10 mph. The MAV has demonstrated rapid stall recovery. Under power the model generally recovers from stall in less than one chord length. Test flights have been flown for 12 minutes with battery to spare. The MAV should be able to fly for 15-20 minutes. The standard NPS flapping wing MAV does not carry a payload. [40, 41]

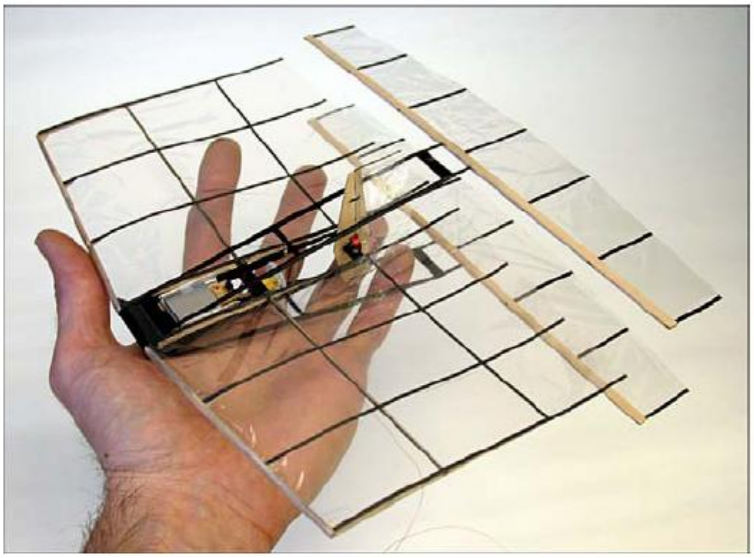

Figure 14: NFS Flapping wing MAV [42]

3.12. NRL MITE

The MITE is a dual propeller fixed wing MAV. The design has a fixed chord of nine inches. MITE variants have been flown with wingspans of 8.0, 14.5, 12.0, and 18.5 inches. The 14.5 inch wingspan MITE2 can carry a one ounce payload. In flight tests the MITE2 has demonstrated 20 minute endurance at speeds from 10 to 20mph. The MITE2 carries an analog camera and is remotely piloted only, although autopilot systems are being developed. The MITE3 wingspan was reduced to 12.0 inches after swapping to lithium batteries and more advanced avionics. The latest variant, MITE4 shown in Figure is a 18.5 inch wingspan configuration with more powerful coreless motors for testing developmental payloads up to 4.0 ounces. Performance numbers are not readily available because each variant has multiple configurations using different battery packs, motor gearing ratios, and propellers. Many MAVs experience unpredictable rolling, especially at low velocities such as during launch due to torque in the body from the motor. The MITE's counter-rotating propeller design avoids the torque problem that many MAVs can experience. The propeller wash also has a net upward component at the leading edge of the wing because of the rotation directions of the propellers. The upward velocity causes an increase in effective angle of attack. The increased effective angle of attack can be used to gain aerodynamic benefits. [42]

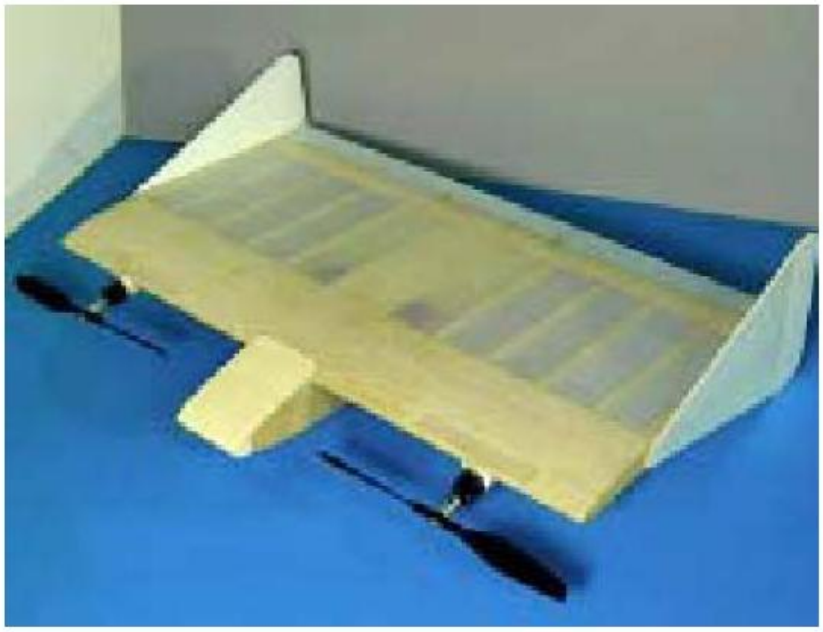

Figure 15: NRL MITE4 [42]

Chapter 4

4. SYSTEM REQUIREMENTS

Micro air vehicles (MAVs) belong to a class, whose dimensions are comparable to those of bees and insects. These significantly small vehicles are not scaled down versions of larger unmanned air vehicles (UAVs). These are fully functional small flight vehicles in a class of their own. The definition employed in Defense Advanced Research Projects Agency's (DARPA's) program limits these craft to a size less than 15 cm in length, width or height [1]. The implications of this physical size can be seen in the technology requirements for the development of these vehicles.

4.1. TECHNICAL REQUIREMENTS

Technological feasibility follows from advances in several micro technologies. The desire to downsize components to micro levels has led to many innovative developments in the field of electronics, propulsion, controls and structures. An interesting synergistic development is the micro electro-mechanical systems known as MEMS. These combine microelectronics components with comparably sized mechanical elements of varying complexities to achieve useful, and often unique functionality (e.g. integrated systems of sensors, actuators and processors). Another interesting developmental field is that of sensors. Microsystems, such as tiny CCD-array cameras, equally small infrared sensors and chip-sized hazardous substance detectors are in the pipeline [1]. Small size of an MAV results in severely constrained weight and volume. This has resulted in a situation where the aerodynamics of the vehicle are completely different from that used in the existing flight vehicles. Scientists are looking at nature for aerodynamic solutions from the flight of small birds, bees and insects. Conventional designs will not work for MAVs. Innovative technical solutions are being sought for aerodynamics and control, propulsion and power, navigation, and communication.

4.1.1. Aerodynamics

The flight regime of MAVs results in a fundamental shift in aerodynamics. Prominently, it is an environment more common to the smallest birds and the largest insects. Basic understanding of the aerodynamics encountered here is at present very limited. The flight behavior of these exotic creatures of nature cannot be predicted with the familiar high Reynolds number aerodynamics commonly used in UAV design [43]. Low Reynolds number aerodynamics 'of MAVs may result in unusual configurations, such as low aspect ratio fixed wings to rotary wings, and even more radical concepts like flapping wings. A plot of optimum aspect ratio requirement for MAV flight duration is shown in Figure below. Aspect ratio imposes a severe limitation on the performance of MAVs [44].

4.1.2. Propulsion System

Small-scale propulsion systems will have to satisfy extraordinary requirements for high energy density and high power density. Acoustically, quiet systems will also have to be developed to assure covertness. It is noted that propulsion would require 90 percent of the available power and 70 per cent of the total weight for an MAV. A video system that operates at only one frame every two seconds is needed. Higher frame rates will increase the demand for high power and high energy density sources. Additional power would be required for onboard image compression and far higher data rate communication that are yet to be developed. MAVs must be capable of staying aloft, for perhaps 20 min to 60 min, while carrying a payload of 20 g or less, to a distance of perhaps 10 km. Finding high density sources of propulsion and power is a pivotal challenge. Some of the propulsion issues are linked with low Reynolds number aerodynamics of MAVs. The usual high lift-to-drag ratio concept used in larger vehicles does not hold. The low Reynolds number wings

have '113 to 114 the lift-to-drag ratio of conventional aircraft. Propellers less than 7.62 cm in diameter have poor efficiency, of the order of 50 per cent less. One way envisaged to overcome these limitations is to maximize the wing area leading to low-wing loadings, and the power required will be reduced considerably [25]. The 15 cm limitation of MAVs requires increasing the wing chord to maximize wing area, leading to low aspect ratio configurations. Finally to reduce power requirements, technologies like MEMSs, low power electronics, and component multi-functionality will help. High energy density (1.e. lightweight) power sources are essential. Battery-based systems would power the first-generation MAVs, but more exotic technologies, like fuel cells are being developed for follow-on systems. The reciprocating chemical muscle (RCM) is a mechanism that takes advantage of the superior energy density of chemical reactions as opposed to that of electrical energy storage, which is the approach currently being taken by most MAV researchers3. For example, the energy potential in one drop of gasoline is enormous as compared to that which can be stored in a battery of the same volume and weight. The **RCM** is a regenerative device that converts chemical energy into motion through a direct non-combustive chemical reaction. Hence, the concept of a muscle as opposed to an engine. There is no combustion taking place, nor is there an ignition system required. The RCM is capable of producing autonomic wing flapping as well as small amounts of electricity for control of MEMS devices [26].

4.1.3. Navigation and Communication

MAVs inherently suffer from control degradation because of their low wing loadings and inertial forces, which are stabilizing factors on full-scale aircraft. Because of the size of MAVs, perturbances such as wind gusts cause significantly large disturbances. A successful MAV will require a sophisticated stability and

navigation suite in order to be able to survive gusty wind conditions and avoid obstacles in unfamiliar territory. Without an auto-stabilizing system, pilots in the field will be burdened by the constant attention required by marginally stable MAVs. Current navigation methods, such as GPS and inertial navigation systems, are either too heavy, require too much power, or need brand new technology to make their use on MAVs feasible. The smallest commercially-available autopilot is Procerus Technologies' Kestrel, weighing 16.65g and measuring 2 inches in length. The Kestrel provides GPS-based navigation, an inertial measurement unit for stability, payload communications, and data logging. However, this autopilot is prohibitively heavy for MAVs that weigh less than 100 g. In order to reduce the weight of autopilot systems, innovative research is being conducted that utilizes optic flow methods for navigation. Optic flow refers to the apparent visual motion relative to an object in motion itself [27].

Inertial navigation [28] for MAVs awaits the development of low-drift micro gyros and accelerometers. Real time human interaction to provide vehicle stabilization and guidance is being considered for early designs. In some of the more demanding applications, for example vehicle agility for gust response, may well surpass a human operator's ability to cope with, and real-time human control may not be possible except in the simplest scenarios. Significant advances in miniature navigation, guidance and control systems are yet to be developed. Communication problems relate to small antenna size and limited power available to support the bandwidth required for image transmission. Control functions demand much lower bandwidth capabilities, in the 10's of Kbit range. One approach to solve communication problems relating to MAVs is to explore cellular communication architectures.

4.1.4. Payload Capabilities

A variety of sensors will have to be adapted and integrated into MAV systems. These may include optical, IR, acoustic, biochemical, nuclear, and others. Severe weight restrictions demand new types of avionics systems to fit within the 50'g allowed for the vehicle and its payload. Synthetic aperture radar (SAR), a micro sensor of extremely low weight and power, and small size, is being developed as an imaging payload for MAVs. The sensor offers all-weather/tall-visibility conditions, high resolution imaging capability to small units for surveillance and targeting purposes. In addition to being able to see through smoke, fog, etc. and its round-the-clock mission capability, SAR provides the valuable range information and it is particularly sensitive to man-made metallic objects, such as tanks, artillery pieces. Video camera system which would weigh only 1 g and occupy roughly 1 cm3 and would have 1000 × 1000 pixels and require as little as 25 mW is in the pipeline. Depending on system parameters, the total weight of the imaging payload can be expected to range between 45.359 g to 226.796 g.

4.1.5. Control System

MAV flight control would require miniature motion sensors and control surface actuators based on technology under development by the micro electromechanical systems (MEMS) community. As designed, the MAV would fly in a low Reynolds-number regime at airspeeds of 10 to 15 m/sec. Propulsion would be provided by a combination of an electric motor with either an advanced lithium battery or fuel cell, or by a miniature internal combustion engine, which is a more efficient option. Because of the close coupling between vehicle elements, system integration would be a significant challenge, requiring tight packaging and multifunction components to meet mass limitations.

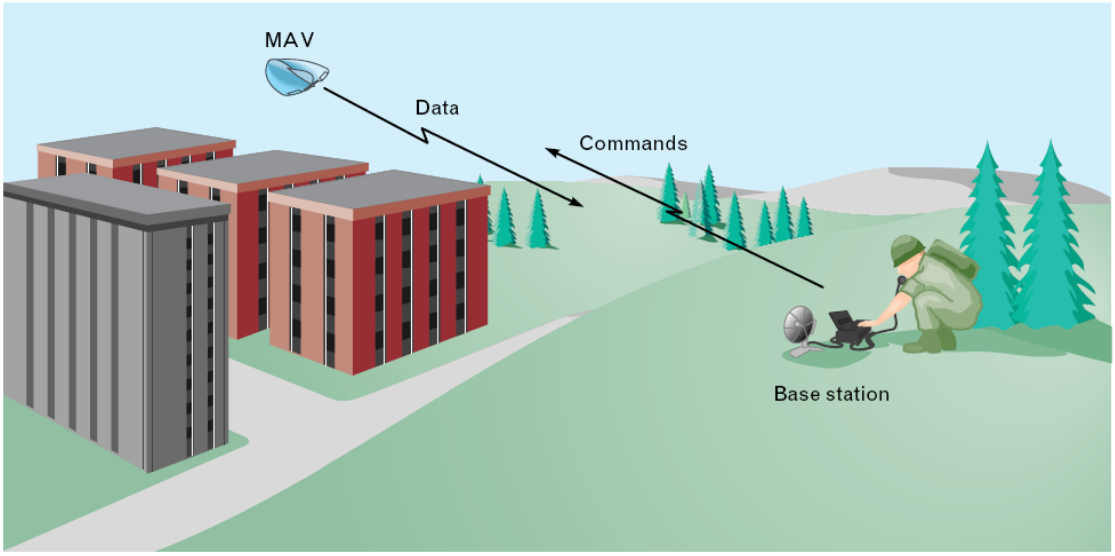

Figure 16: Micro air vehicle (MAV) used for Reconnaissance

Design capabilities for MAVs are tightly coupled to their missions, most of which could be carried out by using fixed-wing aircraft that can circle areas of interest. The vehicle must fly 10 to 15 m/sec, fast enough to overcome head winds, and have an endurance of 20 to 60 min to provide adequate range and mission time. For information-gathering missions, simple acoustic, seismic, or magnetic sensors can detect the presence of personnel, vehicles, and structures. Additional sensors can permit the MAV to detect chemical, biological, and nuclear contaminants in the atmosphere. Non-imaging sensors can detect light sources or measure local temperature. Visible and infrared imaging systems can provide useful data for surveillance applications.

Aerodynamic and propulsion factors limit the MAV to narrow ranges of airspeed and angle of attack, rendering the vehicle more vulnerable to gust upset. Flight control allows the MAV to fly at low airspeed in the presence of wind gusts and turbulence, stabilizes the vehicle with the aid of appropriate sensors, and provides aerodynamic controls.

Following figure illustrates the elements in the MAV flight-control system.

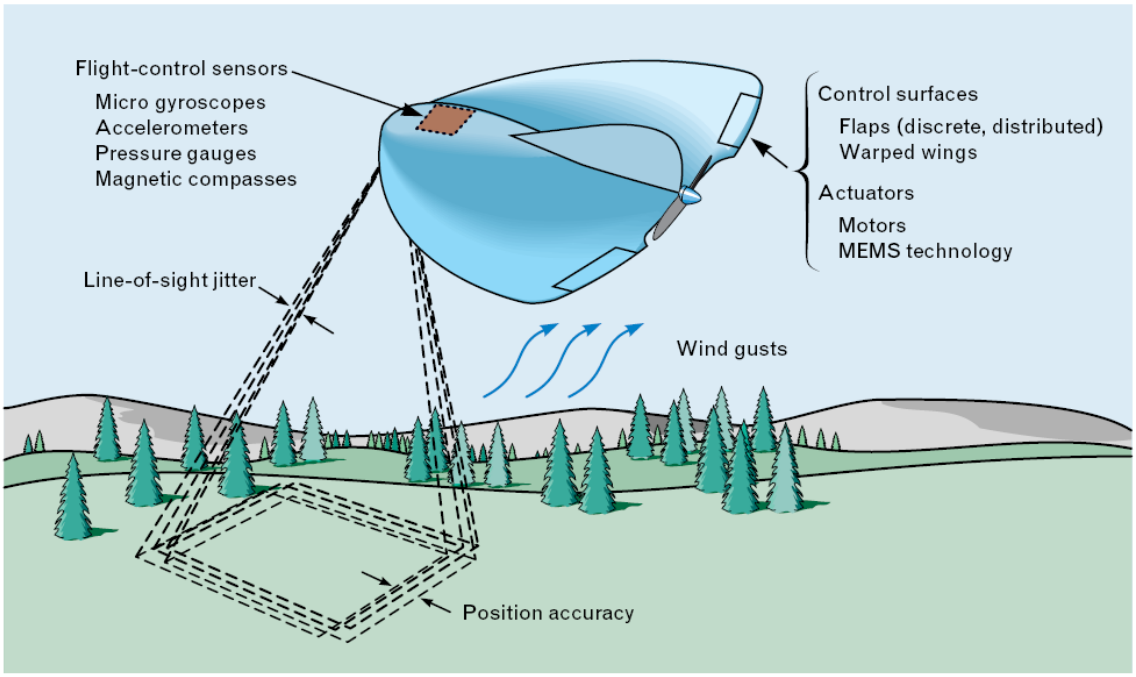

Figure 17: MAV Flight-Control System

Because the MAV airframe dynamic modes, such as Dutch roll and the short-period longitudinal mode will occur at higher frequencies compared with larger vehicles, the MAV will need some means of augmenting the natural stability of the airframe. In addition, the MAV should have the capability to fly itself to preprogrammed waypoints selected by the operator. Micronized pressure gauges and accelerometers are currently available and miniature magnetic compasses may also be feasible soon. Most useful for this application, however, are rate sensors. Microchip angular-rate sensors are now being produced, and will be useful for MAVs as soon as they are mated to miniaturized readout electronics. Drift rates from these sensors will be adequate for vehicle stabilization applications.

The ability to generate aerodynamic forces and moments is also required to stabilize and maneuver the MAV. These controls could be achieved with

conventional discrete hinged surfaces such as ailerons and elevators; distributed micro-actuated control surfaces; or wings that change shape or warp. All methods require micromechanical actuators. Because of recent advances in MEMS, a number of different actuator candidates should be available in the next one to two years. Examples include integrated force arrays, which generate electrostatic attraction force, and several approaches using piezoelectric crystals. These actuators can generate linear forces or be used in the construction of rotary machines that produce torque. They have the advantage of employing fabrication approaches that lend themselves to high production rates. Tiny conventional electromagnetic actuators, those used in watches, may also be tapped for some first-generation MAVs. The flight-control sensors and actuators must be integrated into the flight-control system by using a digital processor with the necessary signal interfaces. A custom microcontroller chip that also serves as the central processor for the communications and optical- sensor subsystem will accomplish this function.

4.2. DESCRIPTION OF ON-BOARD SENSORS USED FOR NAVIGATION OF MICRO AIR VEHICLES

The MAV could provide significant new capabilities to a wide range of users. Several MAVs and a base station could be transported and operated by a single individual, providing real-time data directly to the local user. The MAV promises to be particularly useful for covert operations. A variety of vehicle configurations and sensors could be used for many possible missions. The Micro Air Vehicle is a challenging environment for a navigation system. The MAV requires a small, lightweight navigation system, which must be extremely robust, easy to use, and inexpensive. This stands in contrast to traditional unmanned aerial vehicles, which have used large, expensive navigation systems similar to those found on conventional aircraft. The MAV navigation system has shown that the benefits of

MEMS based inertial navigation systems can be effectively used in MAVs. Although sensors with MEMS (Micro Electronic Mechanic System) technology have become smaller and lighter, some small sensors have sacrificed accuracy for size and weight and the precision of them cannot meet the demand of MAVs. Moreover, most MEMS sensors are more vulnerable to the temperature, which impedes their applications.

Flight control system basically consists of the following two sections:

1. On-board section
2. ground section

Control surfaces play an important role in the control and flight system of the micro air vehicles. The throttle, rudder, elevator, and aileron control are used to control the aircraft's altitude, yaw, pitch and roll respectively.

On-board control architectures for MAV have to integrate a variety of sensor information (GPS, MEMS gyro, accelerometer, magnetometer, aircraft attitude reference sensor, altimeter and barometer) in general control systems and all of them are integrated in an Inertial Measurement Unit (IMU). Optical flow sensors can be used for the navigation purpose of the MAV. Onboard hardware is seriously constrained by the load and energy consumption.

4.2.1. MEMS gyro

MEMS Gyroscopes are of great importance in commercial, medical, automotive and military fields. They can be used in cars for ABS systems, for anti-roll devices and for navigation in tall buildings areas where the GPS system might fail. The military market is in need for highly accurate, high-G- sustainable Inertial Measuring Units (IMU's). The ability to make low-cost, accurate, small dimension devices in MEMS answers many of the above mentioned needs. It should be noted

that most of these designs are manufactured using an SOI wafer, using the mono-crystalline silicon's excellent vibration and fatigue-resistant properties [49].

MEMS gyroscopes are typically designed to measure angular rate of rotation. A measurement of the angle itself is useful in many applications but cannot be obtained by integrating the angular rate due to the presence of bias errors which cause a drift. MEMS gyroscopes are micro-scaled or millimeter-scaled inertial rate sensors. Nowadays they have played a dominant role in auto-motives (rollover detection, anti-sliding control and GPS), aerospace (GPS assisted inertial navigation), and consumer electronics (camera image stabilization, cell phone GPS, and 3-D mouse). Compared to traditional electro-mechanical gyroscopes, the MEMS gyroscopes are small in size, inexpensive, and energy efficient. However, the imperfection of micro-fabrication and surrounding disturbances degrade the performance of the MEMS gyroscope and consequently cause measurement error of rotation rates. Therefore, a robust control system is essential for improving the performance of the MEMS gyroscopes through effectively compensating for the fabrication imperfections and disturbances [50].

All MEMS gyroscopes take advantage of the Coriolis Effect. In a reference frame rotating at angular velocity Ω, a mass M moving with velocity v sees a force:

$$F = 2Mv \times \Omega$$

Many types of MEMS gyroscopes have appeared in the literature, with most falling into the categories of tuning-fork gyros, oscillating wheels, Foucault pendulums, and wine glass resonators. Conventional (non-MEMS) spinning wheel gyros are common, but levitation and rotation of a MEMS device with no springs has not yet been commercialized.

4.2.2. Accelerometer

Accelerometers are commonly used for the measurement of acceleration of Micro Air Vehicles. Due to the weight and mass limitations, MEMS accelerometers are used. 3-axis accelerometers are normally preferred because they can measure the acceleration in all the three axes. Conceptually, an accelerometer behaves as a damped mass on a spring. When the accelerometer experiences an external force such as gravity, the mass is displaced until the external force is balanced by the spring force. The displacement is translated into acceleration. Modern accelerometers are often small micro electro-mechanical systems (MEMS), and are indeed the simplest MEMS devices possible, consisting of little more than a cantilever beam with a proof mass (also known as seismic mass). Damping results from the residual gas sealed in the device. An Inertial Navigation System (INS) is a navigation aid that uses a computer and motion sensors (accelerometers) to continuously calculate via dead reckoning the position, orientation, and velocity (direction and speed of movement) of a moving object without the need for external references. Other terms used to refer to inertial navigation systems or closely related devices include inertial guidance system, inertial reference platform, and many other variations. An accelerometer alone is unsuitable to determine changes in altitude over distances where the vertical decrease of gravity is significant, such as for aircraft and rockets. In the presence of a gravitational gradient, the calibration and data reduction process is numerically unstable [51].

Accelerometers are used to detect apogee in both professional and in amateur rocketry. Accelerometers are also being used in Intelligent Compaction rollers. Accelerometers are used alongside gyroscopes in inertial guidance systems. One of the most common uses for MEMS accelerometers is in airbag deployment systems for modern automobiles. In this case the accelerometers are used to detect the rapid negative acceleration of the vehicle to determine when a collision has

occurred and the severity of the collision. Another common automotive use is in electronic stability control systems, which use a lateral accelerometer to measure cornering forces. The widespread use of accelerometers in the automotive industry has pushed their cost down dramatically. Another automotive application is the monitoring of noise, vibration and harshness (NVH), conditions that cause discomfort for drivers and passengers and may also be indicators of mechanical faults. Tilting trains use accelerometers and gyroscopes to calculate the required tilt [52].

4.2.3. Magnetometer

A magnetometer is a scientific instrument used to measure the strength and/or direction of the magnetic field in the vicinity of the instrument. Magnetism varies from place to place and differences in Earth's magnetic field (the magnetosphere) can be caused by the differing nature of rocks and the interaction between charged particles from the Sun and the magnetosphere of a planet. Magnetometers are often a frequent component instrument on spacecraft that explore planets. The use of three orthogonal vector magnetometers allows the magnetic field strength, inclination and declination to be uniquely defined. Examples of vector magnetometers are fluxgates, superconducting quantum interference devices (SQUIDs) and the atomic SERF magnetometer [52].

4.2.4. Pressure Sensors

Small autopilots typically have two pressure sensors: a static pressure sensor which is used to measure altitude, and a dynamic pressure sensor which is used to measure airspeed. These sensors will be discussed in the following two sections.

4.2.4.1. Altitude Sensor

Pressure is a measure of force per unit area or

$$P = \frac{F}{A}$$

Where P is the pressure, F is the force, and A is the area. The static pressure at a particular altitude is determined by the force exerted by a column of air at that altitude:

$$P = \frac{m_{column} g}{A}$$

Where m_{column} is the mass of the column of air, g is the gravitational constant, and A is the area upon which the column is exerting pressure. The density of air is the mass per unit volume. Since the volume is given by the area times the height we get

$$P = \rho h g$$

where ρ is the density of air and h is the altitude

4.2.4.2. Air Speed Sensor

When the MAV is in motion, the atmosphere exerts dynamic pressure on the UAV in the direction of airflow. The dynamic pressure is given by

$$P_I = \frac{1}{2} \rho V_a^2$$

where V_a is the airspeed of the UAV. Bernoulli's theorem states that

$$P_S = P_I + P_o$$

where P_S is the total pressure, and P_o is the static pressure. The static and differential pressure sensors are analog devices that are sampled by the on-board processor.

4.2.5. GPS

The Global Positioning System (GPS) can provide long-term stability with high accuracy and worldwide coverage. Since the performance of the low cost micro GPS receiver can be easily degraded in high maneuvering environments, fusing the navigation data with other sensors such as a magnetometer or barometer is necessary. A GPS receiver calculates its position by precisely timing the signals sent by the GPS satellites high above the Earth. Each satellite continually transmits messages containing the time the message was sent, precise orbital information, and the general system health and rough orbits of all GPS satellites. The receiver measures the transit time of each message and computes the distance to each satellite. Many GPS units also show derived information such as direction and speed, calculated from position changes. [53]

The National Marine Electronics Association (NMEA) has developed a standard for all GPS devices. The string containing the most relevant information is the $GPRMC data line which is the Recommended Minimum Specific GPS/TRANSIT Data. The $GPRMC data string contains 12 pieces of information separated by commas within the string [58]:

1. Time Stamp
2. Validity: A for OK, V for invalid
3. Current Latitude
4. North or South
5. Current Longitude
6. East or West
7. Speed (in knots)
8. True Course
9. Date Stamp

10. Variation
11. East or West
12. Checksum

The most useful pieces of data are the latitude (3), longitude (5), and true course (8). The true course is the current heading of the aircraft in degrees and is measured clockwise from the north direction. If the MAV is heading east, for example, then the true course would be equal to 90 degrees. This single value saves an enormous amount of computation. Otherwise, a vector would have to be drawn from the previous latitude/longitude point to the current latitude/longitude point. The angle it forms with the north direction would then have to be calculated.

4.2.6. Optic Flow Sensors (navigation purpose)

The MAV should be able to fly towards its goal autonomously. This includes "small scale navigation", which refers to collision avoidance, altitude control, landing, and other similar tasks. All processing and control, including any collision avoidance, must be performed onboard. Thus due to the MAV's small size, any on-board collision avoidance system needs to weigh no more than several grams.

The term "optic flow" refers to the speed at which texture moves in an image focal plane as a result of relative motion between the observer and objects in the environment. Optic flow is typically formulated as a vector field over an image, in which the vectors define the velocity that the texture is moving in the image plane. A unit of measure for optic flow could be either "pixels per second" or "radians per second", with the latter used when considering how the visual field maps onto the image focal plane. Figure depicts how a micro air vehicle (MAV) might experience optic flow while in-flight, and how the optic flow could be used for small scale navigation and collision avoidance. In this example, we consider an MAV flying in a straight line over ground. Figure shows two optic flow fields as seen by two sensors:

one aimed downward and one aimed forward. The optic flow in the downward direction moves backward, simply because the MAV is flying forwards. The optic flow will be slightly faster for objects that are higher in altitude, and hence closer to the MAV. Thus a tree or bush whose height is just below the flight altitude of the MAV will have a corresponding large optic flow vector. The magnitude of this optic flow in radians per second is simply the MAV's altitude above the ground (or object on the ground) divided by its flight speed [54].

The optic flow in the forward direction is more complex and depends on the presence of any obstacles in the front. The focus of expansion (FOE) is the point from which the optic flow vectors radiate. The FOE indicates the MAV's direction of heading. If the MAV is approaching an obstacle, then the forward optic flow field will have a large divergence or expansion, and the FOE will be inside the obstacle in the visual field. If the MAV has a flight path that will cause it to fly nearby an obstacle but without collision, the associated optic flow field will have a large expansion but only on the side of the image containing the obstacle. In this case the FOE will not be located inside the obstacle. If there are no obstacles in the flight path, then only the ground and the horizon will contribute to the optic flow. In this case the divergence will be relatively small.

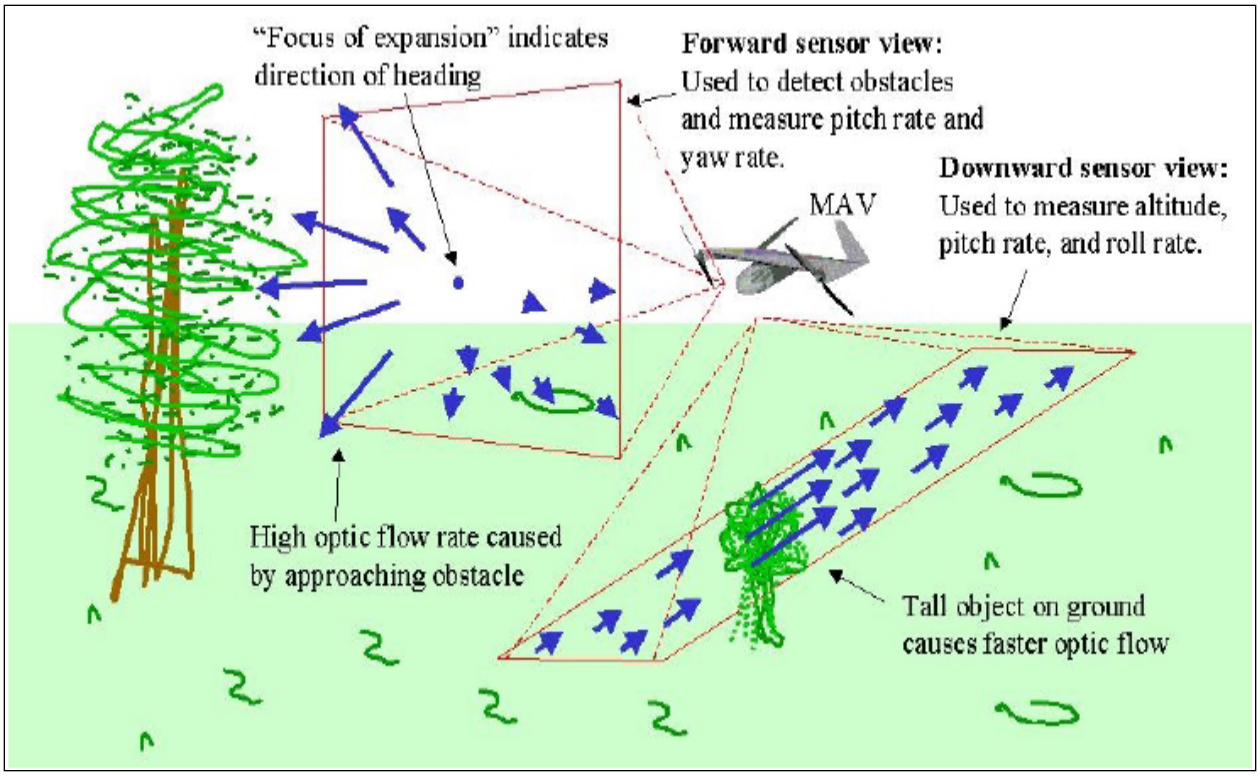

Figure 18: Optic flow as seen by an MAV flying above ground [54]

4.3. GUIDANCE AND FLIGHT CONTROL LOOP

The guidance loop forms an outer control loop in autonomous mode. It computes guidance demands to force the vehicle to follow the desired way-point. The flight control (or autopilot) loop forms the inner control loop and it generates the actual control signals to follow the guidance objectives as well as to stabilize the vehicle attitude and its rate [55]. Proposed control system for the Micro Air Vehicle is given below:

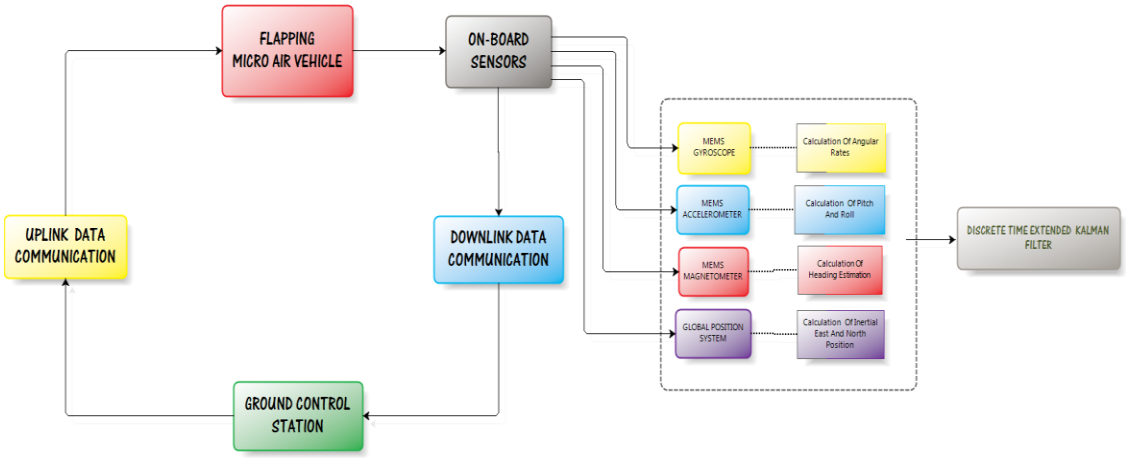

Figure 19: Proposed Control System

The flight control system for the fixed wing MAV is as given below:

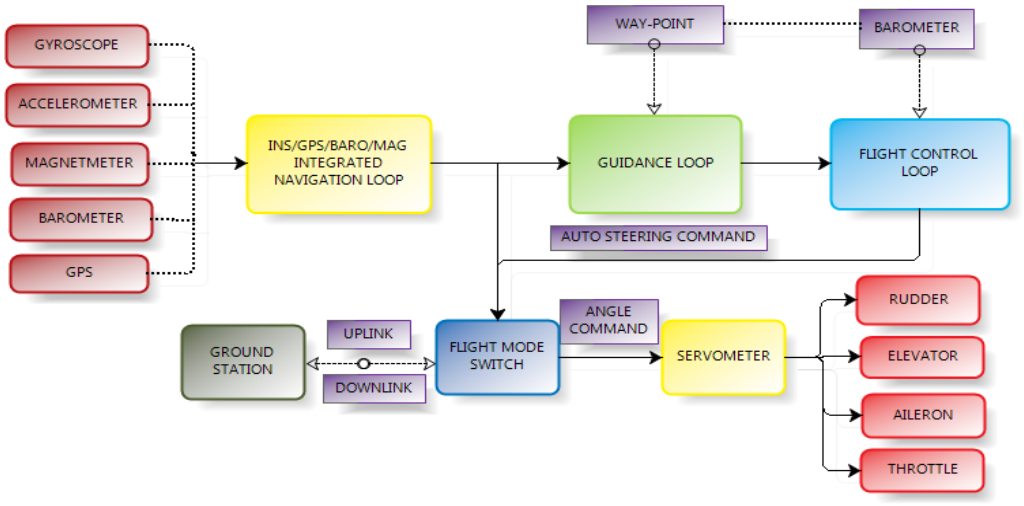

Figure 20: Flight control system for the Fixed wing MAV

The controls of fixed wing MAV are:

1. Throttle control
2. Elevator control
3. Aileron control
4. Rudder Control

In fixed wing MAV elevon can be used to replace the aeliron and elevator. In flapping MAV, for the case of simplicity, we can only consider rudder and throttle while ignoring elevon. So the proposed flight control system for flapping MAV is shown below:

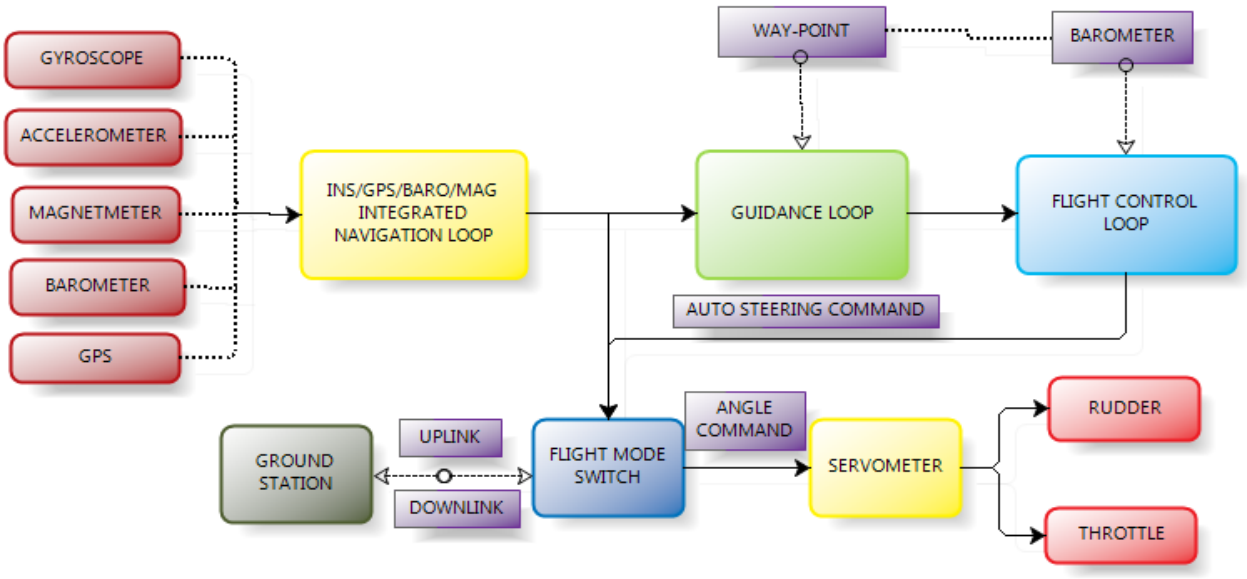

Figure 21: Proposed Flight Control System for flapping MAV

4.3.1. The Guidance Loop

The guidance loop generates the guidance demands from the current vehicle states and the next waypoint information. The guidance loop remains same for both the fixed-wing MAV and Flapping MAV. The guidance demands are desired vehicle speed with respect to the air, desired height and bank angle as shown in following figure. If the autonomous mode is activated, it selects the appropriate next waypoint depending upon the guidance state [56]. Then it decides if the waypoint has been intercepted or missed. If it is not intercepted it determines the Line Of Sight (LOS) angles and LOS rates to the next waypoint. Based on this information it computes the lateral acceleration required to intercept the next waypoint and converts this acceleration to the desired bank angle with a set of additional guidance demands: airspeed and height. The guidance loop implemented in this work updates its guidance demands every 10Hz [57].

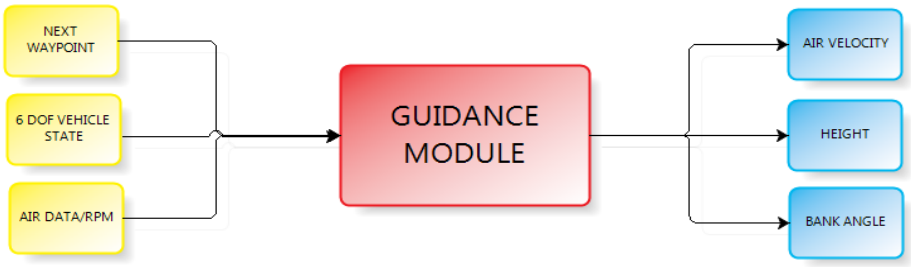

Figure 22: The Guidance Module

4.3.2. The Flight Control Loop

The flight control loop controls the vehicle's attitude and attitude rates as well as the vehicle speed with respect to the air. The block diagram of the control loop is shown in following figure. It performs speed control, height and height rate control, bank angle control, heading control, turn compensation and elevation control by using the guidance demands and measured vehicle states.

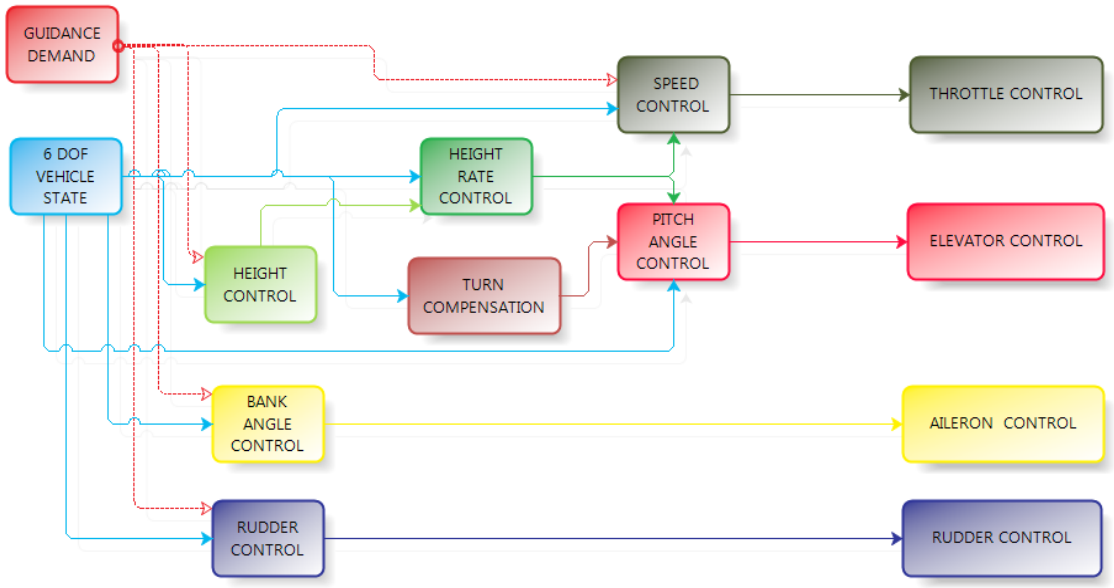

Figure 23: Flight Control Loop

The Flight Control Loop generates actuator signals for the engine throttle, rudder, elevator, and aileron. In this work, the control loop generates the control signals every 50Hz which is limited by the bandwidth of the electric servo actuators. The control loop is the most time critical task in autonomous flight so it is allocated to the highest priority inside the FCS. Most of the guidance and control algorithms

were verified and tested using the Hardware-In-The-Loop (HWIL) simulator which uses the vehicle model and simulated sensor data in the laboratory. However the true vehicle model and control action to the vehicle can only be verified through real-time flight tests [58].

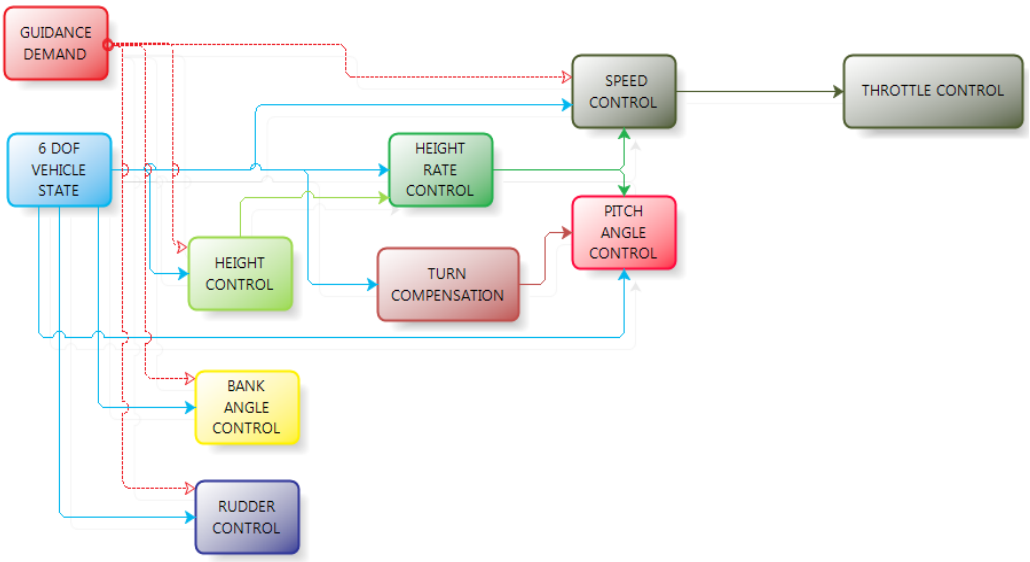

Figure 24: Proposed Control System for Flapping MAV

In the proposed design of Flapping MAV the elevon control is neglected for simplicity. So the controls are:

1. Throttle control
2. Rudder Control

And the controlling parameters are:

1. Flapping Frequency
2. Rudder Movement

Chapter 5

5. WORKING ON MATHEMATICAL MODEL

The use of GPS has allowed much progress in control and coordination of MAV's. The Information from GPS is limited, however, in that it gives only information about the direction of the ground track of the MAV, without regard or estimation of the direction the nose of the MAV is pointed, or heading. Determination of heading allows for greater precision of several MAV missions, such as those which require the aiming of cameras, as well as cooperative timing missions, for which knowledge of wind is helpful in determining the range of possible arrival times for individual agents. Accurate heading determination is accomplished independently of GPS by the use of solid state rate gyros and Magnetometers.

The MAV body coordinate frame is a right handed system centered at the MAV center of mass. The x axis points out the nose, the y axis points out the right wing, and the z axis points out the belly. The airspeed of the airplane is expressed in terms of velocity components on each of these axes, or alternatively, as the magnitude of these components of velocity, with a side slip and angle of attack. An inertial coordinate frame is also used, which is centered at a home base, with the x axis pointed north, the y axis pointed east, and the z axis pointed down into the earth. An additional frame, called the vehicle frame, is centered at the MAV and is oriented to the inertial frame. MAV state variables relate these frames, with positions giving the translation from the inertial frame to the vehicle frame, and attitude variables rotating from the vehicle to the body frame.

Standard MAV state variables

P_N	Inertial North position of MAV
P_E	Inertial East position of MAV
h	Inertial MAV altitude
u	Airspeed along body x-axis
v	Airspeed along body y-axis
w	Airspeed along body z-axis
ϕ	Roll angle
θ	Pitch angle
ψ	Heading
p	Angular rate about body x-axis
q	Angular rate about body y-axis
r	Angular rate about body z-axis

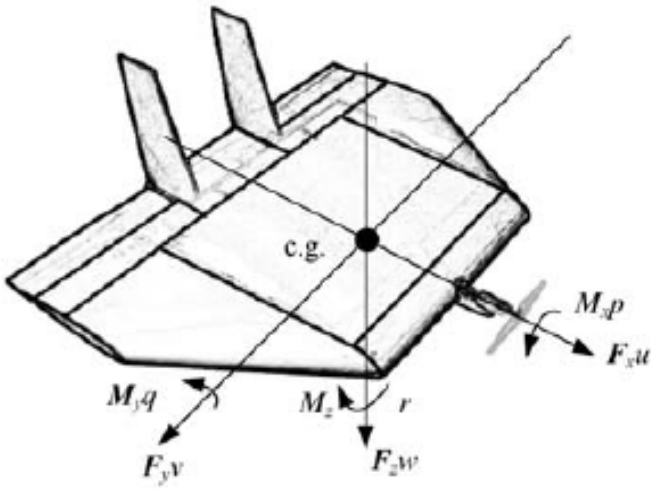

Alternate state variables

V_{air}	Total airspeed
α	Angle of attack
β	Sideslip angle

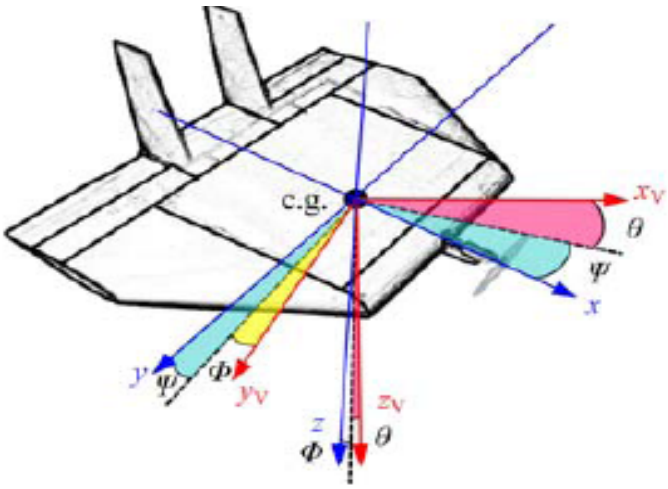

Variables representing sensor measurements

$accc_x$	x accelerometer reading
acc_y	y accelerometer reading
acc_z	z accelerometer reading
GPS_N	GPS northing
GPS_E	GPS easting
$GPS_{velocity}$	GPS ground speed
$GPS_{heading}$	GPS ground track
mag_x	x-axis magnetometer reading
mag_y	y-axis magnetometer reading
mag_z	z-axis magnetometer reading

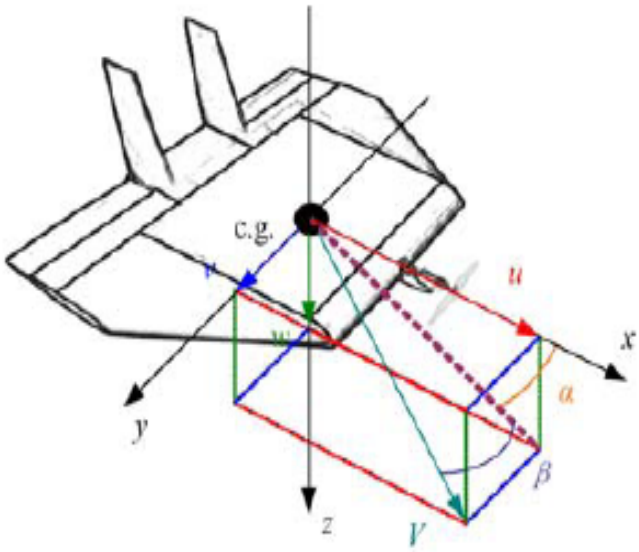

Variables representing External States

W_N	Wind from north
W_E	Wind from east
m_{ox}	Northern magnetic field component
m_{oy}	Eastern magnetic field component
m_{oz}	Vertical magnetic field component

5.1. STATE EQUATIONS

The state equations which relate body frame rotations to changes in roll, pitch and heading are nonlinear. Letting the states be roll angle and pitch angle, ϕ and θ, and letting angular rates p, q and r and Airspeed V_{air} be inputs. The update of the states is related to the inputs as shown following [59]:

$$\begin{bmatrix} \dot{\phi} \\ \dot{\theta} \\ \dot{\psi} \\ \dot{P}_N \\ \dot{P}_E \\ \dot{W}_N \\ \dot{W}_E \end{bmatrix} = \begin{bmatrix} p + q\sin\phi\tan\theta + r\cos\phi\tan\theta \\ q\cos\phi + r\sin\phi \\ q\dfrac{\sin\phi}{\cos\theta} + r\dfrac{\cos\phi}{\cos\theta} \\ V_{air}\cos\psi + W_N \\ V_{air}\sin\psi + W_E \\ 0 \\ 0 \end{bmatrix}$$

For the state equations above, body frame accelerations ax, ay and az may be calculated as system outputs. Following is an expected output from the sensors in terms of state variables, rather than representing a physical law which will dictate that output.

5.2. EXPECTED SENSORS OUTPUT

Expected Accelerometer Output

$$\begin{bmatrix} acc_x \\ acc_y \\ acc_z \end{bmatrix} = \begin{bmatrix} \dfrac{\dot{u} + qw - rv}{g} + \sin\theta \\ \dfrac{\dot{v} + ru - pw}{g} - \cos\theta\sin\phi \\ \dfrac{\dot{w} + pv - qu}{g} - \cos\theta\cos\phi \end{bmatrix}$$

Expected Magnetometer Output

$$\begin{bmatrix} mag_x \\ mag_y \\ mag_z \end{bmatrix} = \begin{bmatrix} \cos\theta\cos\phi & \cos\theta\sin\psi & -\sin\theta \\ (\sin\phi\sin\theta\cos\psi - \cos\phi\sin\psi) & (\sin\phi\sin\theta\sin\psi + \cos\phi\cos\psi) & \sin\phi\cos\theta \\ (\cos\phi\sin\theta\cos\psi + \sin\phi\sin\psi) & (\cos\phi\sin\theta\sin\psi - \sin\phi\cos\psi & \cos\phi\cos\theta \end{bmatrix} \begin{bmatrix} m_{ox} \\ m_{oy} \\ m_{oz} \end{bmatrix}$$

Expected GPS Output

$$\begin{bmatrix} GPS_N \\ GPS_E \\ GPS_{velocity} \\ GPS_{heading} \end{bmatrix} = \begin{bmatrix} P_N \\ P_E \\ \sqrt{V_{air}^2 + 2V_{air}(W_N\cos\psi + W_E\sin\psi) + (W_N^2 + W_E^2)} \\ \tan^{-1}\left(\dfrac{V_{air}\sin\psi + W_E}{V_{air}\cos\psi + W_N}\right) \end{bmatrix}$$

Although the GPS sensor will output ground speed and ground track data, the usefulness of the information is questionable. The speed and heading data in from the GPS are calculated from successive points, so the reading of each is a reflection of a historical average. The data could be used effectively if a log of estimation, sensor and input data were kept, and a correction applied to a historical estimate, then the model forward propagated in time to the current time, but the merit of using the GPS speed and track data must be weighed against the computational overhead.

5.3. ASSUMPTIONS

Normally aerodynamic angles (angle of attack (α) and the sideslip angle (β)) and air speed (V) are used instead of the body axis velocities in order to express the aerodynamic forces [59].

$$\begin{bmatrix} u \\ v \\ w \end{bmatrix} = V_{air} \begin{bmatrix} \cos\alpha\cos\beta \\ \sin\beta \\ \sin\alpha\sin\beta \end{bmatrix}$$

An alternative expression of the Body frame component velocities is shown:

$$V_{air} = \sqrt{u^2 + v^2 + w^2} \qquad \beta = \tan^{-1}\left(\frac{v}{u^2 + w^2}\right) \qquad \alpha = \tan^{-1}\left(\frac{w}{u}\right)$$

However, since we do not have a method for directly measuring $\dot{u}$, $\dot{v}$, $\dot{w}$, u, v, and w, we will assume that $\dot{u} = \dot{v} = \dot{w} \approx 0$ and assume that $\alpha \approx \theta$ and $\beta \approx 0$ to obtain

The MAV equations of motion assume knowledge of body frame component airspeeds. Although this information is not known, the same information can be approximated for level flight. If the MAV is not climbing or descending: $\begin{bmatrix} u \\ v \\ w \end{bmatrix} = V_{air} \begin{bmatrix} \cos\theta \\ 0 \\ \sin\theta \end{bmatrix}$ $\alpha = \theta$

Further we may assume zero side slip:

$$\beta = 0$$

Assume also that linear accelerations are small: $\begin{bmatrix} \dot{u} \\ \dot{v} \\ \dot{w} \end{bmatrix}$

$$\begin{bmatrix} \dot{u} \\ \dot{v} \\ \dot{w} \end{bmatrix} = 0$$

Under these assumptions:

$$V_{air} = \begin{bmatrix} \cos\theta \\ 0 \\ \sin\theta \end{bmatrix}$$

And

$$\begin{bmatrix} acc_x \\ acc_y \\ acc_z \end{bmatrix} = \begin{bmatrix} \dfrac{V_{air} q \sin\theta}{g} + \sin\theta \\ \dfrac{V_{air}(r\cos\theta - p\sin\theta)}{g} - \cos\theta\sin\phi \\ \dfrac{-V_{air} q \cos\theta}{g} - \cos\theta\cos\phi \end{bmatrix}$$

5.4. KALMAN FILTER

Filtering is desirable in many situations in engineering and embedded-systems. For example, radio communication signals are corrupted with noise. A good filtering algorithm can remove the noise from electromagnetic signals while retaining the useful information. Another example is power supply voltages. Uninterruptible power supplies are devices that filter line voltages in order to smooth out undesirable fluctuations that might otherwise shorten the lifespan of electrical devices such as computers and printers. The Kalman Filter is a tool that can estimate the variables of a wide range of processes [60].

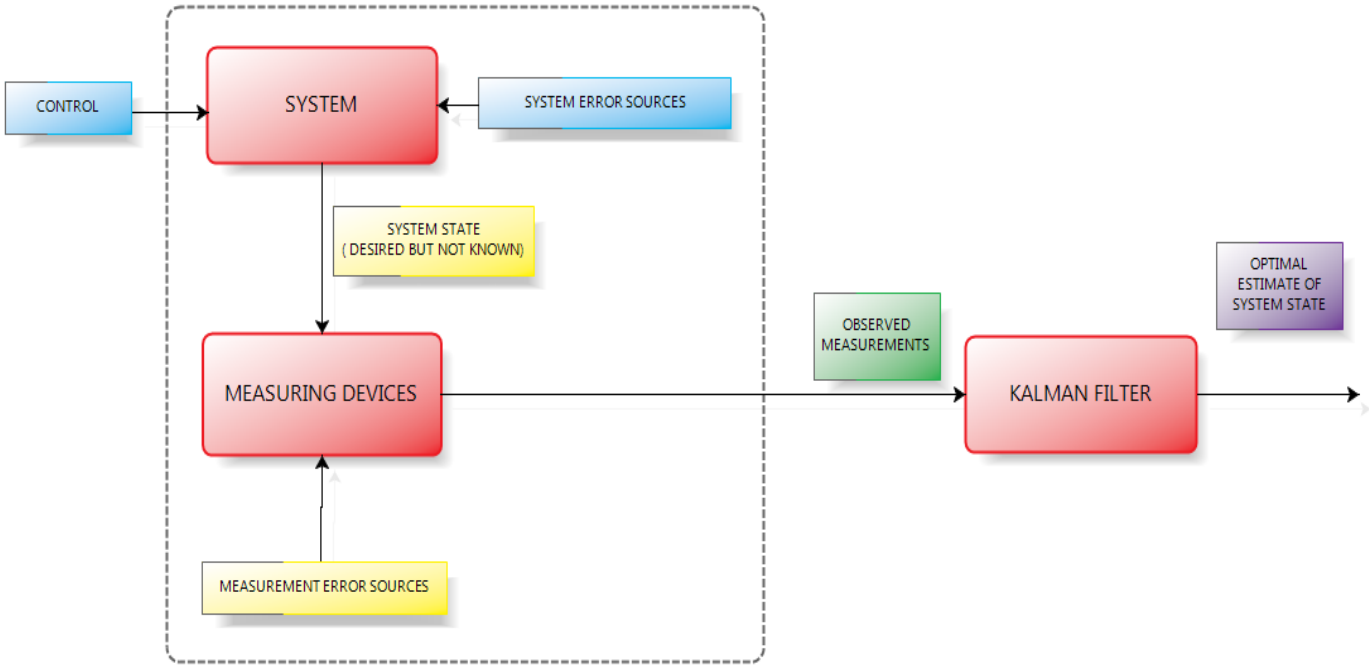

Figure 25: Typical Application of Kalman Filter

In mathematical terms we would say that a Kalman Filter estimates the states of a linear system. The Kalman Filter not only works well in practice, but it is theoretically attractive because it can be shown that of all possible filters, it is the

one that minimizes the variance of the estimation error. Kalman Filters are often implemented in embedded control systems because in order to control a process, you first need an accurate estimate of the process variables. In order to use a Kalman Filter to remove noise from a signal, the process that we are measuring must be able to be described by a linear system. Many physical processes, such as a vehicle driving along a road, a satellite orbiting the earth, a motor shaft driven by winding currents, or a sinusoidal radio-frequency carrier signal, can be approximated as linear system.

5.5. EXTENDED KALMAN FILTER

While no proof has been discovered to show that applying a Kalman Filter to a set of linearized state equations will yield optimal observation results, experience has shown that very effective observation can be achieved using an Extended Kalman Filter (EKF).

The system and measurement equations are given as follows:

$$\begin{aligned} x_k &= f_{k-1}(x_{k-1}, u_{k-1}, w_{k-1}) \\ y_k &= h_h(x_k, v_k) \\ w_k &\approx (0, Q_k) \\ v_k &\approx (0, R_k) \end{aligned}$$

initialize the filter as follows:

$$\hat{x}_0^+ = E(x_0)$$

$$P_0^+ = E\left[(x_0 - \hat{x}_0^+)(x_0 - \hat{x}_0^+)^T\right]$$

for k = 1,2,3 . . . .

Compute the following partial derivative matrices:

$$F_{k-1} = \left.\frac{\partial f_{k-1}}{\partial x}\right|_{\hat{x}_{k-1}^{+}}$$

$$L_{k-1} = \left.\frac{\partial f_{k-1}}{\partial w}\right|_{\hat{x}_{k-1}^{+}}$$

Perform the time update of the state estimate and estimation error covariance as follows:

$$P_k^- = F_{k-1} P_{k-1}^+ F_{k-1}^T + L_{k-1} Q_{k-1} L_{k-1}^T$$
$$\hat{x}_k^- = f_{k-1}\left(\hat{x}_{k-1}^+, u_{k-1}, 0\right)$$

- compute the following partial derivative matrices

$$H_K = \left.\frac{\partial h_k}{\partial x}\right|_{\hat{x}_k^-}$$
$$M_K = \left.\frac{\partial h_k}{\partial v}\right|_{\hat{x}_k^-}$$

- perform the measurement update of the state estimate and estimation error covariance as follows

$$K_k = P_k^- H_k^T \left(H_k P_k^- H_k^T + M_k R_k M_k^T\right)^{-1}$$
$$\hat{x}_k^+ = \hat{x}_k^- + K_k\left(y_k - h_k\left(\hat{x}_k^-, 0\right)\right)$$
$$P_k^+ = \left(I - K_K H_k\right) P_k^-$$

5.6. CASCADED EXTENDED KALMAN FILTER STATE ESTIMATION SCHEME

5.6.1. Single 7 State Extended Kalman Filter

The state equations which relate body frame rotations to changes in roll, pitch and heading are nonlinear. Letting the states be roll angle and pitch angle, ϕ and θ, and letting angular rates p, q and r and Airspeed V_{air} be inputs.

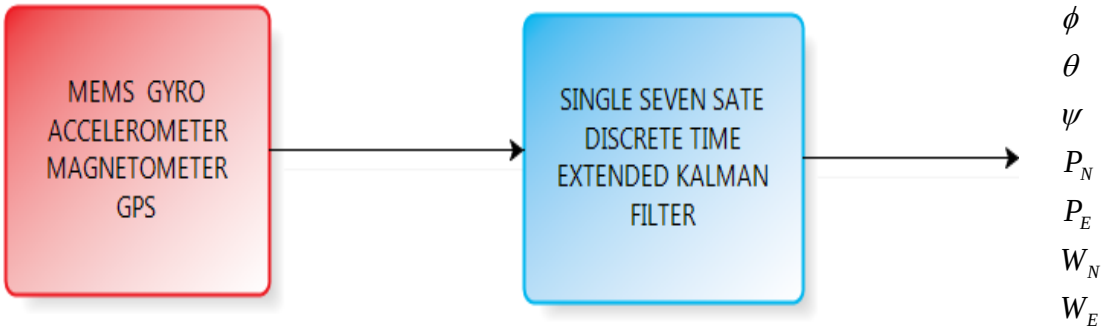

Figure 26: Single Seven State Extended Kalman Filter Scheme

The update of the states is related to the inputs as shown following [59,60]:

$$\begin{bmatrix} \dot{\phi} \\ \dot{\theta} \\ \dot{\psi} \\ \dot{P}_N \\ \dot{P}_E \\ \dot{W}_N \\ \dot{W}_E \end{bmatrix} = \begin{bmatrix} p + q\sin\phi\tan\theta + r\cos\phi\tan\theta \\ q\cos\phi + r\sin\phi \\ q\dfrac{\sin\phi}{\cos\theta} + r\dfrac{\cos\phi}{\cos\theta} \\ V_{air}\cos\psi + W_N \\ V_{air}\sin\psi + W_E \\ 0 \\ 0 \end{bmatrix}$$

linearization of EKF through Jacobian method [60]

$$\frac{\partial f(\hat{x},u)}{\partial x} = \begin{bmatrix} q\cos\phi\tan\theta - r\sin\phi\tan\theta & q\dfrac{\sin\phi}{\cos^2\theta} + r\dfrac{\cos\phi}{\cos^2\theta} & 0 & 0 & 0 & 0 & 0 \\ -q\sin\phi + r\cos\phi & 0 & 0 & 0 & 0 & 0 & 0 \\ q\dfrac{\cos\phi}{\cos\theta} - r\dfrac{\sin\phi}{\cos\theta} & (q\sin\phi + r\cos\phi)\sec\theta\tan\theta & 0 & 0 & 0 & 0 & 0 \\ 0 & 0 & 0 & 0 & 0 & -1 & 0 \\ 0 & 0 & 0 & 0 & 0 & 0 & -1 \\ 0 & 0 & 0 & 0 & 0 & 0 & 0 \\ 0 & 0 & 0 & 0 & 0 & 0 & 0 \end{bmatrix}$$

Measurement

$$h(\hat{x},u)=\begin{bmatrix} \frac{V_{air}q\sin\theta}{g}+\sin\theta \\ \frac{V_{air}(r\cos\theta-r\sin\theta)}{g}-\cos\theta\cos\phi \\ \frac{-V_{air}q\cos\theta}{g}-\cos\theta\sin\phi \\ P_N \\ P_E \\ \sqrt{V_{air}^2+2V_{air}(W_N\cos\psi+W_E\sin\psi)+(W_N^2+W_E^2)} \\ \tan^{-1}\left(\frac{V_{air}\sin\psi+W_N}{V_{air}\cos\psi+W_E}\right) \end{bmatrix}$$

linearization of EKF through Jacobian [60]

$$H_k=\frac{\partial h(\hat{x},u)}{\partial x}=\begin{bmatrix} 0 & \frac{V_{air}q\cos\theta}{g}+\cos\theta & 0 & 0&0&0&0 \\ -\cos\theta\cos\phi & \frac{-V_{air}(r\sin\theta-p\cos\theta)}{g}+\sin\theta\sin\phi & 0 & 0&0&0&0 \\ \cos\theta\sin\phi & \frac{V_{air}q\sin\theta}{g}+\sin\theta\cos\phi & 0 & 0&0&0&0 \\ 0 & 0 & 0 & 1&0&0&0 \\ 0 & 0 & 0 & 0&1&0&0 \\ -\cos\theta\cos\phi & \frac{-V_{air}(r\sin\theta-r\cos\theta)}{g}+\sin\phi & 0 & 0&0&0&0 \\ 0 & 0 & \frac{\frac{V_{air}\cos\psi}{v_{air}\cos\psi+W_E}+\frac{V_{air}\sin\psi+W_E}{V_{air}\sin\psi(V_{air}\sin\psi+W_E)^2}}{1+\frac{(V_{air}\sin\psi+W_E)^2}{(V_{air}\cos\psi+W_E)^2}} & 0&0&0 & \frac{\frac{1}{(V_{air}\cos\psi+W_E)-(V_{air}\sin\psi+W_W)}}{1+\frac{(V_{air}\sin\psi+W_E)^2}{(V_{air}\cos\psi+W_E)^2}} \end{bmatrix}$$

Process Covariance Matrix

Process Covariance Matrix [41] is given as follows:

$$Q=E(ww^T)$$

where,

$$w=\begin{bmatrix} w_\phi \\ w_\theta \\ w_\psi \\ w_{P_N} \\ w_{P_E} \\ w_{W_N} \\ w_{W_E} \end{bmatrix}$$

and

$$w^T = \begin{bmatrix} w_\phi & w_\theta & w_\psi & w_{P_N} & w_{P_E} & w_{W_N} & w_{W_E} \end{bmatrix}$$

so,

$$Q = E\begin{bmatrix} w_\phi^2 & w_\phi w_\theta & w_\phi w_\psi & w_\phi w_{P_N} & w_\phi w_{P_E} & w_\phi w_{W_N} & w_\phi w_{W_E} \\ w_\theta w_\phi & w_\theta^2 & w_\theta w_\psi & w_\theta w_{P_N} & w_\theta w_{P_E} & w_\theta w_{W_N} & w_\theta w_{W_E} \\ w_\psi w_\phi & w_\psi w_\theta & w_\psi^2 & w_\psi w_{P_N} & w_\psi w_{P_E} & w_\psi w_{W_N} & w_\psi w_{W_E} \\ w_{P_N} w_\phi & w_{P_N} w_\theta & w_{P_N} w_\psi & w_{P_N}^2 & w_{P_N} w_{P_E} & w_{P_N} w_{W_N} & w_{P_N} w_{W_E} \\ w_{P_E} w_\phi & w_{P_E} w_\theta & w_{P_E} w_\psi & w_{P_E} w_{P_N} & w_{P_E}^2 & w_{P_E} w_{W_N} & w_{P_E} w_{W_E} \\ w_{W_N} w_\phi & w_{W_N} w_\theta & w_{W_N} w_\psi & w_{W_N} w_{P_N} & w_{W_N} w_{P_E} & w_{W_N}^2 & w_{W_N} w_{W_E} \\ w_{W_E} w_\phi & w_{W_E} w_\theta & w_{W_E} w_\psi & w_{W_E} w_{P_N} & w_{W_E} w_{P_E} & w_{W_E} w_{W_N} & w_{W_E}^2 \end{bmatrix}$$

Noise is uncorrelated [62]:

$$Q = E\begin{bmatrix} w_\phi^2 & 0 & 0 & 0 & 0 & 0 & 0 \\ 0 & w_\theta^2 & 0 & 0 & 0 & 0 & 0 \\ 0 & 0 & w_\psi^2 & 0 & 0 & 0 & 0 \\ 0 & 0 & 0 & w_{P_N}^2 & 0 & 0 & 0 \\ 0 & 0 & 0 & 0 & w_{P_E}^2 & 0 & 0 \\ 0 & 0 & 0 & 0 & 0 & w_{W_N}^2 & 0 \\ 0 & 0 & 0 & 0 & 0 & 0 & w_{W_E}^2 \end{bmatrix}$$

Measurement Covariance Matrix is given as follows:

$$R = E(vv^T)$$

Where,

$$v = \begin{bmatrix} v_{acc_x} \\ v_{acc_y} \\ v_{acc_z} \\ v_{GPS_N} \\ v_{GPS_E} \\ v_{GPS_{velocity}} \\ v_{GPS_{Heading}} \end{bmatrix}$$

and

$$v = \begin{bmatrix} v_{acc_x} & v_{acc_y} & v_{acc_z} & v_{GSPS_N} & v_{GPS_E} & v_{GPS_{velocity}} & v_{GPS_{Heading}} \end{bmatrix}$$

so,

$$R = E\begin{bmatrix} v^2_{acc_x} & v_{acc_x}v_{acc_y} & v_{acc_x}v_{acc_z} & v_{acc_x}v_{GPS_N} & v_{acc_x}v_{GPS_E} & v_{acc_x}v_{GPS_{Velocity}} & v_{acc_x}v_{GPS_{Heading}} \\ v_{acc_y}v_{acc_x} & v^2_{acc_y} & v_{acc_y}v_{acc_z} & v_{acc_v}v_{GPS_N} & v_{acc_y}v_{GPS_E} & v_{acc_y}v_{GPS_{Velocity}} & v_{acc_y}v_{GPS_{Heading}} \\ v_{acc_z}v_{acc_x} & v_{acc_z}v_{acc_y} & v^2_{acc_z} & v_{acc_z}v_{GPS_N} & v_{acc_z}v_{GPS_E} & v_{acc_z}v_{GPS_{Velocity}} & v_{acc_z}v_{GPS_{Heading}} \\ v_{GPS_N}v_{acc_x} & v_{GPS_N}v_{acc_y} & v_{GPS_N}v_{acc_z} & v^2_{GPS_N} & v_{GPS_N}v_{GPS_E} & v_{GPS_N}v_{GPS_{Velocity}} & v_{GPS_n}v_{GPS_{Heading}} \\ v_{GPS_E}v_{acc_x} & v_{GPS_E}v_{acc_y} & v_{GPS_E}v_{acc_z} & v_{GPS_E}v_{GPS_N} & v^2{}_{GPS_E} & v_{GPS_E}v_{GPS_{Velocity}} & v_{GPS_E}v_{GPS_{Heading}} \\ v_{GPS_{Velocity}}v_{acc_x} & v_{GPS_{Velocity}}v_{acc_y} & v_{GPS_{Velocity}}v_{acc_z} & v_{GPS_{Velocity}}v_{GPS_N} & v_{GPS_{Velocity}}v_{GPS_E} & v^2{}_{GPS_{Velocity}} & v_{GPS_{Velocity}}v_{GPS_{Heading}} \\ v_{GPS_{Heading}}v_{acc_x} & v_{GPS_{Heading}}v_{acc_y} & v_{GPS_{Heading}}v_{acc_z} & v_{GPS_{Heading}}v_{GPS_N} & v_{GPS_{Heading}}v_{GPS_E} & v_{GPS_{Heading}}v_{GPS_{Velocity}} & v^2{}_{GPS_{Heading}} \end{bmatrix}$$

Noise is uncorrelated [62]

$$R = E\begin{bmatrix} v^2{}_{acc_x} & 0 & 0 & 0 & 0 & 0 & 0 \\ 0 & v^2_{acc_y} & 0 & 0 & 0 & 0 & 0 \\ 0 & 0 & v^2_{acc_z} & 0 & 0 & 0 & 0 \\ 0 & 0 & 0 & v^2_{GPS_N} & 0 & 0 & 0 \\ 0 & 0 & 0 & 0 & v^2{}_{GPS_E} & 0 & 0 \\ 0 & 0 & 0 & 0 & 0 & v^2{}_{GPS_{Velocity}} & 0 \\ 0 & 0 & 0 & 0 & 0 & 0 & v^2{}_{GPS_{Heading}} \end{bmatrix}$$

5.6.2. 2-Stage Extended Kalman Filter Scheme

Because the heading update equation uses the same inputs as the Pitch and Roll equations, it is not unnatural to lump them together in the same estimation block. The exclusiveness of the heading state lies in the output equations. There is not a

sensor output equation which will relate heading to accelerometer readings, which is why it was convenient to split heading estimation into it's own stage as mentioned earlier. One of the merits of heading and attitude at the same time is that magnetometer information may be beneficial in the estimation of pitch and roll, since no maneuver will upset the earth's magnetic field, as they may the accelerometer readings. And, depending on the attitude and heading of the MAV, projecting pitch and roll onto the magnetic field vector may refine the pitch and roll estimates.

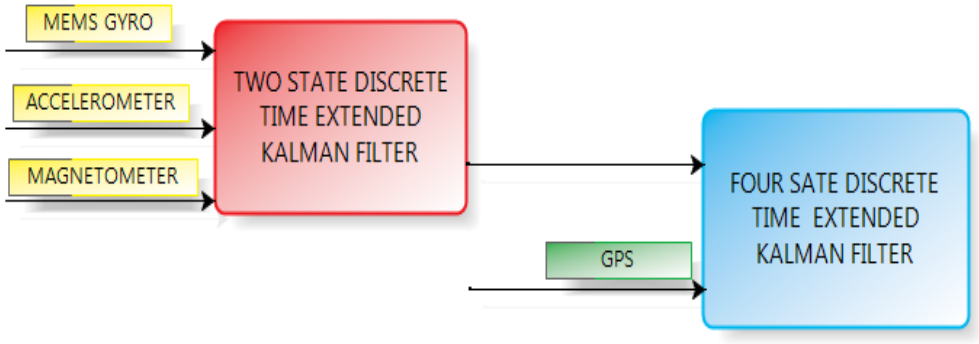

Figure 27: Two Stage Cascaded Scheme

Stage#01: Pitch, Roll and Yaw Estimation:

$$x = \begin{bmatrix} \phi \\ \theta \\ \psi \end{bmatrix}, u = \begin{bmatrix} p \\ q \\ r \\ V_{air} \end{bmatrix}, y = \begin{bmatrix} acc_x \\ acc_y \\ acc_z \end{bmatrix}$$ Linearization through jacobian

$$\begin{bmatrix} \dot{\phi} \\ \dot{\theta} \\ \dot{\psi} \end{bmatrix} = f(x,u) = \begin{bmatrix} p + q\sin\phi\tan\theta + r\cos\phi\tan\theta \\ q\cos\phi + r\sin\phi \\ q\dfrac{\sin\phi}{\cos\theta} + r\dfrac{\cos\phi}{\cos\theta} \end{bmatrix}$$

Linearization through jacobian [61]:

$$A=\frac{\partial f(\hat{x},u)}{\partial x}=\begin{bmatrix} q\cos\phi\tan\theta-\sin\phi\tan\theta & \frac{q\sin\phi+r\cos\phi}{\cos^2\theta} & 0 \\ -q\sin\phi+r\cos\phi & 0 & 0 \\ (q\cos\phi-r\sin\phi)\sec\theta & (q\sin\phi+r\cos\phi)\sec\theta\tan\theta & 0 \end{bmatrix}$$

Process Covariance Matrix [62] is given as follows:

$$Q=E\left(ww^T\right)$$

where,

$$w=\begin{bmatrix} w_\phi \\ w_\theta \\ w_\psi \end{bmatrix}$$

and

$$w^T=\begin{bmatrix} w_\phi & w_\theta & w_\psi \end{bmatrix}$$

so,

$$Q=E\begin{bmatrix} w_\phi^2 & w_\phi w_\theta & w_\phi w_\psi \\ w_\theta w_\phi & w_\theta^2 & w_\theta w_\psi \\ w_\psi w_\phi & w_\psi w_\theta & w_\psi^2 \end{bmatrix}$$

Noise is uncorrelated [61]:

$$Q=E\begin{bmatrix} w_\phi^2 & 0 & 0 \\ 0 & w_\theta^2 & 0 \\ 0 & 0 & w_\psi^2 \end{bmatrix}$$

The output equations for attitude estimator are as follows:

$$h(\hat{x},u)=\begin{bmatrix} \frac{V_{air}q\sin\theta}{g}+\sin\theta \\ \frac{V_{air}(r\cos\theta-p\sin\theta)}{g}-\cos\theta\sin\phi \\ \frac{-V_{air}q\cos\theta}{g}-\cos\theta\cos\phi \end{bmatrix}$$

Linearization through jacobian [61]:

$$H_k = \frac{\partial h(\hat{x}, u)}{\partial x} = \begin{bmatrix} 0 & \frac{V_{air} q \cos\theta}{g} + \cos\theta & 0 \\ -\cos\theta\cos\phi & \frac{-V_{air}(r\sin\theta + p\cos\theta)}{g} + \sin\theta\sin\phi & 0 \\ -\cos\theta\sin\phi & \frac{V_{air} q \sin\theta}{g} + \sin\theta\cos\phi & 0 \end{bmatrix}$$

Measurement Covariance Matrix [63] is given as follows:

$$R = E(vv^T)$$

Where,

$$v = \begin{bmatrix} v_{acc_x} \\ v_{acc_y} \\ v_{acc_z} \end{bmatrix}$$

and

$$v = \begin{bmatrix} v_{acc_x} & v_{acc_y} & v_{acc_z} \end{bmatrix}$$

so,

$$R = E\begin{bmatrix} v^2{}_{acc_x} & v_{acc_x} v_{acc_y} & v_{acc_x} v_{acc_z} \\ v_{acc_y} v_{acc_x} & v^2_{acc_y} & v_{acc_y} v_{acc_z} \\ v_{acc_z} v_{acc_x} & v_{acc_z} v_{acc_y} & v^2_{acc_z} \end{bmatrix}$$

Noise is uncorrelated [61]:

$$R = E\begin{bmatrix} v^2{}_{acc_x} & 0 & 0 \\ 0 & v^2_{acc_y} & 0 \\ 0 & 0 & v^2_{acc_z} \end{bmatrix}$$

Stage#02: Position and Wind Estimation

$$x = \begin{bmatrix} P_N \\ P_E \\ W_N \\ W_E \end{bmatrix}, u = \begin{bmatrix} \psi \\ V_{air} \end{bmatrix}, y = \begin{bmatrix} GPS_N \\ GPS_E \\ GPS_{Velocity} \\ GPS_{Heading} \end{bmatrix}$$

$$\begin{bmatrix} \dot{P}_N \\ \dot{P}_E \\ \dot{W}_N \\ \dot{W}_E \end{bmatrix} = \begin{bmatrix} V_{air}\cos\psi - W_N \\ V_{air}\sin\psi - W_E \\ 0 \\ 0 \end{bmatrix}$$

Process Covariance Matrix is given as follows:

$$Q = E\left(ww^T\right)$$

where,

$$w = \begin{bmatrix} w_{P_N} \\ w_{P_E} \end{bmatrix}$$

and

$$w^T = \begin{bmatrix} w_{P_N} & w_{P_E} \end{bmatrix}$$

Noise is uncorrelated:

Output equations by $Q = E\begin{bmatrix} w_{P_N}^2 & 0 \\ 0 & w_{P_E} \end{bmatrix}$ inertial estimator:

$$h(\hat{x}, u) = \begin{bmatrix} GPS_N \\ GPS_E \end{bmatrix} = \begin{bmatrix} P_N \\ P_E \end{bmatrix}$$

Linearization through Jacobian [61]:

$$\frac{\partial h(\hat{x}, u)}{\partial x} = \begin{bmatrix} 1 & 0 \\ 0 & 1 \end{bmatrix}$$

Measurement Covariance Matrix is given as follows:

$$R = E(vv^T)$$

Where,

$$v = \begin{bmatrix} GPS_N \\ GPS_E \\ GPS_{Velocity} \\ GPS_{Heading} \end{bmatrix}$$

$$v^T = \begin{bmatrix} GPS_N & GPS_E & GPS_{Velocity} & GPS_{Heading} \end{bmatrix}$$

So

$$R = E\begin{bmatrix} GPS_N^2 & GPS_N GPS_E & GPS_N GPS_{Velocity} & GPS_N GPS_{Heading} \\ GPS_E GPS_N & GPS_E^2 & GPS_E GPS_{Velocity} & GPS_E GPS_{Heading} \\ GPS_{Velocity} GPS_N & GPS_{VElocity} GPS_E & GPS_{Velocity}^2 & GPS_{Velocity} GPS_{Heading} \\ GPS_{Heading} GPS_N & GPS_{Heading} GPS_E & GPS_{Heading} GPS_{Velocity} & GPS_{Heading}^2 \end{bmatrix}$$

The noise is uncorrelated [61]

$$R = E\begin{bmatrix} GPS_N^2 & 0 & 0 & 0 \\ 0 & GPS_E^2 & 0 & 0 \\ 0 & 0 & GPS_{Velocity}^2 & 0 \\ 0 & 0 & 0 & GPS_{Heading}^2 \end{bmatrix}$$

5.6.3. 3 Stage Extended Kalman Filter Scheme

In this scheme, three Extended Kalman Filters [60] work independently, each imparting the information that it estimates to the stage below. This three stage filter assumes the least coupling.

Stage#01: Pitch and Roll Estimation:

First stage state variables and inputs:

$$x=\begin{bmatrix}\phi\\ \theta\end{bmatrix}, u=\begin{bmatrix}p\\ q\\ r\\ V_{air}\end{bmatrix}, y=\begin{bmatrix}acc_x\\ acc_y\\ acc_z\end{bmatrix}$$

The Kalman Filter time update includes updating the states with the state update equation, and a calculation of the linearized state equations for the update of the filter covariance matrix [61].

$$\dot{x}=\begin{bmatrix}\dot{\phi}\\ \dot{\theta}\end{bmatrix}=f(x,u)=\begin{bmatrix}p+q\sin\phi\tan\theta+r\cos\phi\tan\theta\\ q\cos\phi+r\sin\phi\end{bmatrix}$$

$$A=\frac{\partial f(\hat{x},u)}{\partial x}=\begin{bmatrix}q\cos\phi\tan\theta-r\sin\phi\tan\theta & \frac{q\sin\phi+rxos\phi}{\cos^2\theta}\\ -q\sin\phi+r\cos\phi & 0\end{bmatrix}$$

The output equations for the attitude estimator are shown below:

$$h(\hat{x},u)=\begin{bmatrix}\frac{V_{air}q\sin\theta}{g}+\sin\theta\\ \frac{V_{air}(r\cos\theta-p\sin\theta)}{g}-\cos\theta\sin\phi\end{bmatrix}$$

$$h(\hat{x},u)=\begin{bmatrix}0 & \frac{V_{air}q\cos\theta}{g}+\cos\theta\\ -\cos\theta\cos\phi & \frac{-V_{air}(r\sin\theta+p\cos\theta)}{g}+\sin\theta\sin\phi\end{bmatrix}$$

Process Covariance Matrix is given as follows:

$$Q=E(ww^T)$$

where,

$$w=\begin{bmatrix}w_\phi\\ w_\theta\end{bmatrix}$$

$$w^T = \begin{bmatrix} w_\phi & w_\theta \end{bmatrix}$$ and

Noise is uncorrelated [42]:

$$Q = E\begin{bmatrix} w_\phi^2 & 0 \\ 0 & w_\theta^2 \end{bmatrix}$$

Measurement Covariance Matrix is given as follows:

$$R = E(vv^T)$$

Where,

$$v = \begin{bmatrix} v_{acc_x} \\ v_{acc_y} \end{bmatrix}$$

and

$$v^T = \begin{bmatrix} v_{acc_x} & v_{acc_y} \end{bmatrix}$$

So

$$R = E\begin{bmatrix} v^2{}_{acc_x} & v_{acc_x} v_{acc_y} \\ v_{acc_y} v_{acc_x} & v_{acc_y}^2 \end{bmatrix}$$

Noise is uncorrelated

$$R = E\begin{bmatrix} v^2{}_{acc_x} & 0 \\ 0 & v_{acc_y}^2 \end{bmatrix}$$

Stage#02: Heading Estimation

$$x = [\psi], u = \begin{bmatrix} \phi \\ \theta \\ q \\ r \end{bmatrix}, y = \begin{bmatrix} acc_z \end{bmatrix}$$

$$\dot{\psi} = f(x,u) = q\frac{\sin\phi}{\cos\theta} + r\frac{\cos\phi}{\cos\theta}$$

$$A = \frac{\partial f(\hat{x},u)}{\partial x} = 0$$

Process Covariance Matrix [61] is given as follows:

$$Q = E\left(ww^T\right)$$

where,

$$w = \left[w_\psi\right]$$

and

$$w^T = \left[w_\psi\right]$$

Noise is uncorrelated [62]:

$$Q = E\left[w_\psi^2\right]$$

Output equations by heading estimator:

$$h(\hat{x},u) = \left[\frac{-V_{air}q\cos\theta}{g} - \cos\theta\cos\phi\right]$$

Linearization through jacobian method [62]:

$$H_k = \frac{\partial h(\hat{x},u)}{\partial x} = [0]$$

Measurement Covariance Matrix [63] is given as follows:

$$R = E(vv^T)$$

where, $v = \left[acc_z\right]$

and

$$v^T = [acc_z]$$

Noise is uncorrelated [61]:

$$R = E[acc_z^2]$$

Stage#03: Position and Wind Estimation:

$$x = \begin{bmatrix} P_N \\ P_E \\ W_N \\ W_E \end{bmatrix}, u = \begin{bmatrix} \psi \\ V_{air} \end{bmatrix}, y = \begin{bmatrix} GPS_N \\ GPS_E \\ GPS_{Velocity} \\ GPS_{Heading} \end{bmatrix}$$

$$\begin{bmatrix} \dot{P}_N \\ \dot{P}_E \\ \dot{W}_N \\ \dot{W}_E \end{bmatrix} = \begin{bmatrix} V_{air}\cos\psi - W_N \\ V_{air}\sin\psi - W_E \\ 0 \\ 0 \end{bmatrix}$$

Process Covariance Matrix

Process Covariance Matrix [62] is given as follows:

$$Q = E(ww^T)$$

where,

and

$$w^T = \begin{bmatrix} w_{P_N} & w_{P_E} \end{bmatrix}$$

Noise is uncorrelated [61]:

$$Q = E\begin{bmatrix} w_{P_N}^2 & 0 \\ 0 & w_{P_E} \end{bmatrix}$$

Output equations by inertial estimator:

$$h(\hat{x},u)=\begin{bmatrix} GPS_N \\ GPS_E \\ GPS_{velocity} \\ GPS_{heading} \end{bmatrix}=\begin{bmatrix} P_N \\ P_E \\ \sqrt{V_{air}^2+2V_{air}\left(W_N\cos\psi+W_E\sin\psi\right)+\left(W_N^2+W_E^2\right)} \\ \tan^{-1}\left(\dfrac{V_{air}\sin\psi+W_E}{V_{air}\cos\psi+W_N}\right) \end{bmatrix}$$

Linearization through jacobian [61]:

$$\frac{\partial h(\hat{x},u)}{\partial x}=\begin{bmatrix} 1 & 0 & 0 & 0 \\ 0 & 1 & 0 & 0 \\ 0 & 0 & 0 & 0 \\ 0 & 0 & 0 & \dfrac{1}{\dfrac{\left(V_{air}\cos\psi+W_E\right)-\left(V_{air}\sin\psi+W_W\right)}{\left(V_{air}\cos\psi\right)+W_E}\cdot\dfrac{\left(V_{air}\sin\psi+W_E\right)^2}{\left(V_{air}\cos\psi+W_E\right)^2}+1} \end{bmatrix}$$

Measurement Covariance Matrix [62] is given as follows:

$$R=E(vv^T)$$

Where,

$$v=\begin{bmatrix} GPS_N \\ GPS_E \\ GPS_{Velocity} \\ GPS_{Heading} \end{bmatrix}$$

and

$$v^T=\begin{bmatrix} GPS_N & GPS_E & GPS_{Velocity} & GPS_{Heading} \end{bmatrix}$$

So

$$R=E\begin{bmatrix} GPS_N^2 & GPS_NGPS_E & GPS_NGPS_{Velocity} & GPS_NGPS_{Heading} \\ GPS_EGPS_N & GPS_E^2 & GPS_EGPS_{Velocity} & GPS_EGPS_{Heading} \\ GPS_{Velocity}GPS_N & GPS_{VElocity}GPS_E & GPS_{Velocity}^2 & GPS_{Velocity}GPS_{Heading} \\ GPS_{Heading}GPS_N & GPS_{Heading}GPS_E & GPS_{Heading}GPS_{Velocity} & GPS_{Heading}^2 \end{bmatrix}$$

The noise is uncorrelated [61]

$$R=E\begin{bmatrix} GPS_N^2 & 0 & 0 & 0 \\ 0 & GPS_E^2 & 0 & 0 \\ 0 & 0 & GPS_{Velocity}^2 & 0 \\ 0 & 0 & 0 & GPS_{Heading}^2 \end{bmatrix}$$

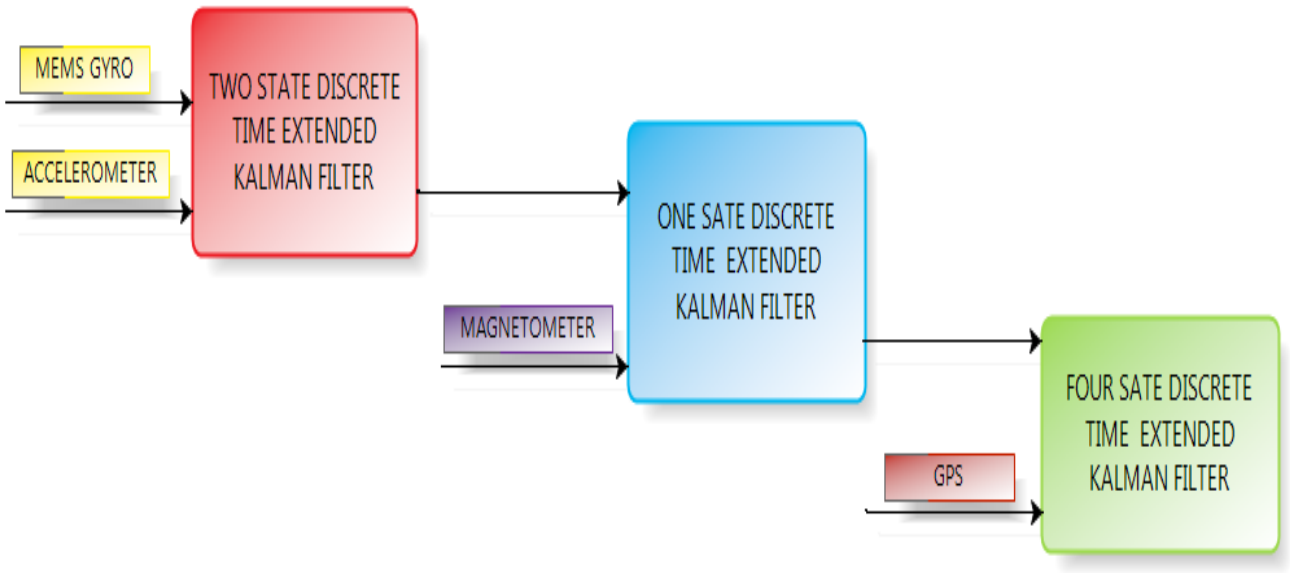

Figure 28: Three Stage Cascaded Scheme

Chapter 6

6. RESULT AND ANALYSIS

The output of the on-board sensors is mathematically modeled and filtered with the help of Single Seven State Discrete Time Extended Kalman Filtering. The inputs to the filter were angular rates in three directions and velocity of air. The state variables were phi, theeta, psi, Pn, Pe and Wn, We. The measurement variables were acceleration in all 3 directions and components of GPS. Coding was performed to analyze the filter's response to variable inputs and also to compare the 3 types of filters p, q and r were varied individually in the trajectory and graphs plotted of state variables and measured variables for different types of filters.

The actual and estimated results are compared as following:

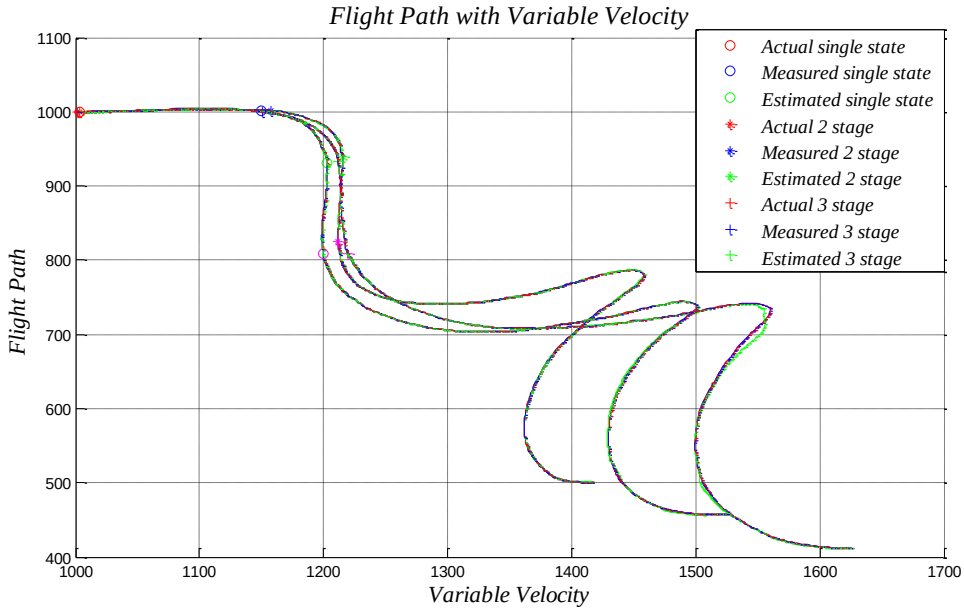

Figure 29: Result 01

The curves shown are that of the flight path of the FMAV through the number of iterations. The values of height as calculated using velocity and the phi angle, the

eastern and the northern position were used to calculate a resultant so as to define the flight path of the aircraft. The FMAV flies straight without nay changes in its orientation for a while before it takes a deep dive, corresponding to the decrease in pitch angle as seen by the plot of the pitch angle, and then levels up again as the pitch angle levels. The curves in the flight path depict the variations in roll and yaw angle that take place during the flight time, owing to variations in velocity. For each filter, the actual and measured flight path almost overlap while the estimated curve shows some inaccuracies, which is primarily due to the errors involved in several calculations that go into the estimation process. The slight difference in flight paths of the three filters could be associated with the different sensitivity levels of each filter that hinder the estimation of steep gradients.

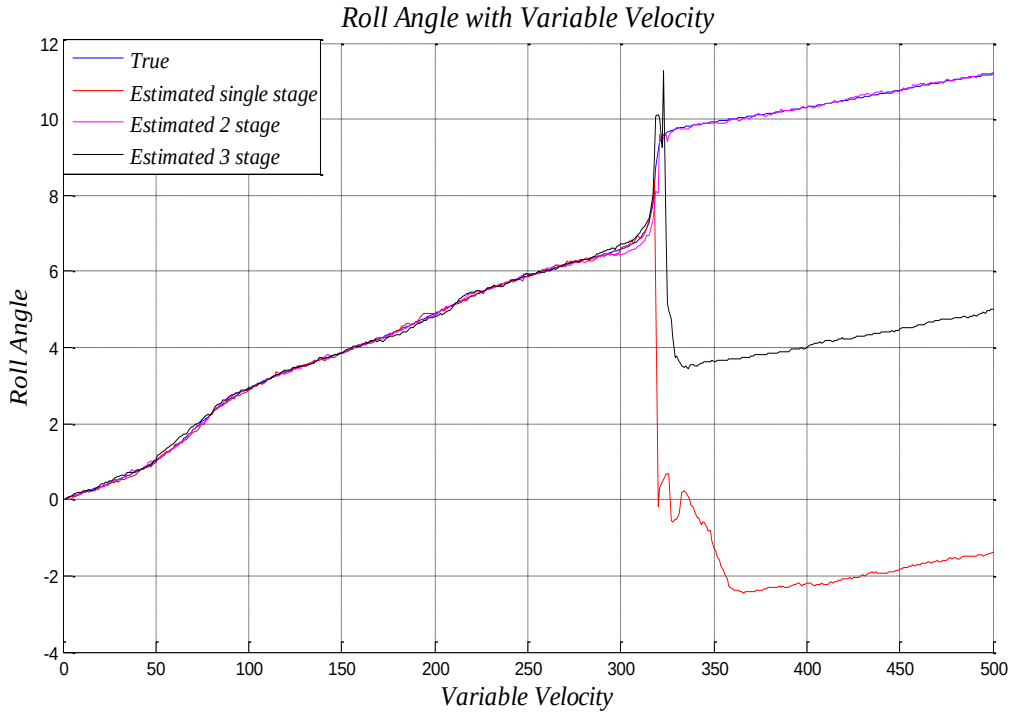

Figure 30: Result 02

The plots shown are those of the state variable phi as it changes with variable velocity. The curves are plotted against the number of iterations, since the

variation in velocity was not unidirectional, and was time/iteration dependant. The roll angle keeps on increasing as velocity first decreases and then increases. The variation in roll angle is huge as velocity varies. The variation in roll angle is not owing to variation in velocity; rather it is due to the constant positive angular rate

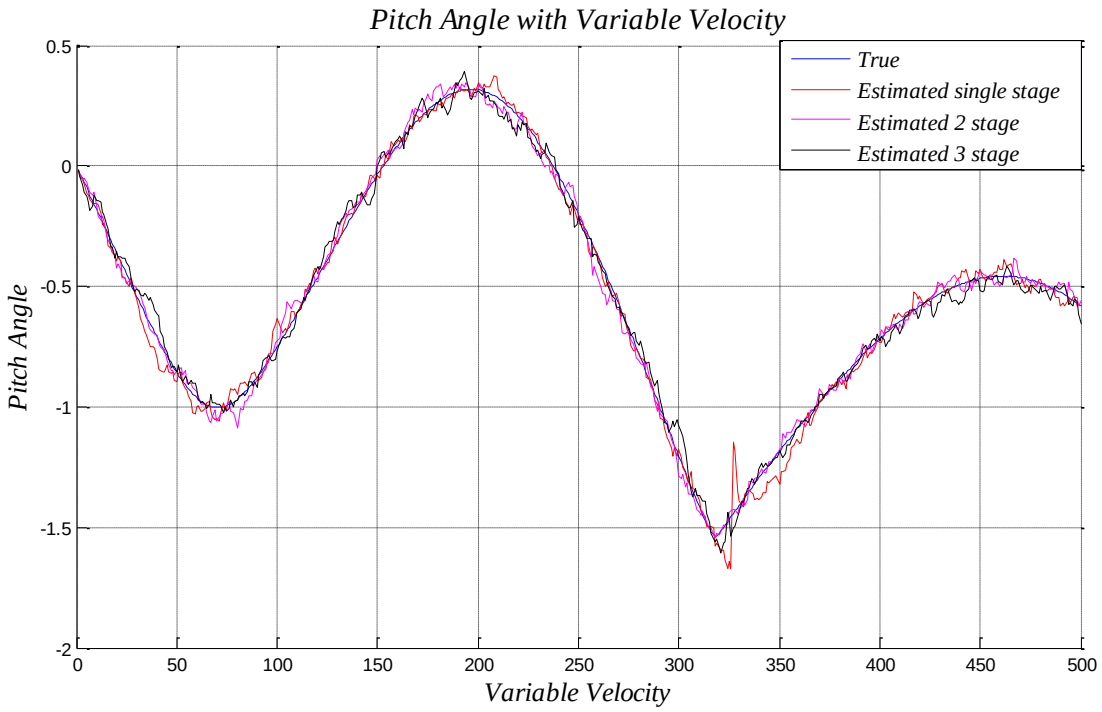

Figure 31: Result 03

about the x axis (p). The roll rate is high enough for minor changes in velocity to be completely ignored. There is however a surge in roll angle between iterations 300 and 350, owing to a surge in velocity. Comparison between the three types of filters shows that it is the first stage Kalman Filter that is the most accurate. The second and third stage tends to fall apart at certain stages, owing to the increased calculation errors involved with a large number of steps.

The plots shown are those of the state variable theeta as it changes with variable velocity. Pitch angle shows a sinusoidal type curve with trend dependent on how much one factor dominates another. Since the pitch rate is negative as velocity first decreases and then increases, the curves show a varied unsymmetrical sinusoidal pattern. As far as the comparison is concerned, all filters are equally good at tracking the trajectory, though owing to the negative value of pitch angle and nonlinear variation in velocity, the filters show some minor limited oscillations.

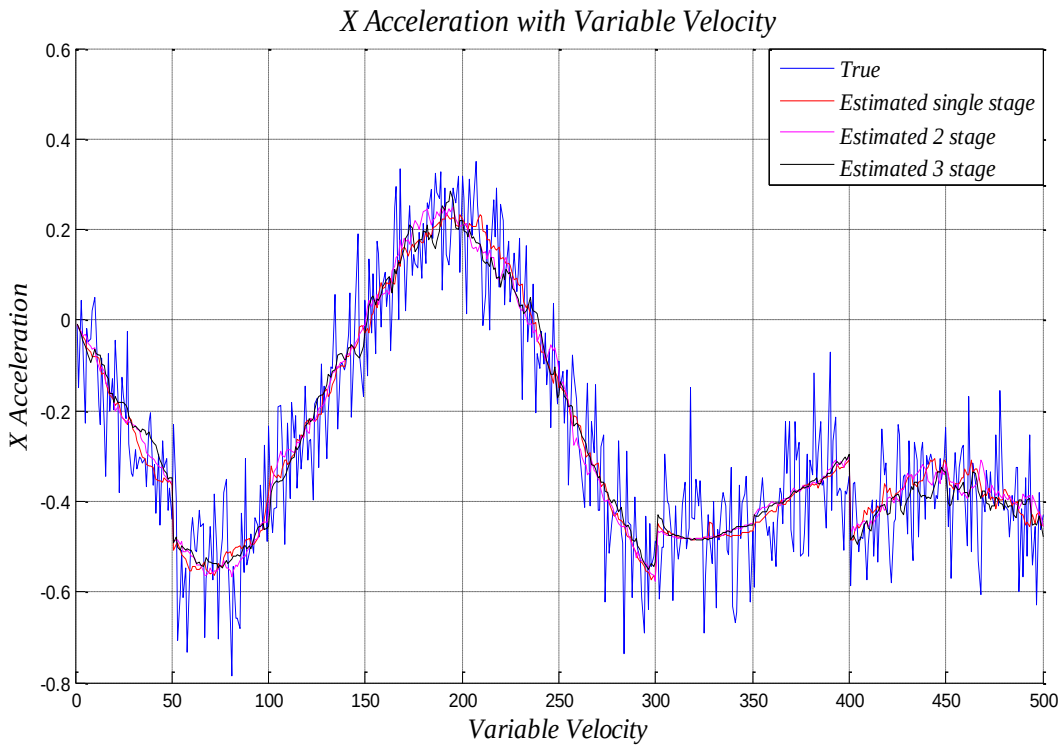

Figure 32: Result 04

The plots shown are those of yaw angle as it changes with variable velocity. The yaw angular rate, as specified, is not very large and therefore the effect of velocity is more

pronounced as compared to any other factor as there were in the case of roll angle and pitch angle. The variation is consistent with the variation of velocity except in iterations where the variation in velocity is not much. All Filters fail to follow the trend very accurately till the end, owing probably to the small value of the yaw angular rate. It is however, the single stage Kalman Filter that follows the trend the most.

The plots shown are those of the measurement variable acceleration in the x direction with variable velocity. The trajectory, as plotted shows many oscillations due to the pronounced effect of process and measurement noise. The variation of acceleration is as per the factors that contribute to the value, i.e. linear acceleration and acceleration due to centripetal forces. All filters show good response, as the noise levels are reduced with all filters. The 3rd stage filter is the most inaccurate amongst the three when following the trend, though it is very accurate itself.

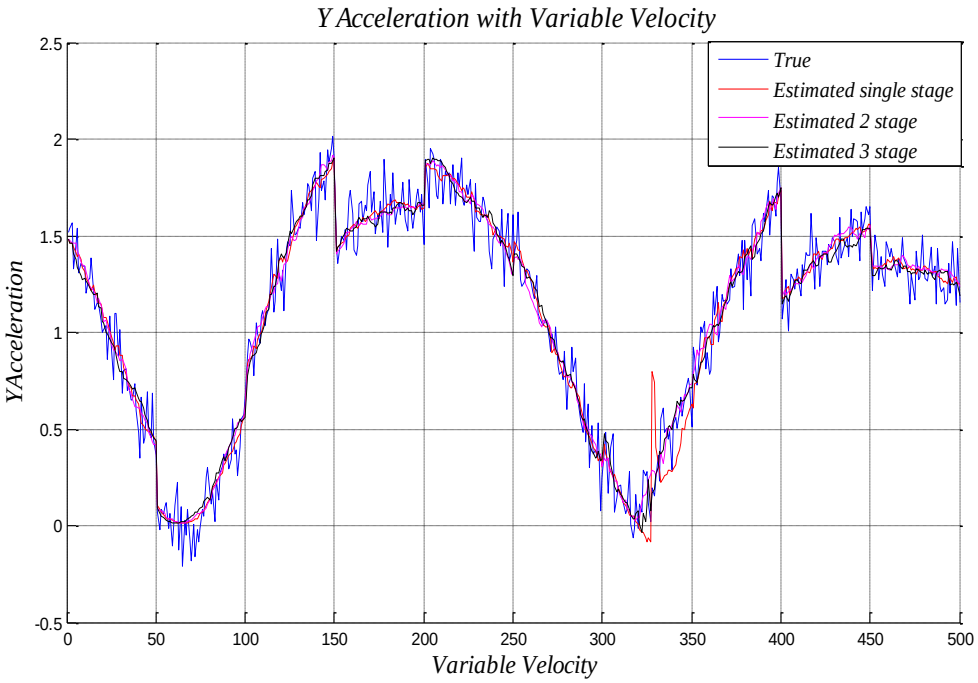

Figure 33: Result 05

The plots shown are those of the measurement variable acceleration in the y direction with variable velocity. The trends of acceleration follow the same trend as expected with variation in velocity and the value of pitch angular rate as specified. Noise in the trajectory or actual value is quite a lot owing to the fact that it combines process noise with measurement noise. It is the filters, though, that reduce the noise to a great extent. All the filters are equally good in that respect.

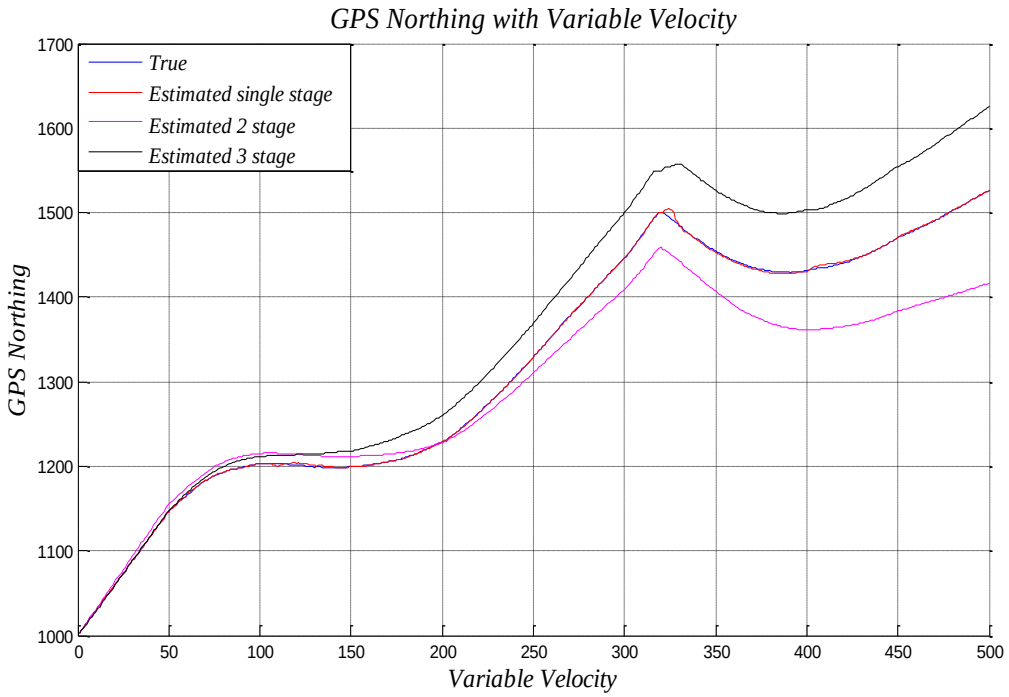

Figure 34: Result 06

The plots shown are those of GPS in the north direction which is also a measurement variable. The value of GPS keeps increasing with variation in velocity because of the continuous increase in roll angle witnessed before. The FMAV continues its flight north bound owing to a positive roll angular rate despite the negative variation in velocity at times. The first stage Kalman Filter plots the trajectory most accurately whereas the 2 stage and 3 stage Kalman Filters lag behind in this regard.

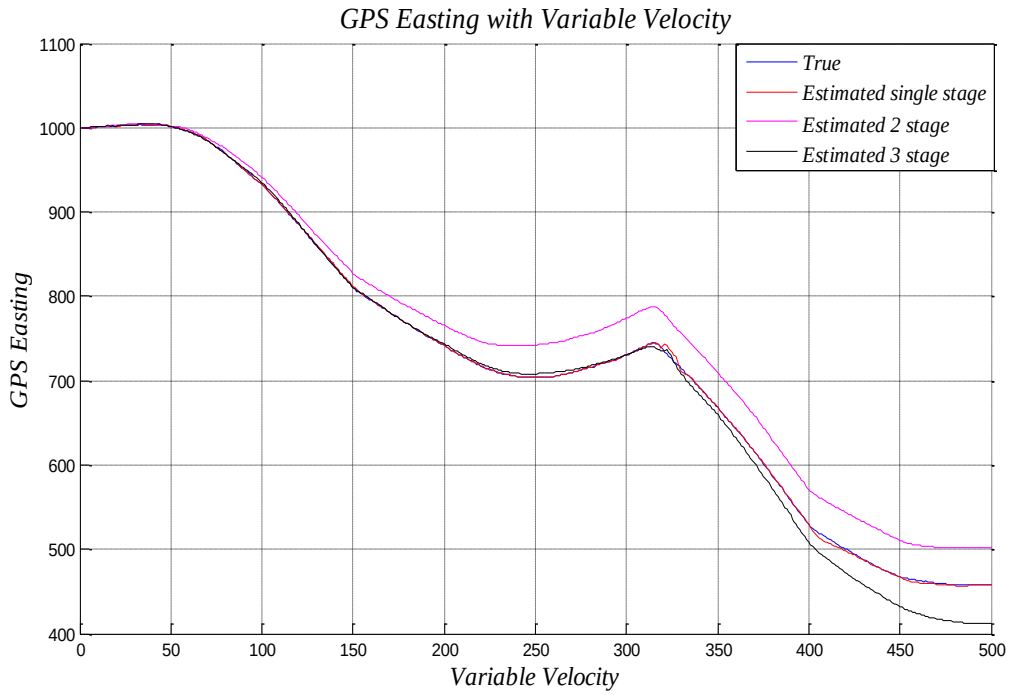

Figure 35: Result 07

The plots shown are those of GPS in the eastern direction. The value of GPS in the eastern direction keeps decreasing with subsequent iterations, which is owing to the negative pitch angular rate and very small yaw angle that has almost no effect on the trends shown. The FMAV continues its flight westwards owing to the variations in the pitch angle, velocity and roll angle. Single stage Kalman Filter is the most accurate whereas the other two types of filters lag behind in one respect or the other.

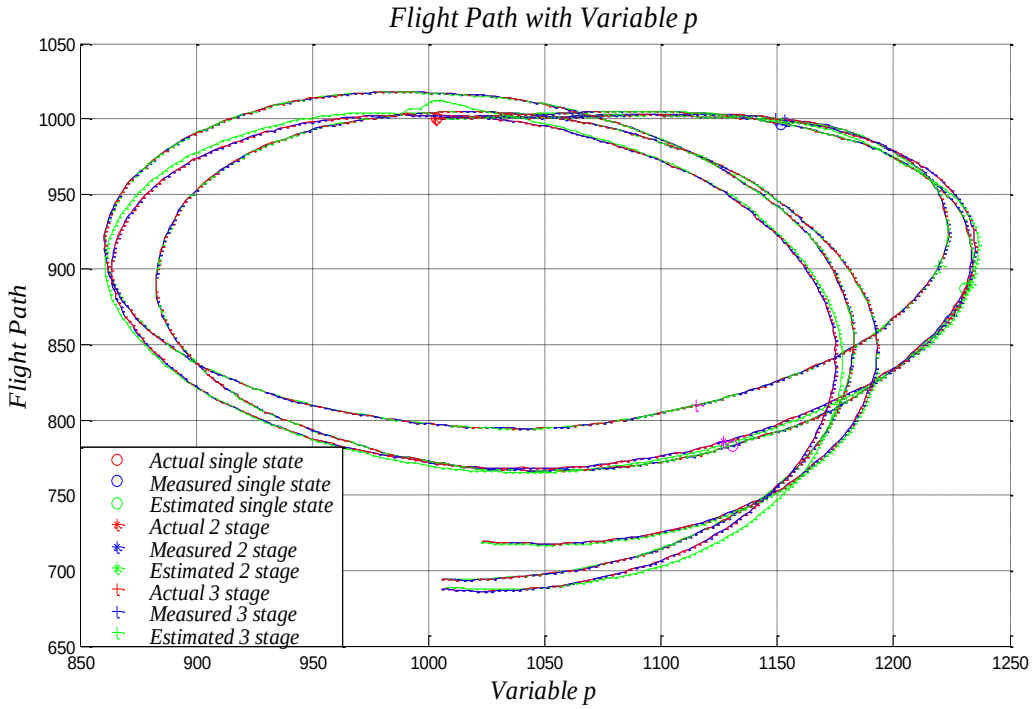

Figure 36: Result 08

The curves shown are that of the flight path of the FMAV. The values of height as calculated using velocity and the phi angle, the eastern and the northern position were used to calculate a resultant so as to define the flight path of the aircraft. The curves are very circuitous, i.e., the FMAV keeps moving around in circles, retracing its path all the while. This type of a flight path can be explained by the shape of the state variables' curves. With a variable p, both roll angle and pitch angle show an oscillatory response, whereas yaw angle keeps decreasing throughout the flight time. As roll and pitch angle both keep repeating their values, the aircraft banks as well as pitches in the same fashion again and again, and thus generates a circuitous path. This circular movement is also verified by the plots of GPS, which are also oscillatory in nature. As in other cases, the three types of filters show slight differences in their flight paths owing to the different levels of sensitivity involved.

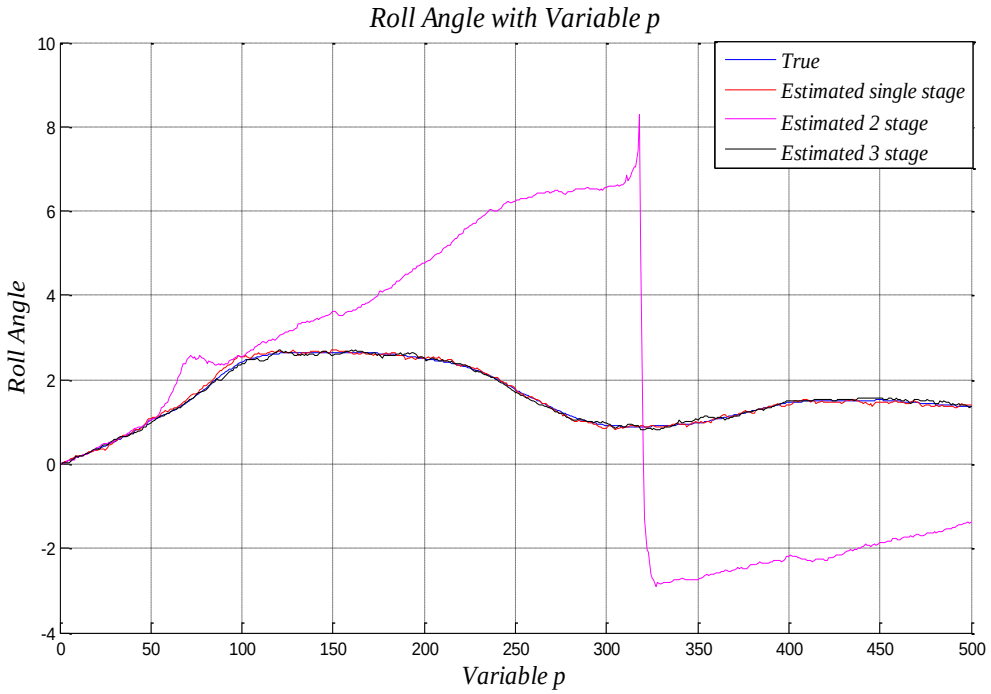

Figure 37: Result 09

The plots shown are that of the roll angle with variable p against the number of iterations. The variation of roll angle as shown is owing to the oscillatory variation in the angular rate itself. Because the angle being plotted and the input variation is about the same axis, the trends conform to the variation in input values. The state estimates produced by the filters show some vibration but overall all the filters are pretty accurate.

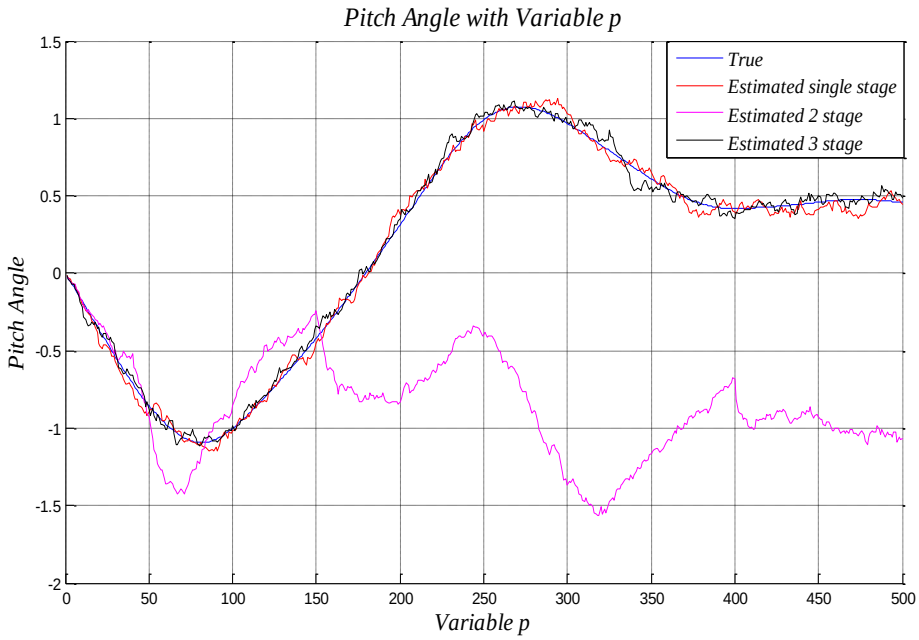

Figure 38: Result 10

The plots shown are that of the pitch angle with variable p against number of iterations. The variation in the pitch angle is more uniform, though sinusoidal as was the variation in roll angle. It is smoother because the lateral non uniform variations have little or no effect on the longitudinal dynamics. The variation, however, is due to the indirect (transformation between inertial and earth frame) effect of the angular rate (p) in the longitudinal dynamics. All the filters are equally good in estimating the state.

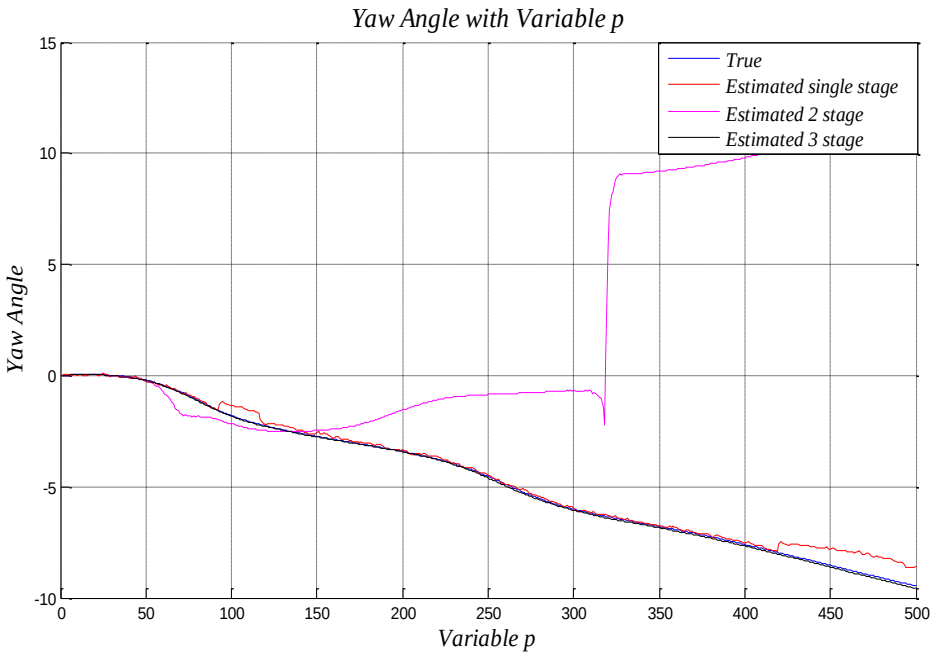

Figure 39: Result 11

The plots shown are that of the yaw angle with variable p against number of iterations. Yaw angle keeps decreasing although there is a bidirectional change in the lateral dynamics via the input. That is owing to the inverse relationship (through cos function) that state variable yaw angle has with the roll and pitch angle estimated before. Therefore, as roll and pitch angle increase, the FMAV yaws towards the negative side, contributing to the westward drift of the FMAV. The single stage filter is not as clean in its estimation of the state as are the other two types.

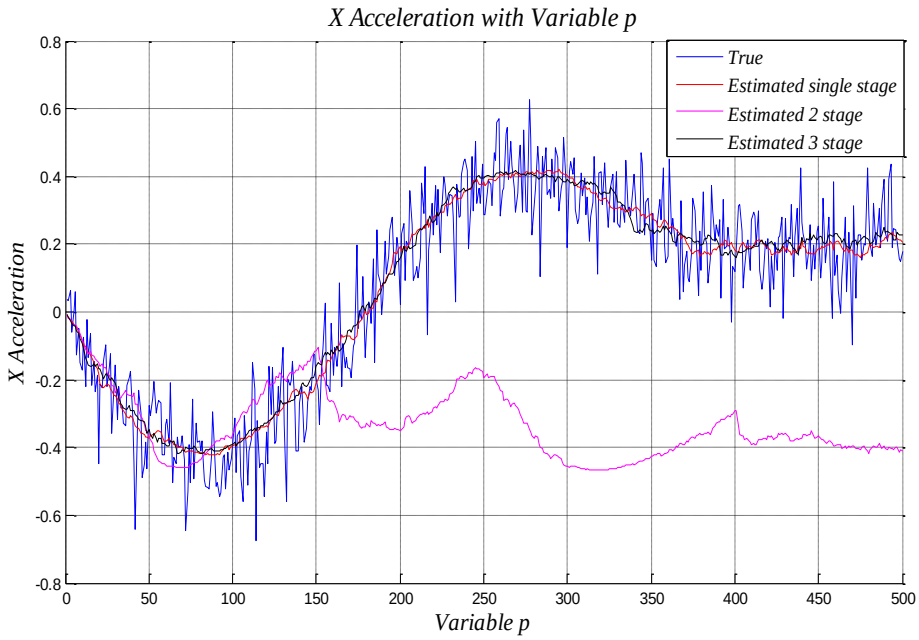

Figure 40: Result 12

The plots shown are that of the measurement variable acceleration in the x direction with variable p against the number of iterations. Acceleration in the x direction, though, not physically related to the angular rate in the x direction, is related indirectly through the effect of centripetal acceleration of the earth's rotation on the FMAV. And therefore, the variation as shown. The variation is almost similar to that of the pitch angle, which makes sense as both fall in the longitudinal dynamics of the aircraft. Single stage Kalman Filter and 3 stage Kalman Filter are the best in noise reduction and precise estimation of the measurement variable, whereas the 2 stage filter, though effective in curtailing noise, does not follow the actual curve accurately.

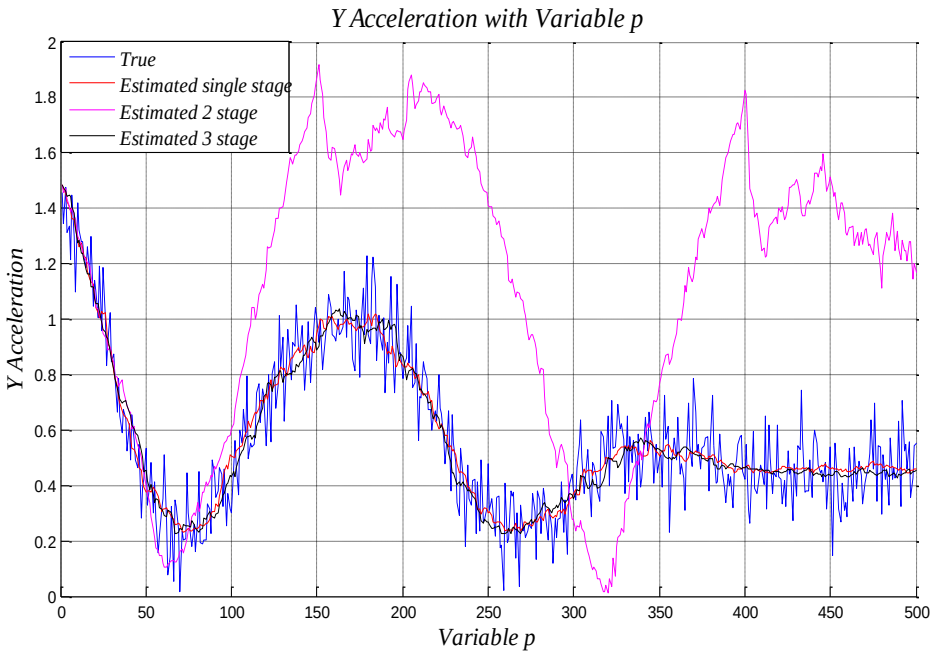

Figure 41: Result 13

The plots shown are that of the measurement variable acceleration in the y direction with variable p against number of iterations. The acceleration in the y direction is directly affected by changes in p, and therefore the non-uniform variations in the value. The noise in the actual curve, owing to the inclusion of random noise; as it is in measuring instruments, is curtailed to a large extent by the filters. The performance of all the filters is equally good.

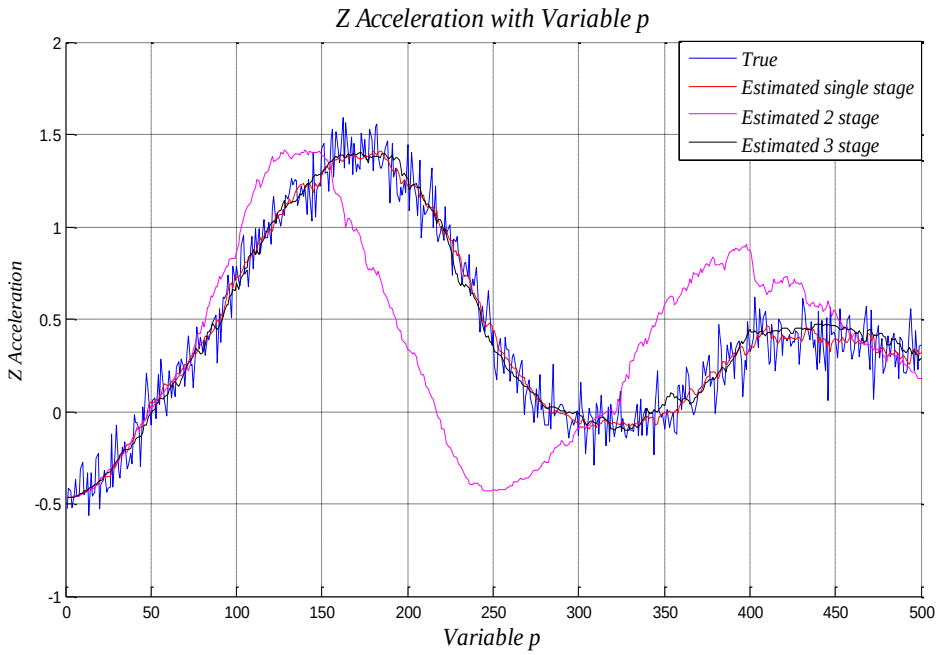

Figure 42: Result 14

The plots shown are that of the measurement variable acceleration in the z direction with variable p against number of iterations. The variable, being a part of the longitudinal dynamics, is not affected directly by the changes in lateral dynamics, but is affected owing to the indirect effect of p through the roll angle that it affects. The trend however, is similar to that of the acceleration in x direction and the pitch angle, as expected. The filters perform very well, tracking the actual measurement very accurately.

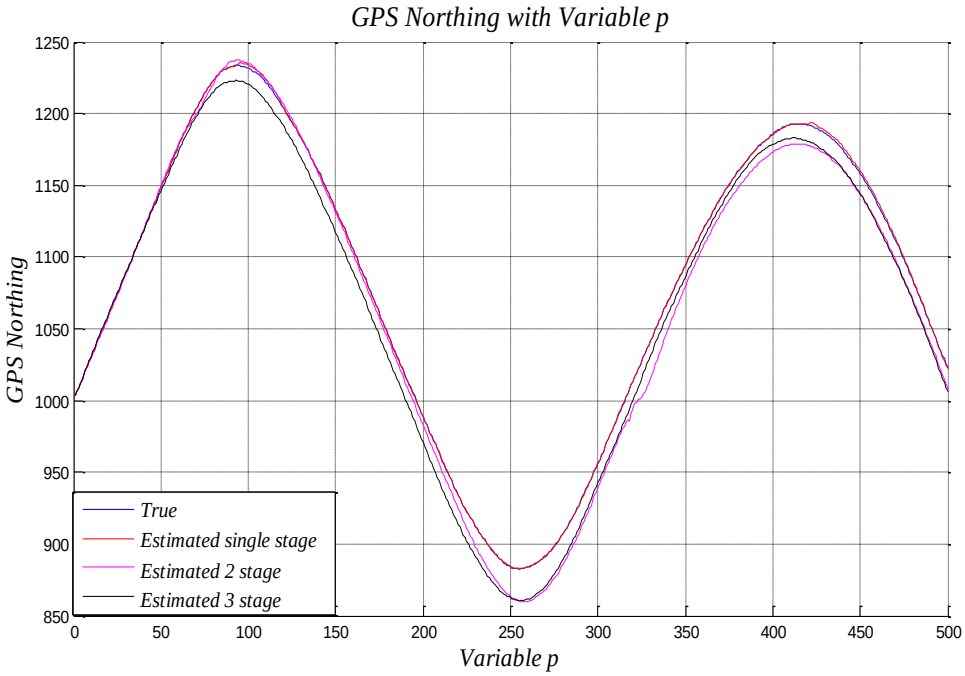

Figure 43: Result 15

The plots shown are that of the measurement variable GPS in the northern direction. The FMAV tends to oscillate in its flight path, owing to the continuous variation in its roll angle and the angular rate associated with that axis. It is because of the oscillatory change in direction of the FMAV due to variable p that the FMAV seems to go due north at some point and due south at some other point. The 3 stage filter, though, following the same trend, is way off track when estimating the value of GPS. This might be due to the compounded effect of uncertainties carried into the third stage where GPS is measured. Single stage Kalman Filter is the most accurate.

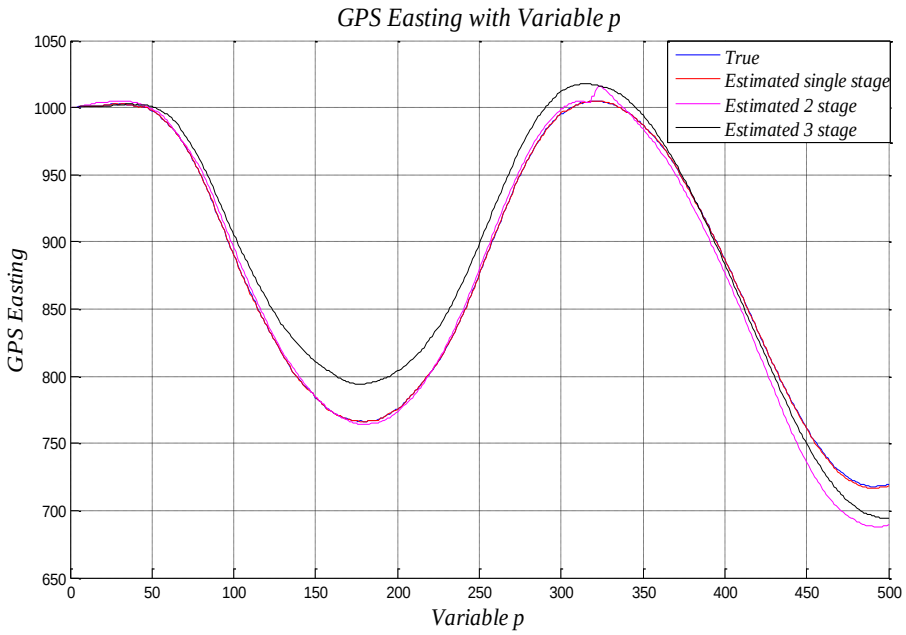

Figure 44: Result 16

The plots shown are that of the measurement variable GPS in the eastern direction with variable p against number of iterations. It is due to the oscillatory nature of all the angles estimated that the aircraft has both westward and eastward directions at separate points in time. The estimates of 2 stage and 3 stage filters are not as accurate as that of the single stage owing the higher number of steps involved.

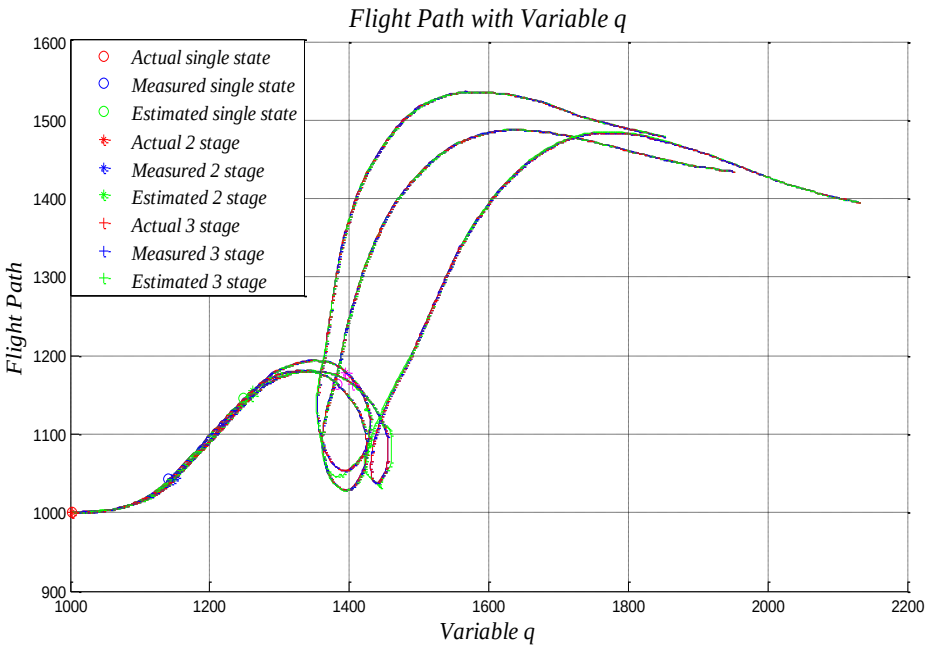

Figure 45: Result 17

The curves shown are that of the flight path as estimated by the three types of curves. The values of height as calculated using velocity and the phi angle, the eastern and the northern position were used to calculate a resultant so as to define the flight path of the aircraft. The FMAV, with variable q, climbs initially and then moves dives into a loop and recovers thereafter to continue with its climb. It takes a smooth dive to level its path in the end. The flight path can be explained by the ever increasing pitch angle, and slight kinks in the yaw and roll angle, that lead to the loop in the middle. The results can also be verified by the GPS curves. The value of GPS in the northern direction has a positive gradient except slightly in the middle where the aircraft takes a dive into the loop. Similarly, GPS in the eastern direction has a positive gradient, except in the middle where the dive into the loop reduces the value of GPS. All filters are equally good at estimating the actual trajectories.

Amongst each other, though, it is at the loop that the three diverge to a certain extent, owing to the steep gradients involved.

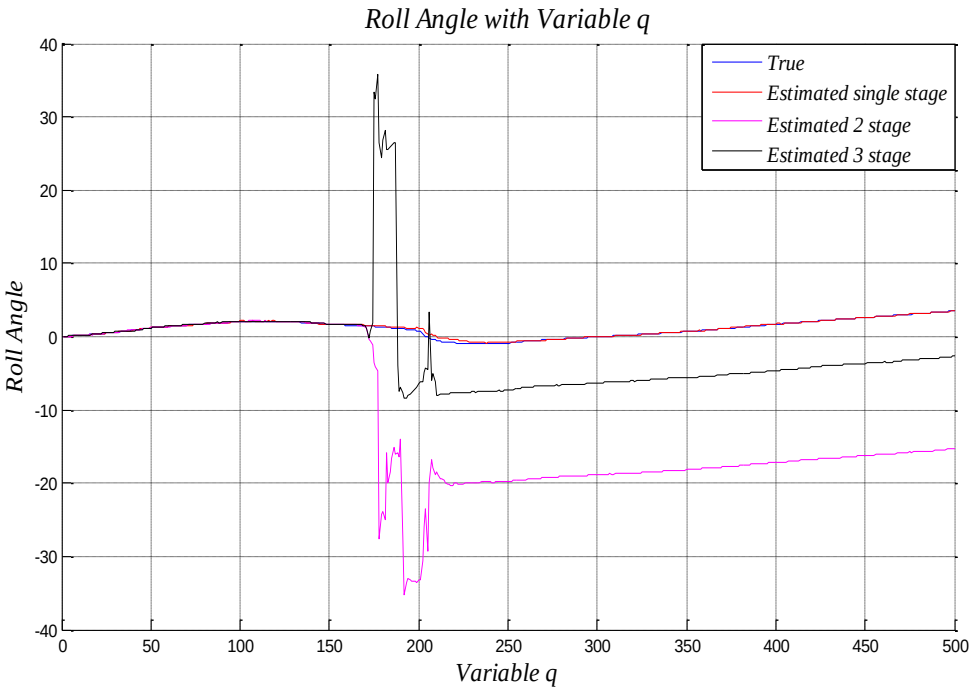

Figure 46: Result 18

The plots shown are those of the roll angle with variable pitch rate against number of iterations. Roll angle doesn't depend much on the pitch rate and therefore does not show a lot of change in its value. The little variation that it does show is owing to the indirect effect of pitch rate on lateral dynamics. Single stage Kalman Filter is the most accurate whereas 2 stage and 3 stage filter are divergent

in their estimate of the state variable. They follow the trend almost accurately but the values are quite off the actual values.

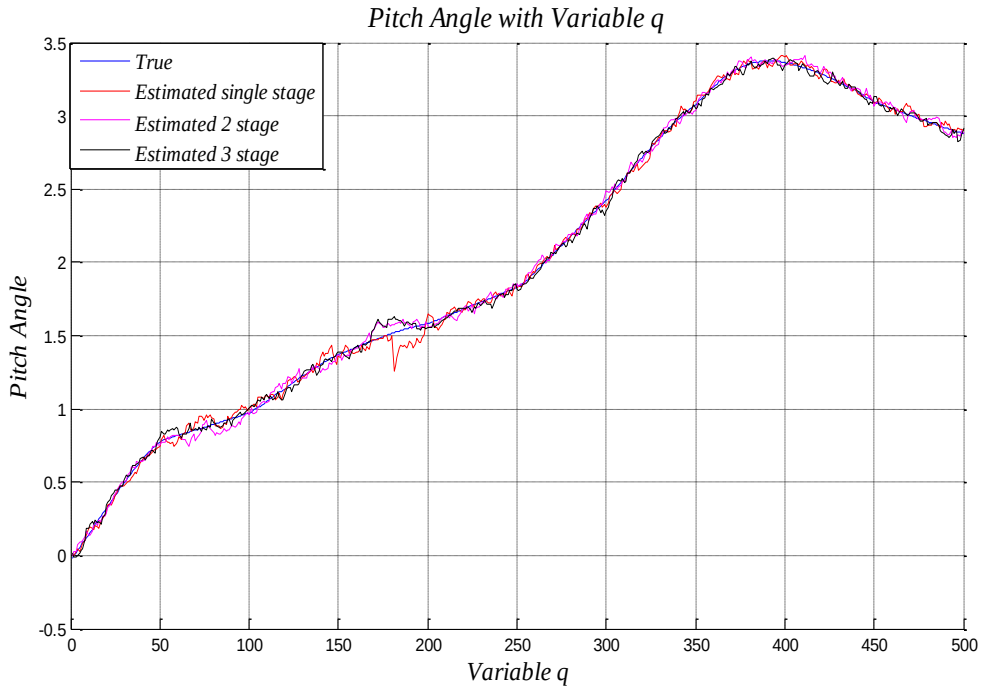

Figure 47: Result 19

The plots shown are those of pitch angle with variable pitch rate against number of iterations. The pitch angle, though, physically affected by pitch rate to a great extent, is not apparently directly affected by the pitch rate. It is, though, through the indirect iterative effect of pitch angle that causes it to continuously increase until the point where the iterative effect is overshadowed by the inverse effect of the value itself. All the filters are equally effective in estimating the state variable, though 3 stage Kalman Filter is the best in terms of noise reduction.

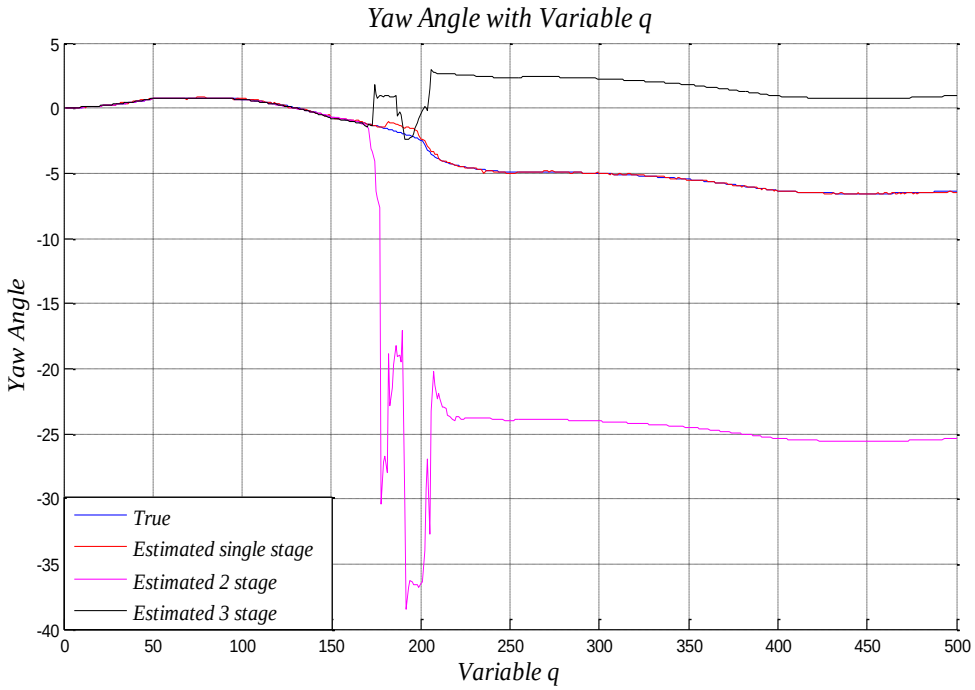

Figure 48: Result 20

The plots shown are those of yaw angle with variable pitch rate against number of iterations. Yaw angle, being a component of lateral dynamics is not affected by longitudinal dynamics. Though, through the indirect effect of centripetal acceleration, yaw angle is affected by variation in the pitch rate. It is also affected by state variables of roll and pitch angle and therefore the trend shown correspond with the trends shown by the other state variables. As before for lateral dynamics, the single stage Kalman Filter is the most accurate filter whereas the other two are not at all accurate.

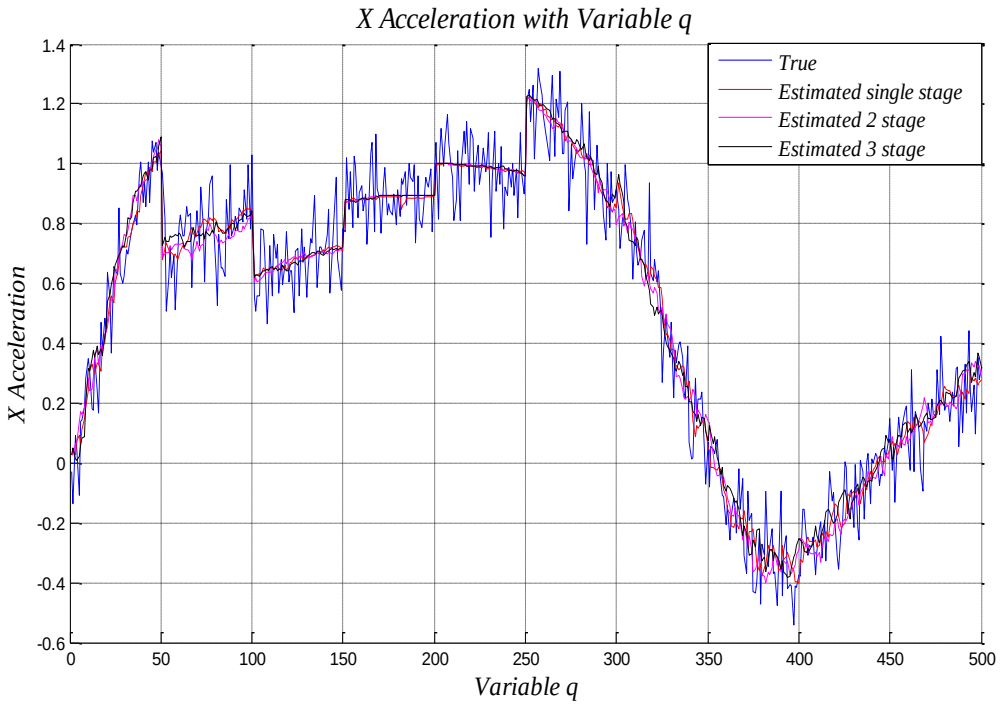

Figure 49: Result 21

The plots shown are those of measurement variable acceleration in the x direction with variable pitch rate against number of iterations. The variations in the measurement variable are in accordance with the changes in the state variables that have been estimated before. The noise in the measurement is curtailed very effectively by all the filters and all the filters follow the trend very accurately.

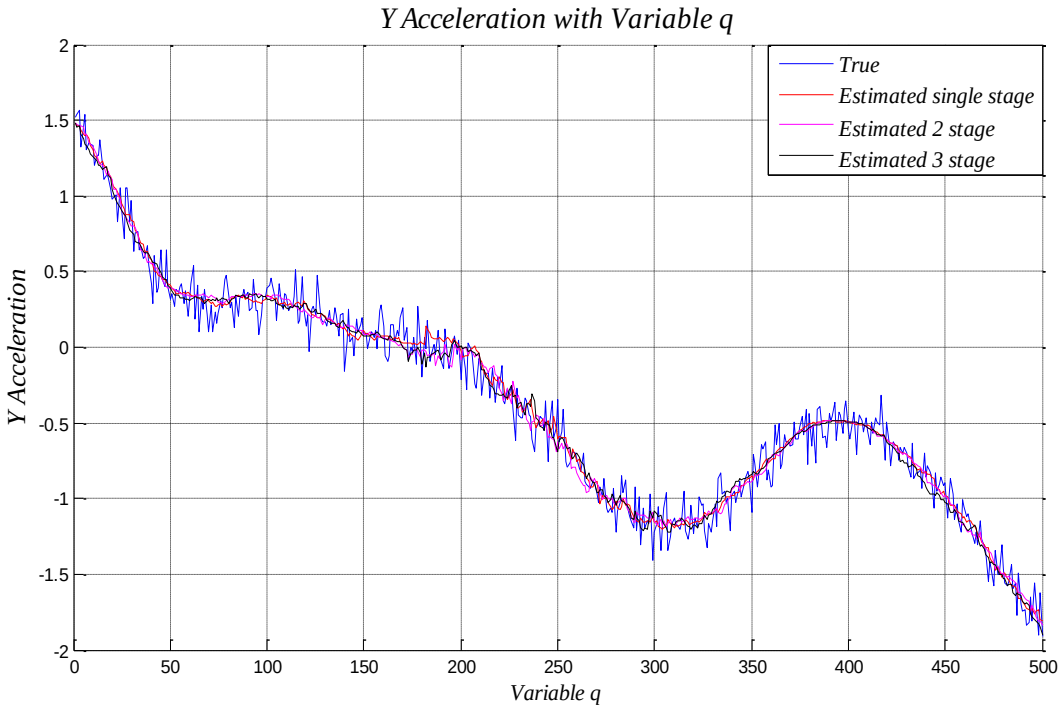

Figure 50: Result 22

The plots shown are those of measurement variable acceleration in the y direction with variable pitch rate against number of iterations. The acceleration in the y direction keeps decreasing because of the decrease in values of yaw angle and roll angle. The iterative process involved further aggravates the negative trend of the curves. The filters, as before, follow the trend very accurately and are quite effective in curtailing measurement noise.

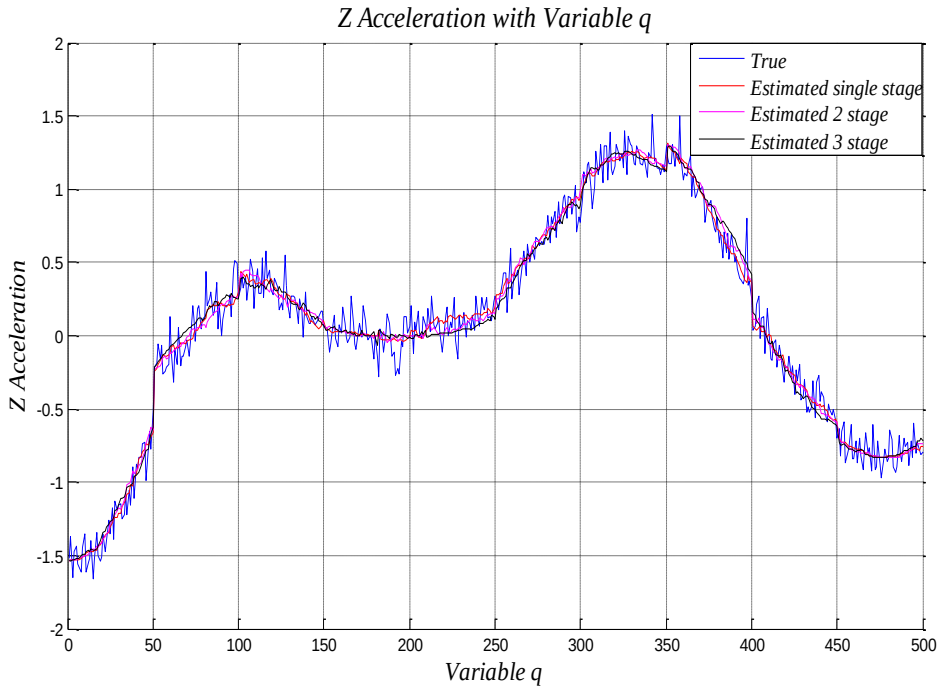

Figure 51: Result 23

The plots shown are those of measurement variable acceleration in z direction with variable pitch rate against number of iterations. The acceleration is affected by the pitch rate along with the state variables, and it is because of that that the response is quite similar to that of the first measurement variable (acceleration in x) owing to their dependence on similar factors. With changes in pitch rate, the aircraft

experiences changes in its forward and vertical accelerations. All types of filters are equally effective in tracking the measurement and curtailing noise.

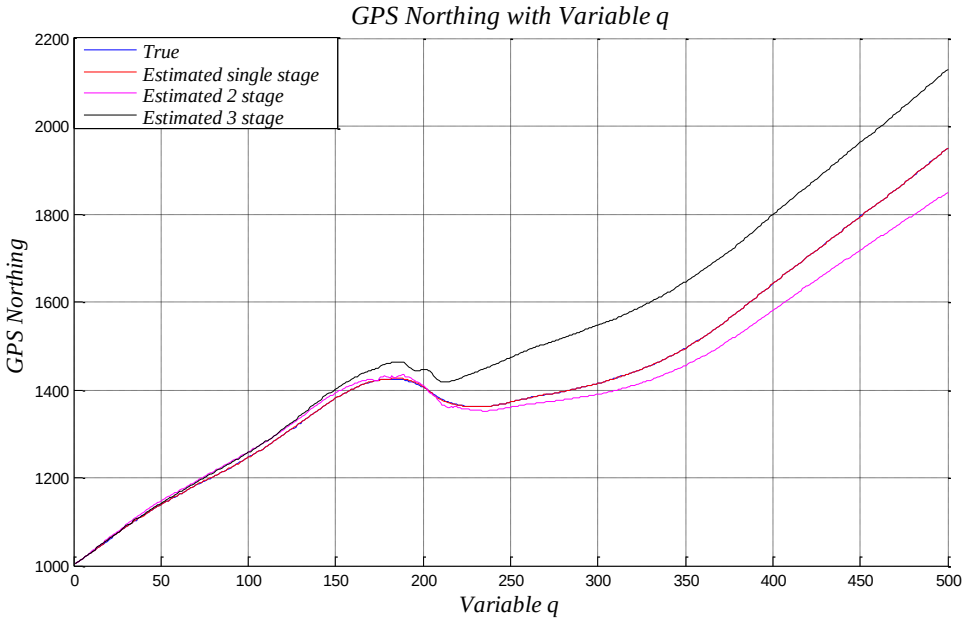

Figure 52: Result 24

The plots shown are those of GPS in the north direction with variable pitch rate against number of iterations. The curve shows an increasing trend owing to the trend shown by the pitch angle. AS the aircraft pitches upwards, it heads more towards the north. The measurement of GPS is almost noise less and so are its estimates. The single stage Kalman Filter is the most accurate, whereas the other two types, though less accurate, follow the trend almost in the similar fashion.

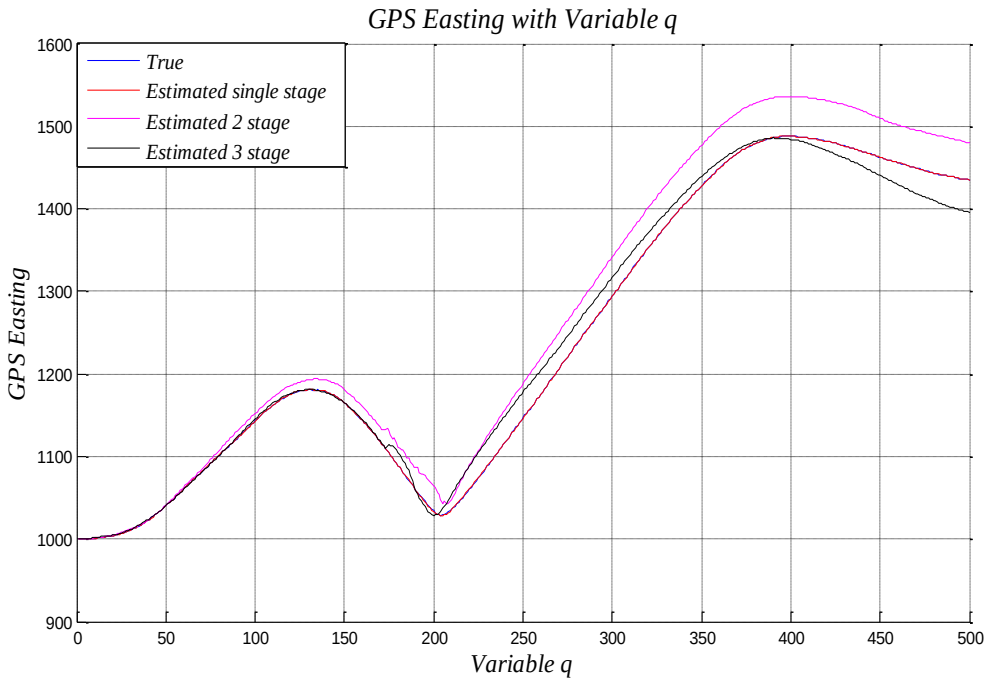

Figure 53: Result 25

The plots shown are those of GPS in the eastern direction with variable pitch against number of iterations. The curve is quite similar to that of GPS in the eastern direction owing to the opposite nature of trends shown by the roll and yaw angles, that affect the movement of the aircraft in the lateral direction and thus eastward

direction. The filters are quite accurate with all of them following the trend very closely. The single stage filter is however the most accurate.

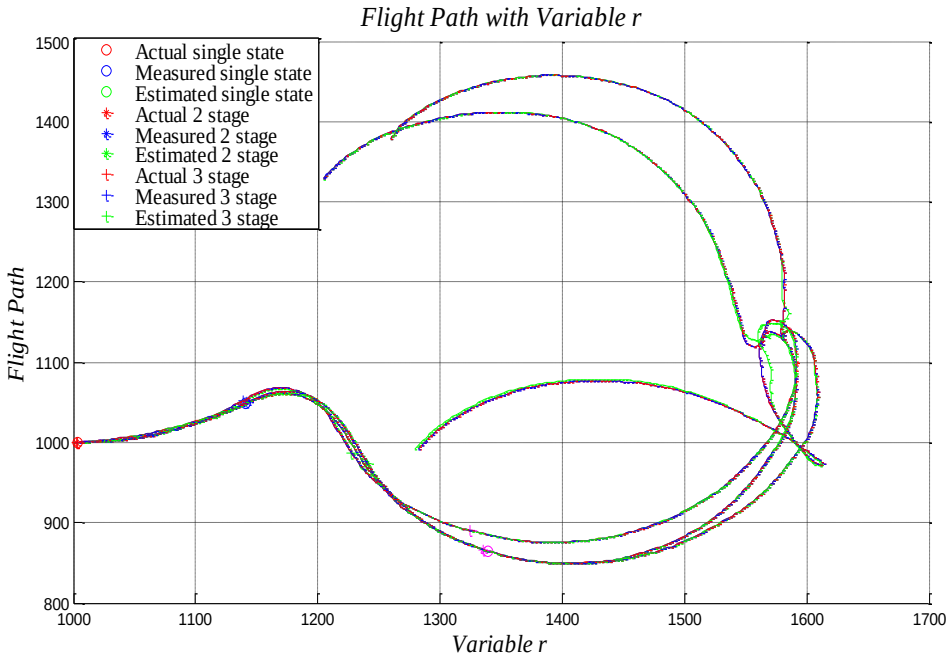

Figure 54: Result 26

The curves shown are those of flight path of the FMAV. The values of height as calculated using velocity and the phi angle, the eastern and the northern position were used to calculate a resultant so as to define the flight path of the aircraft. The FMAV starts with a level flight and then enters into circular turn by decreasing its pitch angle for a while and increasing it afterwards. In between, it enters some tight loops, which can be seen in the GPS curves as well, in the form of small kinks in the both plots. The plots for roll angle and yaw angle contribute to the turn being made by the FMAV during flight. As for pitch angle, the oscillations in its curve indicate the circuitous path that the FMAV generates. All the filters are pretty good at following

the trajectory, but the slight difference amongst them is due to the different levels of calculations involved in the three types.

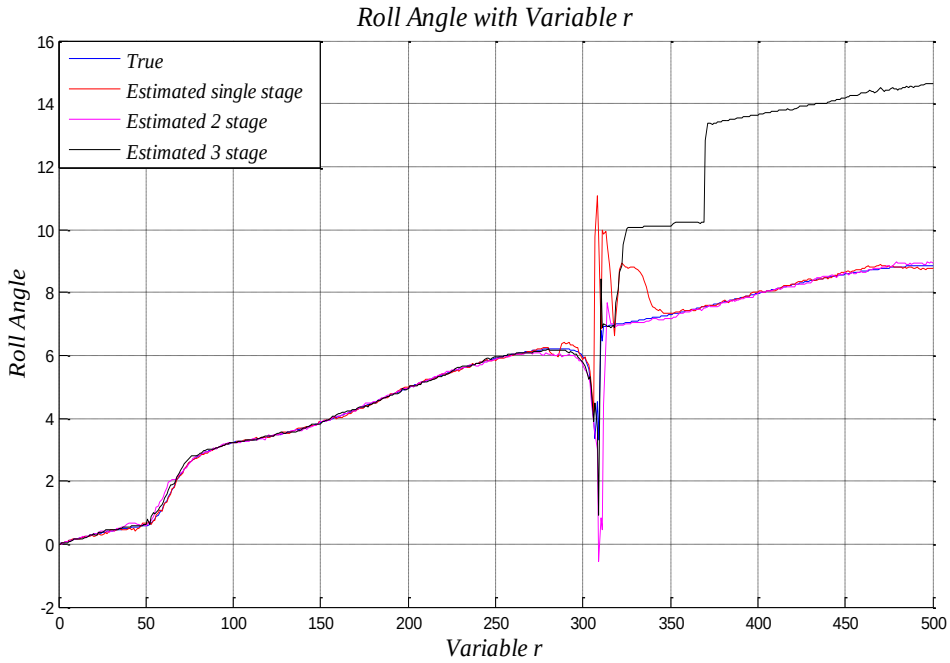

Figure 55: Result 27

The plots shown are that of roll angle with variable yaw rate against number of iterations. The variation has a direct effect on the roll angle, though in an inverse manner. An increase in the yaw rate leads to a decrease in roll angle of the aircraft, which essentially means that as the aircraft turns, its banking angle reduces. The filters do follow the trend to a certain extent, but during a large change in yaw rate, the 2 stage and 3 stage Kalman Filter diverge; an indication of the fact that these two types of filters are not as sensitive as the single stage Kalman Filter.

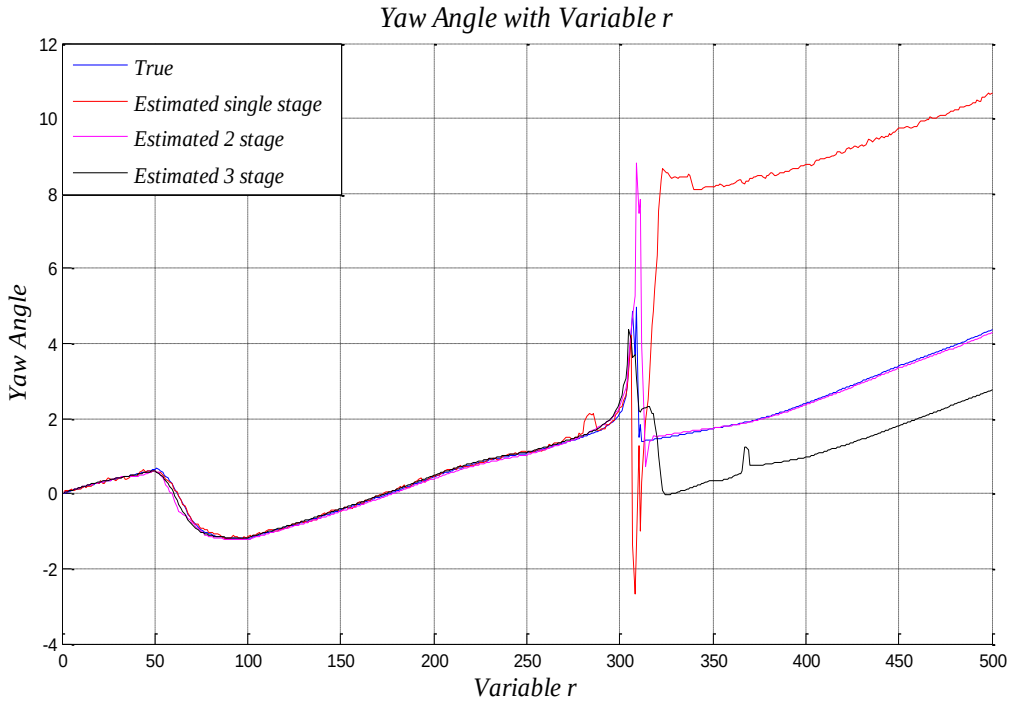

Figure 56: Result 28

The plots shown are that of pitch angle with variable yaw rate against number of iterations. Pitch angle is not directly affected by the yaw rate, but is affected indirectly through changes in the roll angle that contributes in the transformation from inertial to earth frame. All the filters are quite accurate in their estimation of the state variables, though single stage is the most accurate as it follows all the slopes of the curve very smoothly.

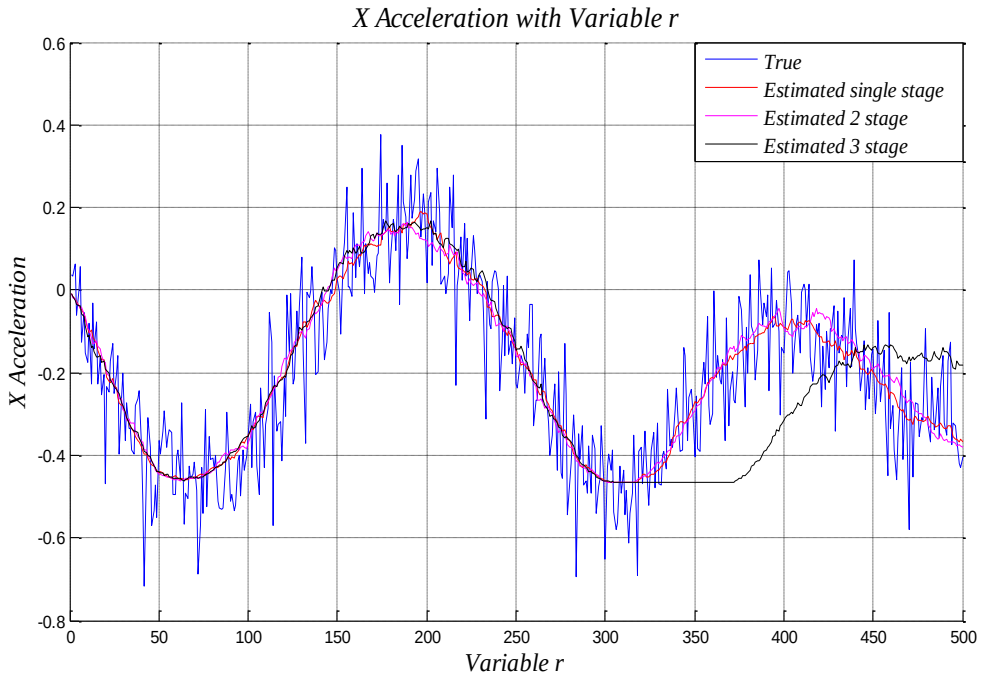

Figure 57: Result 29

The plots shown are that of measurement variable acceleration in the x direction with variable yaw rate against number of iterations. The trend is similar to that of the pitch angle, because of the dependence of the forward dynamics on the pitch angle. As the pitch angle increases, so does the forward velocity and vice versa. The filters are able to curtail the noise in the measurement, but falter at steep slopes, especially the 2 stage Kalman Filter. Single stage is the most accurate as far as values are concerned, though 3 stage is quite accurate also in following the trend along with the single stage Kalman Filter.

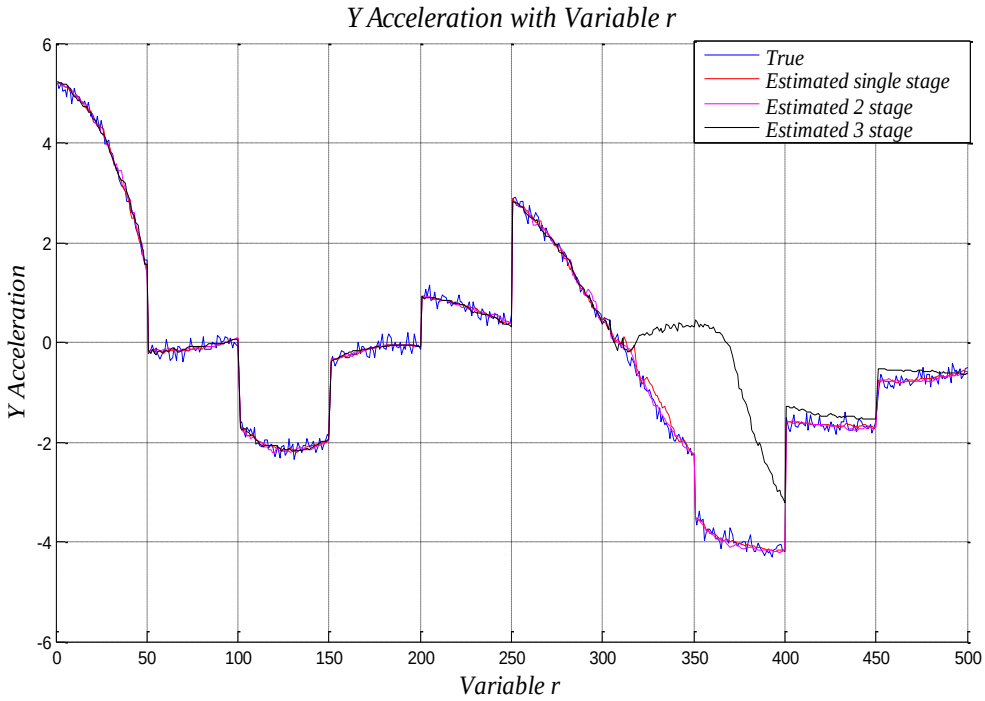

Figure 58: Result 30

The plot shown is that of the measurement variable acceleration in the y direction with variable yaw rate against number of iterations. Since dynamics in the y axis are part of the lateral dynamics, it is under the direct effect of the variation in yaw rate. Moreover, changes in other parameters such as roll angle, pitch angle etc have an effect on the acceleration in the y direction. It is because of the combination of several factors that the trend witnessed cannot be associated with nay one parameter. The highly variable slopes point to the fact that a variation in yaw rate of the aircraft can lead to non-uniform motion in the y axis of the aircraft. The filters are quite successful at reducing the vibrations, though 2 stage, not being as sensitive as the single stage Kalman Filter, tends to waver at times.

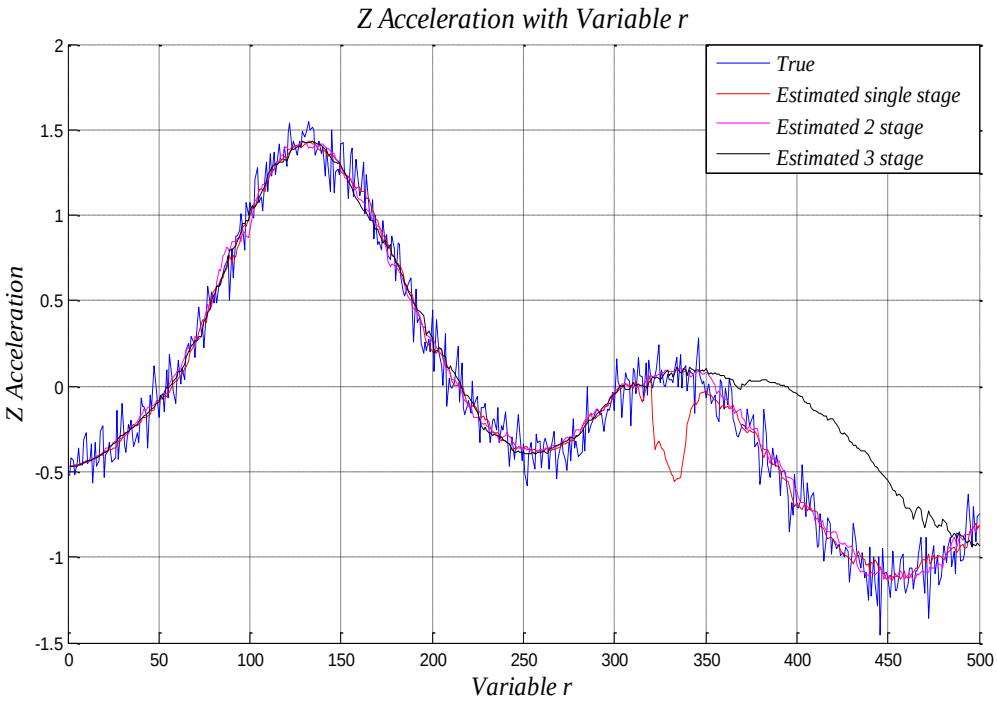

Figure 59: Result 31

The plots shown are that of the measurement variable acceleration in the z direction with variable yaw rate against number of iterations. The dynamics of the z axis are not directly affected by the yaw rate, but are indirectly influenced through the pitch angle that contributes to its strength, and therefore, the trend is quite similar to that of the pitch angle. However, the influence of roll angle on the dynamics alters the trend a tad. The filters are quite good at reducing the effect of vibrations, but as before 2 stage and 3 stage Kalman Filter waver off from the actual curve at some point.

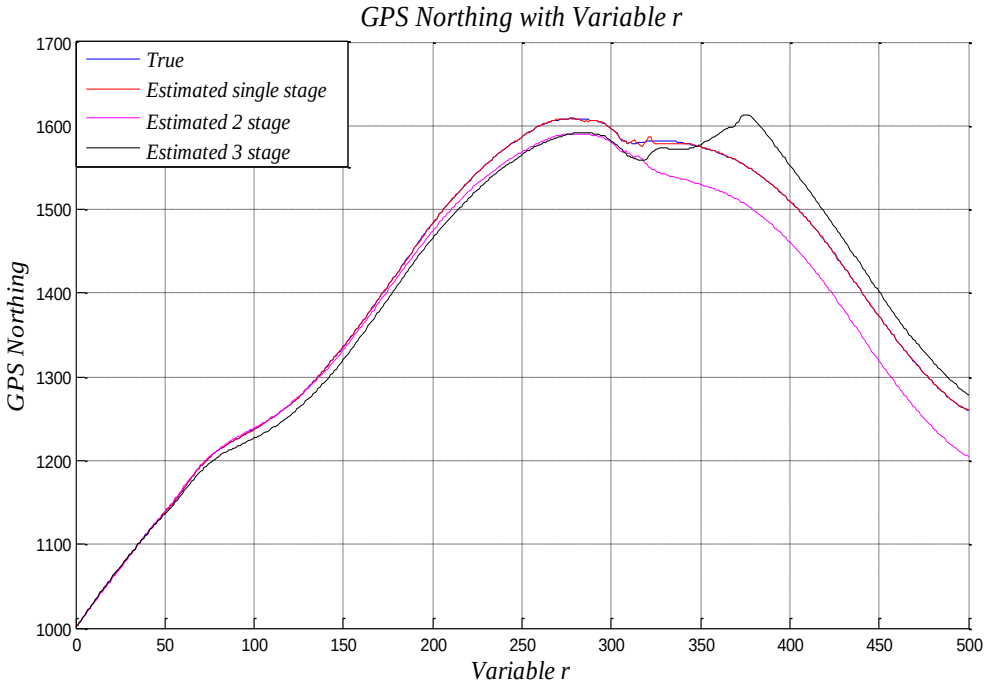

Figure 60: Result 32

The plots shown are that of GPS in the northern direction with variable yaw rate. Because of the involvement of various parameters affected by variation in yaw rate that affect the location of the aircraft the trend shown is not very uniform. The aircraft tends to move northwards and then southwards as the yaw rate first decreases and then increases. Single stage Kalman Filter proves to be the most accurate in determination of aircraft's position.

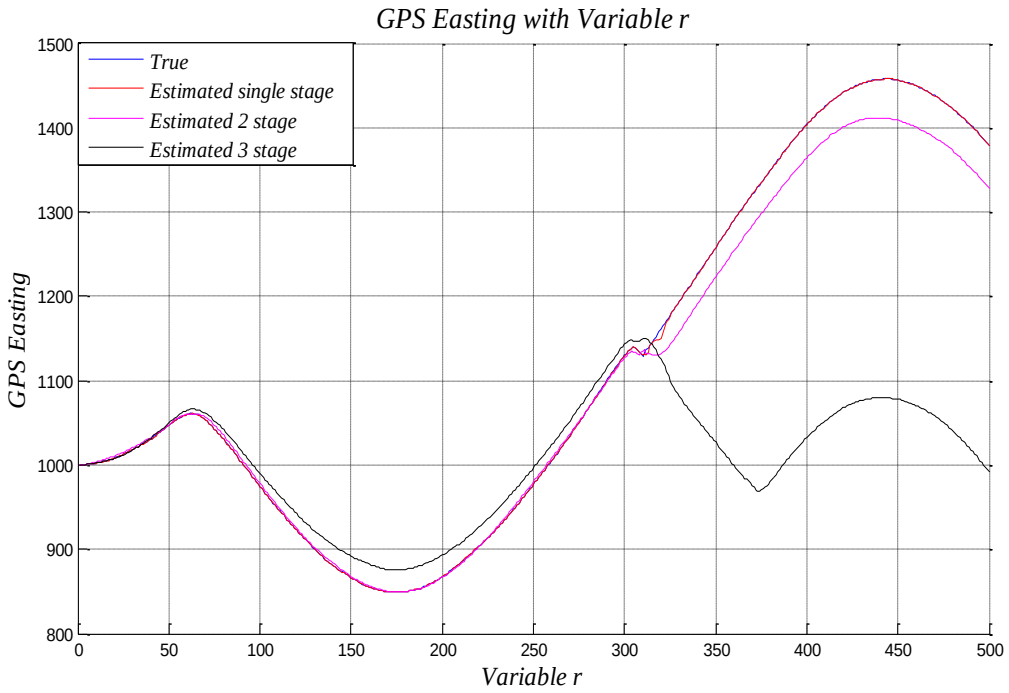

Figure 61: Result 33

The plots shown are that of GPS in the eastern direction with variable yaw rate. The curves are quite similar to that of the yaw angle, which is an indication of the influence of lateral dynamics on the eastward position of the aircraft. All the filters are quite accurate in their estimates, though it is the single stage Kalman Filter that stands out owing to high precision and accuracy.

REFERENCES

1. James M. McMichael (Program Manager Defense Advanced Research Projects Agency) and Col. Michael S. Francis, USAF (Ret.) (Defense Airborne Reconnaissance Office), "*Micro air vehicles - Toward a new dimension in flight*" dated 8/7/97

2. http://www.ornithopter.net/history_e.html.

3. DeLaurier, J.D., "The Development and Testing of a Full-Scale Piloted Ornithopter", 1999.

4. Anderson Jr., J.D., "Fundamentals of Aerodynamics (3rd Ed)", Boston, MA: McGraw Hill, 2001.

5. http://www.ornithopter.org/flapflight/birdsfly/birdsfly.html.

6. http://avdil.gtri.gatech.edu/RCM/RCM/Entomopter/EntomopterProject.html

7. http://robotics.eecs.berkeley.edu/~ronf/MFI.

8. Schmidt, G.T., \Strapdown Inertial Systems - Theory and Applications,"AGARD Lecture Series, No. 95, 1978.

9. Bar-Itzhack, I.Y., and Berman, N., \Control Theoretic Approach to Inertial Navigation Systems," Journal of Guidance, Vol. 11, No. 3, 1988, pp. 237-245.

10. Grewal, M.S., and Andrews, A.P., Kalman Filtering: Theory and Practice using MATLAB, John Wiley and Sons, New York, 2001.

11. Grewal, M.S., Weill, L.R., and Andrews, A.P., Global Positioning Systems, Inertial Navigation, and Integration, John Wiley and Sons, New York, 2001.

12. Wolf, R., Eissfeller, B., Hein, G.W., \ A Kalman Filter for the Integration of a Low Cost INS and an attitude GPS," Institute of Geodesy and Navigation, Munich, Germany.

13. Grejner-Brzezinska, D.A., and Wang, J., \Gravity Modelling for High-Accuracy GPS/INS Integration," Navigation, Vol. 45, No. 3, 1998, pp. 209-220.

14. Srikumar, P., Deori, C.D., \ Simulation of Mission and navigation Functions of the UAV - Nishant," Aeronautical Development Establishment, Bangalore

15. Randle, S.J., Horton, M.A., \ Low Cost Navigation Using Micro – Machined Technology," IEEE Intelligent Transportation Systems Conference, 1997.

16. Gaylor, D., Lightsey, E.G., \ GPS/INS Kalman Filter desing for Spacecraft operating in the proximity of te International Space Station," University of Texas - Austin, Austin.

17. Brown, A., Sullivan, D., \ Precision Kinematic Alignment Using a low costm GPS/INS System," Proceedings of ION GPS 2002, Navsys Corporation, Oregon, 2002.

18. Moon, S.W., Kim, J.H., Hwang, D.H., Ra, S.W., Lee, S.J., \ Implementation of a Loosely Coupled GPS/INS integrated system, " Chungnam National University, Korea.

19. Salychev, O.S., Voronov, V.V., Cannon, M.E., nayak, R., Lachapelle, G., \ Low Cost INS/GPS Integration: Concepts and Testing," Institute of Navigation National Technical Meeting, California, 2000.

20. Wang, J., Lee, H.K., Rizos, C., \ GPS/INS Integration: A Performance Sensitivity Analysis," University of New South Wales, Sydney.

21. Kwon, J.H., \Airborne Vector Gravimetry Using GPS/INS," Ohio State University, Ohio, April 2000.

22. Ronnback, S., \Development of a INS/GPS Navigation Loop for an UAV," University of Sydney, Sydney, February 2000.

23. Gautier, J.D., \ GPS/INS Generalized Evaluation Tool (GIGET) for the design and testing of integrated Navigation Systems," Stanford University, California, 2003.

24. Mayhew, D.M., \Multi-rate Sensor Fusion for GPS Navigation Using Kalman Filtering," Virginia Polytechnic Institute and State University, Virginia, May 1999.

25. Moore, J.B., Qi, H., \Direct Kalman Filtering Approach for GPS/INS Integration", IEEE Transactions on Aerospace and Electronic Systems , Vol 38, No.2, April 2002.

26. Shang, J., Mao, G., and Gu, Q., \Design and Implementation of MIMU/GPS Integrated Navigation Systems,"Tsinghua University, China, 2002.

27. Cao, F.X., Yang, D.K., Xu, A.G., \ Low Cost SINS/GPS Integration for Land Vehicle Navigation, " IEEE International Conference on Intelligent Transport Systems , September 2002, Singapore.

28. Panzieri, S., Pascucci, F., Ulivi, G., \An Outdoor navigation system using GPS and Inertial Platform," IEEE ASME Transactions on Mechatronics, Vol. 7, No. 2, June 2002.

29. Dorobantu, R., Zebhauser, b., \Field Evaluation of a Low-Cost Strapdown IMU by means of a GPS," Technical University of Munchen, Germany.

30. http://www.andrew.cmu.edu/user/deberhar/Mentor.html.

31. Moble Benedict, "Aeroelastic Design and Manufacture of Efficient Ornithopter wing", Dual Degree Dissertation, Department of Aerospace Engineering, IIT Bombay, July 2004.

32. "AeroVironment's "Wasp" Micro Air Vehicle Sets World Record" AeroVironment Inc, Press release, www.aerovironment.com/news/news-archive/wasp62.html, August 2002.

33. "Development of the Black Widow Micro Air Vehicle" by J.M. Grasmeyer and M.T. Keenon, AeroVironment Inc, AIAA Paper No. 2001-0127, January 2001.

34. "AeroVironment's "Hornet" Micro Air Vehicle Performs First Fuel Cell Powered Flight" AeroVironment Inc, Press release, www.aerovironment.com/news/news-archive/hornet62.html, March 2003.

35. "Development of the Black Widow and Microbat MAVs and a Vision of the Future of MAV Design" by M.T. Keenon and J.M. Grasmeyer, AeroVironment Inc.

36. "Mosquito Micro UAV" *Defense Update International Online Defense Magazine*, 2nd Issue, http://www.defense-update.com/products/m/mosquito.htm, 2002.

37. "Desert Hawk Mini UAV Goes Operational" by E. Hehs, *Code One an Airpower Projection Magazine,* Volume 18 No2, 2003.

38. "Army Looks to Miniature Air Vehicles" http://www.blackbirds.net/uav/uavnews.html, November 1998

39. "Unmanned Aerial Vehicles" by G. Goebel, available: http://www.vectorsite.net/twuav.html, January 05, Ch17.

40. "Design and Flight Test Results for Micro-Sized Fixed-Wing and VTOL Aircraft" by S.J. Morris, MLB Company.

41. "Design of Micro Air Vehicles and Flight Test Validation" by Dr. S.J. Morris and Dr. M Holden, MLB Company.

42. "Exploratory Study of the Operationalization of the Flapping Wing MAV" by J. Chan, W.T. Cheng, J. S Choo, S.H. Goh, W.T. Khoo, T.C. Phua, and W.K Tan, Naval Postgraduate School, December 2003.

43. "Experimental Investigation of the Aerodynamic Characteristics of Flapping-Wing Micro Air Vehicles" by K.D. Jones and M.F. Platzer, AIAA Paper No. 2003-0418, January 2002.

44. "The NRL MITE Vehicle" by J. Kellogg, C. Bovais, J. Dahlburg, R. Foch, J. Gardner, D. Gordon, R. Hartley, B. Kamgar-Parsi, H. Mcfarlane, F. Pipitone, R. Ramamurti, A. Sciambi, W. Spears, D. Srull, and C. Sullivan, Naval Research Lab.

45. Z. Jane Wang, "Aerodynamics Efficiency of Flapping Flight: Analysis of Two-Stroke Model", General of Experimental Biology, 2008, No 211, pp 234-238,

46. Sanjay P. Sane and Michael H.Dickinson, "The Aerodynamic Effects of Wing Rotation and Revised Quasi-Steady Model of Flapping Flight ", The General of Experimental Biology 2002, 205, 1087-1096

47. Jae-Hung Han, Jin-Young Lee and Dae-Kwan Kim, "Ornithopter Modeling for Flight Simulation", International Conference on Control, Automation and Systems 2008, Oct 14-17 COEX, Seoul Korea

48. MEMS Mechanical Sensors by Stephen Beeby, Graham Ensell, Michael Kraft, Neil White. Artech House, Inc.Boston • London. www.artechhouse.com

49. "Estimation with Applications to Tracking and Navigation" by Yaakov Bar-Shalom, X-Rong Li, Thiagolingam Kirubarajan. A Wiley- Interscience Publication. John Wiley & sons. INC..

50. "Modern Inertial Technology (Guidance, Navigation and Control) second edition by Anthony Lawrence. Springer.
51. 1. N. Yazdi, F. Ayazi, and K. Najafi. Aug. 1998. "Micromachined Inertial Sensors," Proc IEEE, Vol. 86, No. 8.

52. Jonathan Bernstein, Corning-IntelliSense Corp , MEMS inertial sensing technology

53. S.Nasiri, Wafer Level Packaging of MOEMS Solves Manufacturability Challenges In Optical Cross Connect, 2003,

54. S.Nasiri patent, MEMS Mirrors and MEMS arrays, Pat# 6,480,320 T.B. Gabrielson. May 1993. "Mechanical-thermal noise in micromachined acoustic and vibration sensors," IEEE Trans, Electron. Devices, Vol. 40:903-909.

55. Introduction to GPS The Global Positioning System by Ahmed El-Rabbany Artech House Boston . London. www.artechhouse.com.

56. Mixed-Mode VlSI Optic Flow Sensors for In-Flight Control of a Micro Air Vehicle by G. L. Barrowsa and C. Neely. Naval Research Laboratory, Code 5722. Washington, DC 20375 USA

57. "Ground control station development for autonomous UAV "by Ye Hong, Jiancheng Fang, and Ye Tao. Key Laboratory of Fundamental Science for National Defense, Novel Inertial Instrument & Navigation System Technology, Beijing, 100191, China

58. "Integration of GPS/INS/Vision sensors to navigate unmanned aerial vehicles" by Jinling Wanga, Matthew Garrattb, Andrew Lambertc, Jack Jianguo Wang a, Songlai Hana, David Sinclaird. a School of Surveying & Spatial Information Systems, University of New South Wales, NSW 2052, Australia (Jinling.Wang@unsw.edu.au). b School of Aerospace, Civil and Mechanical Engineering, School of Information Technology and Electrical Engineering, Australia Defence Force Academy, Canberra, Australia. d QASCO Surveys Pty. Limited, 41 Boundary St. South Brisbane, Qld, 4101, Australia.

59. "Development of a flight avionics system for an autonomous micro air vehicle" By Jason Plew, a thesis presented to the graduate school of the University of Florida in partial fulfillment of the requirements for the degree of master of science, University of Florida, 2004.

60. “Integration of MEMS inertial sensor-based GNC of a UAV” by Z. J. Huang and J. C. Fang (huangzhongjun@buaa.edu.cn,fangjiancheng@buaa.edu.cn) from School of Instrumentation & Optoelectronics Engineering Beihang University, Beijing 100083, China. International Journal of Information Technology. Vol. 11 No. 10 2005 (pg 123-132)

61. “State estimation for micro air vehicles” by Randal W. Beard, Department of Electrical and Computer Engineering, Brigham Young University, Provo, Utah. Studies in Computational Intelligence (SCI) 70, 173–199 (2007). Springer-Verlag Berlin Heidelberg 2007

62. “Optimal state estimation Kalman, H_∞ and nonlinear approaches” by Dan Simon, Cleveland State University. A John Wiley &Sons, INC., Publication.

63. Elbert Hendricks, Ole Jannerup, Paul Haase Sorensen, “Linear Systems Control” Deterministic and Stochastic Method, ISBN: 978-3-540-78485-2, Library of Congress Control Number: 208927517, 2008 Springer-Verlag Berlin Heidelberg.